Response to Anonymous Reviewer #1

The authors are grateful to the anonymous reviewer for carefully reading the manuscript and the proposed corrections. Accordingly to the comments following changes were made:

1) Reviewer: *In Introduction, it is difficult to comprehend notations with regards to particles and model coordinates.*

Answer: First paragraph in Introduction (beginning from the line 17, page 1 up to the line 8, page 2) was reformulated as follows:

The relationship between the near-surface flux $F_s(x, y, 0)$ and the flux $F_s(x_M, y_M, z_M)$, measured in point $\mathbf{x}_M = (x_M, y_M, z_M)$, can be formalized via the footprint function f_s:

$$F_s(x_M, y_M, z_M) = \int_{-\infty}^{\infty} \int_{-\infty}^{\infty} f_s(x, y, x_M, y_M, z_M) F_s(x, y, 0) dx dy. \tag{1}$$

Traditionally, footprint functions $f_s^d(x^d, y^d, \mathbf{x}_M) = f_s(x, y, \mathbf{x}_M)$ are expressed in local coordinate system with the origin which coincides with the sensor position (here, $x^d = x_M - x$ is the positive upwind distance from the sensor and $y^d = y_M - y$ is the cross-wind distance, see Fig. 1a). In horizontally homogenous case these functions do not depend on x_M and y_M. In ABL the surface area contributing to the flux is elongated in wind direction, therefore the cross-wind integrated footprint function f_s^y defined as

$$f_s^y(x^d, z_M) = \int_{-\infty}^{\infty} f_s^d(x^d, y^d, z_M) dy^d, \tag{2}$$

is one of the most required characteristics for the practical use.

The measurements of the scalar flux footprint functions in natural environment are restricted (e.g., Finn et al.,1996;Leclerc et al., 1997, 2003; Nicolini et al., 2015) due to the necessity to conduct the emission and detection of artificial tracers. Besides, such measurements are not available for the stably stratified ABL where the area of the surface influencing the point of measurements increases.

Here we avoided introducing of the averaging notations, which bring no additional sense in original version of manuscript. Systems of coordinates are illustrated in additional schematic Fig. 1a.

2) Reviewer: *A new figure would help to explain the analysis and experiment set up.*

E.g. it is unclear why $\mathbf{x}_M$ is a vector but x,y not in Eq. (1). It is hard to understand what the coordinates of particles are and how the weight areas are computed. The figure should refer to Eq. (1) (2) and (3) and to the description on the page 4 lines 20-35..

Answer: New schematic figure was added (Fig.1). It was supplemented with the appropriate description of footprint evaluation algorithm in Section 2.1:

Schematic representation of the algorithm for the footprint function determination in LES is shown in Fig. 1. In accordance with Eq. (3) and the description above, the particle crossing the test area δ_M brings the impact into the value $f_s(x_S, y_S, \mathbf{x}_M)$ then the beginning of its modified trajectory shifted in a such way to superpose the point $\mathbf{x}_1^p$ with sensor position $\mathbf{x}_M$ belongs to the test area δ_S. For example (see, Fig. 1b), red particle is counted while evaluation of the footprint value in point (x_S, y_S), but blue particle is not counted. Such algorithm of averaging was selected because it permits to refine the footprint resolution in the vicinity of sensor independently on the area of δ_M using the assumption of some spatial homogeneity.

Besides, we added description of the grid used for footprint accumulation (see last paragraph of Sect. 2.1 in modified version of manuscript):

Nonuniform Cartesian grid $\mathbf{x}_{ij}^d = (x_i^d, y_j^d)$ (where, $-20 \leq i \leq 160$; $-120 \leq j \leq 120$), stretched with the distance from the sensor position, was selected for the footprint functions accumulation in the following sections of this paper. Grid was prescribed as: $(x_0^d, y_0^d) = (0, 0)$; $x_i^d = \Delta_{x0}\gamma_x^{|i|} i/|i|$ and $y_i^d = \Delta_{y0}\gamma_y^{|j|} j/|j|$ if $i \neq 0$ and $j \neq 0$; $\Delta_{x0} = \Delta_{y0} = 2$ m; $\gamma_x = \gamma_y = 1.05$. This grid is independent on the LES model resolution and coincides with the footprint grids selected for all runs with LSMs and RDMs.

3) Reviewer: *Explain what "ensemble average" means in the context of the study.*

Answer: The following clarification was included after the Eq. (8) in Sect. 2.3:

Here $\left\langle u_i^{(p)} \right\rangle$ is the ensemble averaged Eulerian velocity at point $\mathbf{x}^p$. Note, that LSMs are assumed to be also applicable under the temporal evolution of turbulence statistics. In this paper we shall consider ABL as it approaches a quasi-steady state. Therefore, due to assumption of ergodicity, ensemble averaging can be replaced by averaging in time and in the directions of spatial homogeneity: $\langle\varphi\rangle \approx \langle\varphi\rangle_{x,y,t}$.

4) Reviewer: *Why is the index "p" used both as subscript and superscript in Eq. (7) and later on. Could you make notations more homogeneous?*

Answer: The notation s_p was used to denote evaluated value of scalar concentration by the number of particles (subscript p was not connected with the superscript p). In new version of manuscript we denote this value s_P (with capital P) to avoid misunderstanding.

5) Reviewer: *Page 6, lines 2-3. The sentence is not quite clear. What will happen if a particle leaves the volume and then reappears again in the same volume during the unit time interval? Will it be counted as a new particle? Or do you mean something different under "appearing ... during unit time interval".*

Answer: The word "appearing" was replaced by word "ejected". Here we mean the new particles which were added during the run (appearing of new particles imitates the external source of scalar concentration).

6) Reviewer: *The sentence between Eqs. (8) and (9) is impossible to understand.*

Answer: This sentence was rewritten as follows:

Single particle first-order LSM is formulated as follows. Velocity $u_i'^p$ is described by the stochastic differential equation: ...

7) Reviewer: *Page 9, line 25. Use "provides better agreement" instead of "leads to better coincidence".*

Answer: It was done.

8) Reviewer: *Section 4.2.3, also 5.1.4 and 5.1.5. It would be useful to place a discussion here into some experimental context referring to correlations between resolved and* *unresolved velocities (or velocities and stresses on different spatial scales) , e.g. the work by Charles Meneveau and co-authors (Meneveau and Katz in Annu. Rev. Fluid Mech.* 2000. 32:1–32).

Answer: The paper (Meneveau and Katz, 2000) is devoted to the a priory testing of the scale-similarity approaches for subgrid modelling of Eulerian dynamics in LES. The reference to this paper is useful in Section 3.1 where the mixed subgrid/subfilter model is introduced. So, the following text was added after the Eq. (17):

The a priori tests using the data of laboratory measurements show that scale- similarity models with Gaussian or box filters provide correlation typically as high as 80% between real and modeled stresses (see, overview in Meneveau and Katz, 2000). The significant part of this correlation can be attributed to non-ideality of the spatial filter and use of common information for computing both the real and modeled stresses (see, Liu et al., 1994). The discrete spatial filter used in this study has a smooth transfer function in spectral space, so it can be supposed that the scale-similarity part of Eq. (18) is mainly responsible for the influence of velocity fluctuations belonging to "subfilter" scales.

In Section 4.2.3 we introduced next clarification of high correlation between subfilter velocity and resolved velocity:

In the previous subsection the recovered "subfilter" part of velocity $\mathbf{u}'' = \mathbf{u}^* - \overline{\mathbf{u}}$ and so the subfilter Lagrangian velocity $\mathbf{u}''^{(p)}$ were highly correlated with the resolved velocity $\overline{\mathbf{u}}$ in time and space. This is due to the specifics of spatial filter (Eq. 24) used for the recovering given by Eqs. (25, 26). This filter has a smooth transfer function in spectral space. The analogous effects of non-ideal filters in LES which lead to the high correlations between modelled and measured turbulent stresses were obtained and discussed earlier in (Liu et al., 1994) and (Meneveau and Katz, 2000), where the laboratory data of turbulent flows were studied.

Section 5.1.4 contains the description of the universal function used for correction of dissipation profile. New reference was added to the paper which contains the measurement data of similar nondimensional function. The text after Eq. (43) was modified as follows:

Previous LES studies of stable ABL (e.g., Beare et al., 2006) also give neglectfully small values of the transport terms in TKE balance. The experimental confirmation of the validity of Eq. (42) can be found in (Grachev et al., 2015), where the dissipation in stable ABL was estimated using the spectral analysis of longitudinal velocity in inertial range. In accordance with this paper: $\tilde{\epsilon} \approx \phi_m$, that is almost indistinguishable from Eq. (42) within the accuracy of the experimental data and the ambiguity of the method of dissipation evaluation.

Section 5.1.5 contains the results of the evaluation of diffusion coefficients. Here these coefficients are presented as dimensional values and are specific for the modelled flow. There are no available experimental data on the values of horizontal diffusivity in horizontally homogeneous stable ABL. At least, authors are not aware of such measurements.

9) Reviewer: *Use Figures instead of Pictures in the paper.*

Answer: It was corrected.

10) Reviewer: *General remark in connection to Figure 6. Figure 6 shows a negative footprint. It is hard to understand the physical meaning of the negative values. Could you include a paragraph discussion this aspect?*

Answer: Next explanation was included into first paragraph of Section 4.3:

The negative values of scalar flux footprint show what the vertical turbulent transport of the scalar emitted in the relevant area is basically directed from the upper levels down to the surface. For example the positive surface concentration flux in this area will lead to negative anomaly of the turbulent flux measured in the sensor position. This does not contradict the diffusion approximation of the turbulent mixing, because mean crosswind advection at the upper levels can produce the positive vertical concentration gradient to the right of near-surface wind.

11) Reviewer: *in several places, e.g. line 24 at the page 11, the Equation number is referred without "Eq." so that it is difficult to understand what those numbers are for.*

It was corrected.

Additional references were included into bibliography:

Grachev, A. A., Andreas, E. L., Fairall, C. W., Guest, P. S. and Persson, P. O. G.: Similarity theory based on the Dougherty–Ozmidov length scale. Q.J.R. Meteorol. Soc., 141, 1845–1856, 2015.

Liu S., Meneveau C., Katz J.: On the properties of similarity subgrid-scale models as deduced from measurements in a turbulent jet. J. Fluid Mech. 275, 83–119, 1994.

Meneveau C. and Katz J.: Scale-invariance and turbulence models for large-eddy simulation. Annu. Rev. Fluid Mech., 32, 1–32, 2000. Michalek W.R., J.G. M.Kuerten, J.C.H. Zeegers, R.Liew, J.Pozorski, B.J. Geurts: A hybridstochastic-deconvolution model for large-eddy simulation of particle-laden flow. Physics of Fluids, 25, 123302, 2013

(a)

(b)

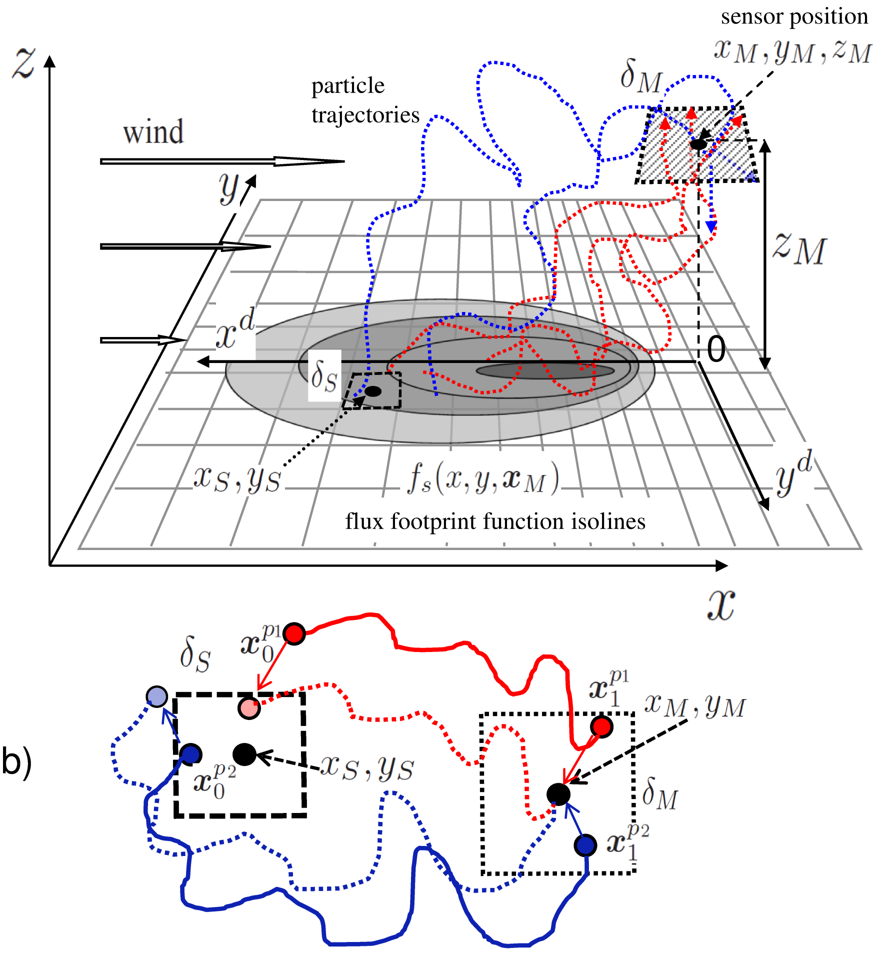

Figure 1: Schematic representation of footprint evaluation algorithm. (a) Setup of numerical experiment. (b) Example of two trajectories (red and blue bold curves). Shifted trajectories are shown by the dashed lines. Particle brings the impact into the value $f_s(x_S, y_S, \mathbf{x}_M)$ if it intersects the test area δ_M in vicinity of the sensor position $\mathbf{x}_M$ and the origin of modified trajectory belongs to the test area δ_S.

Response to Anonymous Reviewer #2

Authors are grateful to the referee for a high assessment of the article. Accordingly to the comments following changes were made:

1) Reviewer: *Page 1, line 18. Replace 'the near-surface flux' by 'the surface flux' because it's defined for z=0 (cf. "L is the Obukhov length at the surface" on page 16, lines 1-2).*

Answer: It was done.

2) Reviewer: *Page 1, lines 18-19. Replace 'denoting the ensemble averaging' by 'denote a time/space average'.*

Answer: Agree. Accordingly to comments of Reviewers #1 and #2 this paragraph was rewritten (see our response #1). In new version of manuscript we avoid ensemble averaging notation in Introduction.

3) Reviewer: *Page 3, line 24. Although abbreviations 'LSM' and 'RDM' are defined in the abstract and later on page 7, they should be also introduced in the text on first occurrence.*

Answer: In new version of the paper the abbreviations 'LSM' and 'RDM' are introduced on page 2, line 12-13.

4) Reviewer: Figures 1-10. I recommend use color version of the plots (similar to Fig. 11) instead black and white.

Answer: Figures 2-6 and 8,10,11 (in previous version 1-5 and 7,9,10) were colorized. Figures 7 and 9 contain a few number of curves, so they remain to be black and white.

Additionally, the typo was corrected in Eq. (49). (ξ_i^p was replaced to ξ_3^p)

Corrected version of the paper is attached (see, pdf file in supplement).

Response to Anonymous Reviewer #3

We are very grateful to reviewer for insightful analysis of our paper. All the comments are very professional and helped us to improve substantially the manuscript. The authors believe, that the material presented in the manuscript became better justified after the revision.

We would like to address two topics raised by the reviewer in a different order than presented in the review. These comments concern the validity of the simulation results (minor comment f) and the correctness of the presented results in Figure 11. It will be impossible to proceed with other comments until we consider these issues.

1) **Reviewer: (f) Wind profile: from Figure 1, it seems that simulated wind speeds in the surface layer part of the domain are smaller than the 'standard' wind profile for stable conditions (e.g., Stull, 1988; Högström, 1996). Please add a couple of sentences to explain why.**

Answer: This comment is suggested as minor but from the authors point of view it is of major importance. There is no sense in discussing anything else, if the numerical model used in this study produces wrong results. We have added the data from eight different LES models in Fig.2 (Fig.AR1 here and Fig.1 in the original version of the manuscript). These data were obtained during LES intercomparison experiment GABLS-1 and are available online at: http://gabls.metoffice.com/lem_data.html. We used the data for 3.125 m resolution, because they were presented for the largest set of the models and because the results do not change substantially with the following grids refining. Wind velocities from the other models shown in Fig.2 (Fig.AR1) are rotated 35 degrees clockwise in accordance with the setup of our runs. The results from the LES model used for the current study fit with the results of the other models very well. Besides, our model gives a good scale invariance, which is not the case for some models presented at http://gabls.metoffice.com/means_125.html. Mean wind profile computed in accordance with [Högström, 1996] is shown by the vertical dashes in Fig.AR1, this profile almost coincides with the longitudinal velocity obtained in LES. Accordingly, the authors have no reason to doubt the results of the simulations. In the opposite case it would have been questionable the LES methodology for the stable boundary layer investigation.

Corrections:

Figure 2 (AR1, former Fig.1) was modified by adding the data from other LES models referred to above.

Following clarification was inserted into the text (p.13 l.21 - p.14 l.3):

This setup is based on the observation data (see, [Kosoviĉ and Curry, 2000]). As it was shown in [Beare et al., 2006], the LES results obtained under the same conditions with the different models converged with the higher grid resolutions. Later, this case was used for testing the LES models e.g. in [Maronga et al., 2015, Zhou and Chow, 2012, Bhaganagar and Debnath, 2015] and many others and for the improvement of subgrid modelling e.g. in [Basu and Porté-Agel, 2006, Zhou and Chow, 2011, Kitamura, 2010]. The LES model presented here was tested earlier under the non-modified setup of GABLS in [Glazunov, 2014], where the turbulent statistics above a flat surface and above an urban-like surface were investigated. In all of these studies, LES results were in agreement with the known similarity relationships for the stable ABL. This allows to consider the LES data for GABLS as a reference case for testing of the approaches utilizing the statistical averaging of the turbulence (e.g., see [Cuxart et al., 2006], where the intercomparison of single-column models was performed). Several of nondimensional relationships in stable ABL were collected and presented in [Zilitinkevich et al., 2013]. Considered case is also included in the LES database for this study and fits well with the different stability regimes after the appropriate normalization. Therefore, the results obtained in this particular case can be generalized for many cases due to similarity of the stable ABLs. Besides, the presented simulations are easily reproducible and they can be repeated using any LES model which contains the Lagrangian particle transport routines.

The mean wind velocity and the potential temperature, calculated with the different spatial steps Δ_g, are shown in Fig. 2 The model slightly overestimates the height of the boundary layer at coarse grids, however, the wind velocity near the surface is approximately the same in all runs. As one can see from the Fig. 2, the results of simulation are in good agreement with the results from other LES presented in [Beare et al., 2006] (see, http://gabls.metoffice.com for more information). Mean wind profile computed in accordance with [Högström, 1996] is shown in Fig. 2 by the vertical dashes, in the surface layer part of the domain this "standard" profile for the stable conditions almost coincides with the longitudinal velocity obtained in LES.

2) **Reviewer: Finally, when comparing to other models, it appears that the authors have not correctly reproduced one of these 'other models' (major comment 5)**.

Answer: Most likely there was an unfortunate misunderstanding. In our paper Obukhov length L was defined as:

$$L = -\frac{U_*^3 \Theta_0}{g Q_s},$$

where Q_s is the kinematic potential temperature flux at the surface, g is the acceleration of gravity and Θ_0 is the reference potential temperature. This definition does not include von Karman constant $\kappa \approx 0.4$ in the denominator. It was pointed out in the original version of the paper, see page 16, line 2: '...note, that the von Karman constant is not included in the definition of the length L here and later...' and in the definition of the local Obukhov length Eq. (40). Such definition of the Obukhov length scale is used alternatively (see, e.g. [Zilitinkevich et al., 2013] Eq.(41)) to its convenience when operating with the stably stratified flows outside the surface layer.

In the original version of the paper we wrote (p.20 l.15–17): "Nevertheless, the final approximations [Kljun et al., 2004] and [Kljun et al., 2015] contain the input parameters, which can be determined from LES: the boundary layer height $z_i \approx 180$ m, Obukhov length $L/\kappa \approx 120$ m, friction velocity $U_* \approx 0.27$ m/s and roughness parameter $z_0 = 0.1$ m. These values were substituted into parameterisations [Kljun et al., 2004] and [Kljun et al., 2015]".

Here L is defined without κ in denominator and the number 120 is the appropriate value for FPP, where this constant is included (see, [Kljun et al., 2015], Appendix B).

We performed the calculations of the footprint functions again using the online tool
http://footprint.kljun.net/ffp.php
and got nearly the same results, as were presented previously in Fig.11 (see short dashed lines in Fig.AR2). The next parameters were used:
L = 120
u_star = 0.272
sigma_v = 0.44
z0 = 0.1
u_mean = 0
h = 180
After substituting L= 120×0.4 =48 m into FPP calculator we got the results shown in Fig.AR2 by the dot-dashed lines. These results are very close to those presented in the review. One can find the values of the Obukhov length which is characteristic for the simulated case provided by other LES models at http://gabls.metoffice.com/times_200.html . It is also close to 120 m (48

m, as defined in our paper).
According to the analysis above we believe that the model FPP of [Kljun et al., 2015] was applied correctly in our paper. The Fig. 11 (Fig. 13 in the revised version) will remain unchanged.

Corrections: Nevertheless, to avoid misunderstanding we insert new equation (40) in Sect. 5.1.1 (the expression for L provided above) and define this length scale explicitly with the following commenting:

Note, that the von Karman constant is not included in the definition of the length L here and later (this alternative definition of the Obukhov length is often used along with the traditional one, see e.g. [Zilitinkevich et al., 2013] Eq.(41)).

Starting from here, we shall follow the order of comments provided in the Review.

Major comments

(1) Model validation and argumentation of approaches

Reviewer: corrections of advection speed due to subgrid-scale turbulence (Eq. 36) are applied only in the lowest grid layer [why exactly one?], p. 13, l. 16 - and somehow 'implemented' in the lowest three layers, p. 13, l. 20

Answer: LSM was implemented in the lowest three layers, but the additional stochastic component of velocity produced by this model was taken into account inside the first layer only during the computation of particle position. Only one layer because the aim of this procedure is to minimize use of computational resources without loss of quality and to test the validity of the Lagrangian particles transport with the minimal use of the nondeterministic terms. The presented results show that it is enough.

Corrections: In new variant of the paper we insert clarification and define this procedure explicitly (see, p. 15, l. 14-17 in new version of the paper):
For the curves marked "st_1l", the resultant velocity of the particles near the surface was calculated

as follows:

$$\vec{u}^p = \vec{u}^{(p)} + r(z^p)\vec{u}''^p,$$

where the function $r(z^p)$ is defined as $r(z^p) = (1 - z^p/\Delta_g)$ if $z_p < \Delta_g$, $r(z^p) = 0$ if $z_p \geq \Delta_g$ and $\vec{u}''^p$ is the random velocity component, calculated using the stochastic subgrid model.

Reviewer: furthermore, this correction is based on using a Langevin type of approach (Eq. 28), which employs a particular value for Kolmogorov's constant for the structure function in the Inertial Subrange [C_0] (which is not specified for this application)

Answer: We agree.

Corrections: Next sentence was included after the Eg.(28) l. 10-11 p. 11:
The parameter C_0 was specified to be equal to 6, because the stochastic part of the model (Eq. 28) is mainly responsible for spatial and time scales in an isotropic inertial subrange of the turbulence.

Reviewer: a further 'correction' is applied (Eqs. 33 and 34) with a somewhat arbitrary coefficient c=0.5, p. 14, l. 3

Answer: We agree that this coefficient was selected quite arbitrarily. Justification for this choice is that,
i) The results of footprint calculation are not very sensitive to this coefficient, see Fig. 4, where the crosses are the footprints, computed without correction (c=0). These footprint functions approximately coincide with the results of other methods applied. The main reasons for the use of correction in addition to the velocity recovering were discussed in Sect 4.2.2 (Spatial variability of scalar concentration inferred by Eulerian and Lagrangian methods).
ii) Other Lagrangian subgrid models (LSM implemented in the whole domain and RDM added to the new version of the paper) give similar results.

Reviewer: particles are released at z0 = 0.1 m, but reflected 'at the ground' (p. 12, l.17). Should this mean z = 0 m? And if so, how are the velocity statistics being evaluated below z0?

Answer: There are no physical arguments for a rigorous specifying of the values of turbulent statistics below z_0, because the roughness length is not more than the parameter in logarithmic velocity profile. In the model the values of turbulent subgrid energy and the dissipation of subgrid

TKE were interpolated linearly for $z > \Delta/2$ and were fixed at the values $\epsilon = \epsilon(\Delta/2)$ $E = E(\Delta/2)$ below. Our experience with LSMs and LES models shows that the details of fast mixing near the ground do not influence the footprints considered here, especially if the grid steps are small enough. For example, in the runs with $\Delta_g = 3.125$ and 2.0 m one can substitute the vertical velocity inside the first layer by the value of reconstructed velocity w^* at the level $z = \Delta_g$ and to perform all simulation without the stochastic terms at all, and when doing so it will lead to extremely overestimated mixing inside the first layer, but the footprints with z_M= 10 m and z_M=30 m will be almost unchanged (not included in the paper, we can supply the appropriate figures or data if it is necessary).

Corrections: In the revised paper the procedure of the interpolation of the turbulent statistics inside the first layer is described explicitly (l. 28-29 p. 11) with the following commenting:

This procedure is rather arbitrary, but it does not have large impact on the results due to the small decorrelation time $T_L(\Delta_g/2)$. Besides, there are no physically grounded reasons for the justification of such interpolations in LES because the resolved velocity in the vicinity of surface is greatly corrupted by the approximation errors. Such procedures should be considered as an adjustments depending on the numerical scheme and on the subgrid closure.

Reviewer: All these settings are likely good (or reasonable) choices but should be substantiated. When serving as a reference for footprint calculations, the LES should be validated on a forward dispersion case from the literature.

Answer: Some examples of such validation were already included in the Supplements to this paper including the simulation results at very rough grids (see, the Supplement S1). It was commented in the Introduction. In this supplement Fig.S1.1(AR9) shows the results of the validation our LES model using [Willis and Deardorff, 1976] data. Figure S1.3(AR10) shows the simulated footprint function and the measured one in convective ABL (case (b) from [Leclerc et al., 1997]). To compare, one can find the results of resolution sensitivity tests with other LES model with embedded particles under the same conditions in ([Steinfeld et al., 2008], Fig.4). There are no available data on footprints in the stable boundary layer which is considered here.

Reviewer: The reasoning for using LES as a reference comes from requiring 'scale invariance', i.e. independence of the results from grid resolution (p. 3, l. 17 - and Figs. 3c, d). This, first of all, is a good criterion in the absence of any true reference - but

one would want to see to what degree the above choices influence this independence.

Answer: Although the authors consider the independence of the results from the grid steps to be the sufficient reason for the justification of the methods applied, nevertheless some imaginable chance exists, that all of these methods provide the 'scale invariance' but at the same time prevent the convergence to the true result. There is no possibility for the grounded rejection of this chance when the models are not free from the adjustable procedures. Subgrid LSM and LSM in the vicinity of the surface combined with our approach are not the exceptions.

Accordingly, we decided to investigate one more subgrid model (RDM), which is rigorously determined by the parameterisations which are already included into the Eulerian LES equations and do not contain any adjustable procedures or parameters. We obtained the results, which are in a close agreement with the results obtained before, except for some details inherent to RDM and known previously from the literature (see, Fig.AR7). Agreement of the different approaches (subgrid LSM, subgris RDM and the recovery of small-scale (sub-filter scale) turbulent motions) provides additional support for correctness of the results.

Corrections: New Section 4.2.4 'LES with subgrid RDM and the comparison of different approaches' (page 17, and the description of this model, page 11) was added to the paper. New Figure 7 (Fig.AR7) was included.

(2) Absorption condition:.

Reviewer: Please provide more information on the absorption height and its impact (p. 12, l. 20 ff). I.e., provide a graph or a reference and list the tests undertaken confirming that "...the upper boundary condition does not have a large impact on the results of calculations of footprints...".

Answer: The confirmation of this sentence was provided in the original version of the paper for the Lagrangian stochastic model (LSMT). See, orange curve in Fig. 11. Here, the absorption was applied above the boundary layer height (a very small portion of the particles can reach this height because there is no turbulent mixing above z =180 m).

Additional confirmation of the validity of our assumption can be done by analyzing the particles trajectories in LES.

In additional run we did not perform any removing of the particles during calculations. We evaluated separately the footprints from the particles trajectories that at least once reached the height z= 100 m. (see, Fig.AR8). As one can see, the footprint for $z_M = 10$ m is not influenced by the artificial boundary condition. The impact of the returned particles into footprint for $z_M = 30$ m is also very small. For the higher level ($z_M = 60$ m) the influence of the upper boundary condition is visible for the distances $x - x_M$ larger then 6 km. The positions and the values of the footprint peaks are not affected by the influence of the top boundary condition and are not directly connected to the value of the vertical turbulent flux at the appropriate levels. To confirm the last conclusion, we present a series of footprints computed with different intervals of averaging in time (see, Fig.AR8). Here, time (in seconds) from the beginning of the particles ejection is shown in the legend. The footprints are developed sequentially - the processes with the small time scales form the peaks first. The value of the vertical concentration flux normalized by its surface value is shown in brackets. One can see that while the total vertical flux grows approximately twice, the positions and the values of the peaks of the crosswind-integrated footprints remain unchanged.

Corrections: We added new Appendix A1 which contains the results of the test presented above.
To be more rigorous, the following sentence in the paper:
'It was verified previously that the upper boundary condition does not have a large impact on the results of calculations of footprints for the heights z_M up to 60 m'.
was replaced by the following one:
'It was verified previously that the upper boundary condition does not have a large impact on the results of calculations of footprints for the heights z_M up to 60 m and for the distances $x - x_M$, considered in this paper (see Appendix A1 and the test with LSM shown by the orange curves in Fig.13)'.

Reviewer: It seems that particles are absorbed at the absorption height and hence removed from the simulation domain.

Answer: Yes, it is really so.

Reviewer: Figure 2 suggests that there is no vertical flux above the absorption height. However, turbulent fluxes should decline almost linearly from their surface value upwards to approach zero at the boundary layer height (i.e. in this case at z = 180 m and not at z = 100 m, cf. Stull, 1988 or Beare et al., 2006).

Answer: The suggestion that the concentration flux declines linearly from their surface value upwards to approach zero at z = 100 m is nonrealistic under the conditions considered here because in this case all the particles will retained in the simulation domain in spite of the absorption. At large simulation times, more realistic final state will be the constant concentration flux from $z = z_0$ up to $z = 100$ m and zero flux if $z < z_0$. We say 'more realistic' because this assumption is based on another assumption that the concentration will reach some limit inside the layer 0–100 m. We did not obtain this state in the presented calculations (the particles simulation time 2 h is not long enough) . The expected flux profile and the concentration profile in the considered case are beyond the scope of this paper, although it is a very interesting task which could be considered in the scope of similarity theory. Taking into account the local nature of the stably stratified turbulence, the authors do not exclude the possibility of nearly the linear profiles of the fluxes, as it is shown in modified Fig.3 (AR11). One can see, what the values of the flux in our simulation are very close to those predicted by Stull, 1988 or Beare et al. 2006 up to the heights $z \approx 60$ m.

In any case, significant differences between the "true" and the modelled footprints will be expected at very large distances from the measurements location, and the flux profile does not affect footprint close to the measurement point position (see, new Appendix A1 and Fig.AR8d).

Reviewer: If the particles cannot reach the boundary layer height, they cannot be reflected at this height and cannot return to the surface. The consequence is that footprints consist of upwards flowing particles only.

Answer: The footprints consist of the upward and the downward flowing particles except those, which already reached the specified level z=100 m. Due to the local nature of the stably-stratified turbulence, and due to the large vertical velocity gradient, the particles, which reach the level z=100 m will return back after a rather big time interval and in a very outlying position (see, new Appendix A1).

Reviewer: If so, this would result in an unrealistic increase in extent of flux footprints as downward flowing particles would weigh out upward flowing particles (when evaluating the vertical flux), with increasing tendency to do so with increasing distance from the measurement location.

Answer: Yes it is indeed so, but for the levels and for the distances which are not considered here. (see, new Appendix A1 and Fig.AR8a,b,c).

Reviewer: Please clarify how this is handled regarding the footprints from the LES.

Answer: See the clarification above. We clearly understand and share all the concerns of the Reviewer. The disadvantages of the proposed setup of the numerical experiment were known for the authors at the beginning of this study. The clear and justified method for the footprint determination in LES up to a limited distance $x - x_M$ will be the appropriate restriction of the particle flight. Nevertheless, we choose this setup deliberately as a way for the direct comparison of statistics obtained by Eulerian and Lagrangian methods. For example, this way permits to compare Schmidt numbers, variances, vertical turbulent fluxes (the resolved and the parameterized separately). All of this give additional possibilities for the LES model validation and development of the optimized procedures for the particles transport in LES.

(3) Normalisation of footprints:

Reviewer: On p. 13, l. 14, it is shown that the integral over the footprint function is normalised to one.

Answer: The normalization of footprints was made only for the Fig.3 (AR3) and Fig.5 (AR5), when the different approaches for the subgrid modeling of particles motions were studied. As all curves in these Figures were normalized identically, the comparison is objective. Besides, while the horizontal particle flight was not restricted, the footprint functions, defined by the Eq. (1) and Eq. (2) and the normalized footprints shown in these figures differ by the multiplier $a = F_s(0)/F_s(z_M)$ (here, F_s is the vertical concentration flux of the particles). The total vertical concentration fluxes are nearly independent from the model, so the only impact of normalization is the scaling of the axis y in Fig. 3 (AR3) and Fig. 5 (AR5) (Fig. 4 (AR4) and Fig. 6 (AR6) in revised paper). This does not influence both the results and the conclusions.

Nevertheless, it was mistake by the authors to include the figures with the different normalization into one paper (figures with the different normalization in one paper but not the curves with different normalization in one figure, as it could have been misunderstood due to the unclear presentation in the former version of the paper).

Corrections: We recalculated all the curves, shown in Fig.3 and Fig.5 and removed the sentence concerning normalization from the text. All the conclusions and the descriptions of the results remain unchanged, as well as other footprints functions shown in the paper (e.g., Fig. 13 (AR2) in the new version coincides with Fig.11 from the original version of the paper).

Reviewer: Does this include negative footprint values, too? Or are these treated separately as mentioned on p. 15?

Answer: Yes, negative values were also included.

Reviewer: Please clarify. The absolute values of the footprint function and hence the cumulated footprint will depend on how negative values are treated. Observed differences in the absolute footprint function values for different footprint approaches (cf. Fig. 11) may be partly due to differences in normalisation procedures.

Answer: Figure 11 was shown without normalization and remains unchanged. The differences are essential.

Reviewer: Also, is there a threshold value for the distance from the measurement up to where footprint values are considered? The 'flat' trend of the cumulative footprint values suggests that the footprint function would only completely diminish at very large distances from the measurement location. If a threshold value is set, again the selected value will have an impact on the normalisation and the absolute value of the footprint function. Please provide more information on the applied procedure.

Answer: See the previous answer. The threshold value for the collection of footprints was selected large enough to include all the particles (see description of the footprint function grid in the answer to Reviewer: #1).

(4) Kolmogorov's constant for the structure function in the Inertial Subrange [C0]:

Reviewer: First of all, this constant is referred to as 'Kolmogorov constant', a name

that is usually associated with that in the energy spectra in the Inertial Subrange (and has a value of approximately 1.5).

Answer: This constant, as well as the formula $E(k) = C_K \epsilon^{2/3} k^{-5/3}$ appeared for the first time in the paper by Obukhov, 1941 ([2], in Russian) which was published a little bit later than the famous paper by Kolmogorov, 1941 ([1], in Russian), where the equivalent form of this law for the velocity structure function $\langle v^2(r)\rangle \sim \epsilon^{2/3} r^{2/3}$ was discovered. In turn, the Lagrangian velocity structure function $\langle (v(t+\tau) - v(t))^2 \rangle = C_0 \epsilon \tau$ was introduced in Landau and Lifshitz, 1944 ([3], first edition, in Russian) and later independently in [Obukhov A. M., 1959].

From this historical point of view both of these constants C_K and C_0 have the equal right to be called the "The Kolmogorov constant" - both of them were introduced first in the papers or the books of other authors and both of them were related to Kolmogorov's (1941) theory.

Although C_0 for LSMs is very often referred as the 'Kolmogorov constant' and the dissipation rate ϵ stands as the single determining parameter for the generative terms in LSMs, we agree with this comment. In practice, the constant C_0 in LSMs of ABL is not connected directly with the motions in the inertial subrange and is responsible for the scales outside the range of isotropy.

Corrections: Accordingly, we replaced naming 'Kolmogorov constant C_0' by the 'parameter C_0' or 'value of C_0' everywhere except page 7, line 4, where this constant is related to the Lagrangian velocity structure function in the inertial subrange.
In the Conclusions the sentence concerning the constant C_0 was extended as follows:

The optimal value for the parameter C_0 for LSMs is found to be close to 6 under the conditions considered here. This value coincides with the estimation of Kolmogorov Lagrangian constant in isotropic homogeneous turbulence. It provides additional justification for use of LSMs in stable ABL, due extending their of its applicability over a wider range of scales including the inertial subrange. Stochastic models that use smaller values $C_0 \approx 3-4$ (this choice is widespread now) may produce extra mixing and the shorter footprints, respectively. Note that the estimation $C_0 = 6$ is based on the LES results combined with the SHEBA data [Grachev et al., 2013], where the nondimensional vertical velocity RMS was evaluated as $\tilde{\sigma}_w \approx 1.33$ (the exact estimation of this value in LES is restricted by the resolution requirements). In the cases when LSMs utilize smaller values of $\tilde{\sigma}_w$ the parameter C_0 should be reduced accordingly (for example, $C_0 \approx 4.7$ will be the best suited parameter for LSMs with the widely used value $\tilde{\sigma}_w \approx 1.25$ prescribed).

Reviewer: The authors discuss the range of proposed values in the literature, and it is felt that i) the paper by Rizza et al. (2010) might be a valuable addition to the discussion of possible values in the PBL

Answer: We agree. This reference was added with the appropriate commenting (see next answer).

Reviewer: ii) the employed value in the LES subfilter correction (Eqs. 28 ff) should be provided.

Corrections: We provide the value $C_0 = 6$ in the revised paper, see page 11, line 10.
Besides, the constant C_K was also not specified in the paper. We clarified the procedure of the evaluation of subgrid energy by its extension on non-equidistant grids in accordance with the formulas employed in LES code (p. 11 l. 21-26).

Reviewer: However, in the present paper it is demonstrated that the results of the LSMs (and in particular LSMT) are sensitive to the choice for C_0 – which is per se not particularly new (see, e.g., Rotach et al. (1996) who have sought the 'optimal' value based on comparison to water tank (dispersion) measurements of Willis and Deardorff – and many others, such as Du et al. (1995), Reynolds (1998), as cited in Rizza et al).

Answer: We completely agree with the Reviewer.

Corrections:

1) The text beginning from line 13 p, 7 in original version was rewritten as follows (p.7 l.23 - p.8 l. 8):

There is no consensus on the value of C_0 as well. Formally, C_0 has the meaning of a universal Kolmogorov constant in Eq. (11). The estimation of this constant for an isotropic turbulence using the data of laboratory measurements and DNS provides an interval $C_0 = 6. \pm 0.5$ (see, [Lien and D'Asaro, 2002]). However, the values $C_0 \sim 3 - 4$ are often used for LSM of particle transport in ABL independently from the type of the stratification. These values have been obtained by the different methods. For instance, the value $C_0 = 3.1$ for a one-dimensional LSM corresponds to a calibration performed in [Wilson et al., 1981] according to observation data [Barad, 1958, Haugen, 1959]. This calibration (see, [Wilson, 2015]) assumes that the turbulent

Schmidt number $Sc = K_m/K_s = 0.64$ near the surface (here K_m is the eddy viscosity). It is known that determination of the turbulent Prandtl number $Pr = K_m/K_h$ (K_h - heat transfer eddy diffusivity) and Schmidt number based on observation data is complicated by large statistical errors associated with the problem of self-correlation [Anderson, 2009, Grachev et al., 2007]. Therefore, this method of estimation of C_0 cannot be considered as final and should be confirmed by future studies. In [Rizza et al., 2010] the values of C_0 were determined using the LES-based evaluations of the velocity structure functions and the Lagrangian spectra in convective and neutrally-stratified ABLs. In this study the LES model had relatively low resolution, which can be insufficient for accurate determination of this constant in the inertial subrange (see discussion on the resolution requirements in [Lien and D'Asaro, 2002]). Nevertheless, the value $C_0 \sim 3$, in the paper by [Rizza et al., 2010] is relevant for LSMs applied to the convective ABL, in that case the constant is also responsible for the energy containing time scales which are well resolved in LES. The detailed overview of the methods of determination of the constant C_0 can be found in [Poggi et al., 2008], where the discussion on the disagreements of the different approaches is also included. The results of the LSMs are very sensitive to the choice for C_0 as it was shown earlier by [Du et al., 1995, Rotach et al., 1996, Wilson, 2015] and many others. Below we show that the commonly used value of $C_0 \sim 3 - 4$ can be greatly underestimated for LSMs applied to the stably stratified ABL.

2) We excluded the sentence concerning the value of C_0 in the Abstract.

Reviewer: If indeed the LES were fully validated and all the choices substantiated (see major comment 1), the present simulations would correspond to 'one more tessera' in the picture of a possible nonuniversality of C0, be it due to stability dependence or employed time scales (outside those corresponding to the Inertial Subrange). It is felt that the conclusions drawn in the present paper (one 'case' – even with three heights) do not warrant the quite general conclusions drawn (p. 21, l. 18), i.e. 'the optimal value is found to be close to 6'

Answer: We agree with the Reviewer.

Corrections: *We add next clarification:*

The optimal value for the parameter C_0 for LSMs is found to be close to 6 under the conditions considered here.

(5) Footprints plotted in Fig. 11:

Reviewer: The footprints plotted in Fig. 11 of the manuscript and listed as Kljun et al. (2015) do not coincide with FFP model results. Plotted below are footprints derived from FFP for the input values mentioned in the manuscript, and optimised parameters for neutral and stable conditions as listed in Kljun et al. (2015). (Note: using the universal FFP parameters, e.g. from the online footprint tool still results in different footprints than those plotted in Fig. 11). It can be seen in Fig. R1 that the peak location of FFP fits very well the peak of LSMT with C0=3 in Fig. 11. Footprint peak values, however, do differ, especially for larger measurement heights. Regarding the absolute values of these peak values please see major concerns (2 and 3) above.

Answer: See answer to this comment above.

Reviewer: Also, the model of Kljun et al. (2004) is outdated; issues in stable conditions were known and were one of the reasons for the update to the model of Kljun et al. (2015).

Answer: We leave the decision concerning the model of Kljun et al. (2004) up to Reviewer and Editor. This model is available online http://footprint.kljun.net/m2004/varinput.php without notice for caution, so we have used this tool.

Reviewer: As FFP compares well with the Lagrangian footprint model it is based on (see Fig. R2), and as different settings of C_0 produce similar shifts in footprints in LPDM-B (Kljun et al. 2002) and the LPDM used in this study (Fig. R2) - the main question boils down to: what is the 'ultimate truth' and what should a footprint parameterisation be based upon? (See comments above.) This is a very important question and I suggest that the authors highlight this fact even more in their manuscript.

Answer: We are confident that the results presented in this paper are accurate for the purpose of footprint evaluation (see answers to comments above) and will not change substantially if any other LES model with sufficiently good resolution will be used.

The questions remain:

Are the conditions of the numerical setup of the experiment GABLS-1 characteristic for the stable ABL in nature and is this case appropriate for making general conclusions?
We believe that it is true because:

i. This setup is based on the observation data [Kosoviĉ and Curry, 2000] and LES reproduces this case quite well.

ii. Usual nondimensional functions of the similarity theory are well satisfied in this case (see e.g. [Basu and Porté-Agel, 2006, Beare et al., 2006, Glazunov, 2014, Zhou and Chow, 2011]).

iii. A lot of single column models were tested in similar conditions [Cuxart et al., 2006] and the results of their comparison with the LES were treated as the indicator of models performance under stable stratification.

iiii. Similarity of the turbulent stable ABLs permits to conclude that the results obtained in one case can be generalized for many others.

The fact that FPP predicts footprints based on LPDM-B indicates that it is able to reproduce the correct form of footprint function, that the scaling approach proposed by [Kljun et al., 2015] is well justified and that FPP is able to be calibrated with respect to this stochastic model and with respect to the postulated nondimensional functions. Most probably, FPP, can be rescaled using the other parameters for LPDM-B or any other data set, including the LES results.

We believe, this paper provides sufficient amount of information, concerning model development techniques and the models evaluation. The investigation of other cases will require development of additional scenarios which should be considered as a separate problem.

The authors would be pleased to work in cooperation with the author of the review if he/she is interested in collaboration. In this case, please contact us directly.

Minor Comments

Reviewer: (a) The term "Analytical footprint model" is commonly used for footprint models based on analytical solutions of the diffusion equation by applying a K-theory approach. This is a distinctly different approach than used in the models of Kljun et al. (2004, 2015). The latter models are footprint parameterisations. Please correct throughout the manuscript.

Corrections: The term "Analytical footprint model" was substituted by "footprint parameterisations"

Reviewer: (b) p. 2, l. 5: '...commonly, the application of these models is limited by the constant flux approximation': this is not true at least for the Kljun et al. papers cited above.

Corrections: This sentence was modified as follows:

Commonly, the applicability of the analytical models is limited by a "constant flux layer" simplification, assuming that the measurement height z_M is much less than the thickness of the ABL z_i.

FPP is referred everywhere in the revised paper as the 'footprint parametirization'.

Reviewer: (c) p. 5, l. 26: If reference is made to 'the lake', this lake must be introduced beforehand. It is not appropriate to explain in brackets that the author apparently works on a 'lake problem'.

Corrections: The term ' lake' is substituted for more neutral 'inhomogeneous surface' which has no direct association with another topic in which authors are involved.

Reviewer: (d) p. 8, l. 15: Euclidean: spelling?

Answer: It is not the spelling, it is a mistake. The continuous space is considered at this stage of description, so it will be better to write:

... reduces to minimization of the functional $\Psi(X) = \int_\Omega \varepsilon_{ij}(\vec{x})\ \varepsilon_{ij}(\vec{x})d\vec{x}$ where Ω is the model domain and $\varepsilon_{ij}(\vec{x})$ is the the residual of the overdefined system of equations ...

It was corrected.

Reviewer: (e) According to Eq. 2, fys corresponds to the crosswind-integrated footprint. Please use this well established term rather than 'crosswind averaged footprint' (e.g. p. 14, l. 3 or p. 20, l. 18). Further, in the captions of Figs. 9 and 11, the graphs are referred to as "One-dimensional footprints fys". This would suggest that the footprint at y=0 is plotted. Please clarify.

Corrections: It was corrected.

Reviewer: (f) Wind profile: from Figure 1, it seems that simulated wind speeds in the surface layer part of the domain are smaller than the 'standard' wind profile for stable conditions (e.g., Stull, 1988; Högström, 1996). Please add a couple of sentences to explain why.

Answer: See the first answer.

Summary

In this table we summarise shortly all the comments which were accepted with the following revision of the paper or rejected with the following minor corrections and the justification if it is needed.

#	Comment	Answer and corrections
Major comments		
(1)	Model validation and argumentation of approaches	Accepted partially. Confirmed by the adding of new results. Some clarifications were included.
(2)	Absorption condition	Rejected. New confirmations were added.
(3)	Normalisation of footprints	Accepted partially. Corrected with the minor revision. Main results remain to be unchanged.
(4)	Kolmogorov's constant for the structure function in the Inertial Subrange [C0]	Accepted. Corrected using the exclusion of too general conclusions and with the correction of the terminology.
(5)	Footprints plotted in Fig. 11	Rejected. Minor clarification was inserted.
Minor comments		
(a)	The terminology	Accepted. The appropriate corrections were included.
(b)	Mistake then citing	Accepted and corrected.
(c)	Embedded advertising (the use of the word 'lake')	Accepted and excluded.
(d)	Spelling?	Accepted by the other reason than spelling. Improved.
(e)	The terminology	Accepted. Appropriate corrections were included.
(f)	Correctness of the LES results (wind profile)	Rejected. The confirmation was included.

References

[1] Колмогоров А. Н. Локальная структура турбулентности в несжимаемой жидкости при очень больших числах Рейнольдса. // Докл. АН СССР.Т. 30, No 4. С. 299–303. 1941.
Kolmogorov A.N.: The Local Structure of Turbulence in Incompressible Viscous Fluid for Very Large Reynolds Numbers. Dokl. Acad. Nauk SSSR, v. 30 No. 4, 299–303. 1941 (in Russian)

[2] Обухов А. М. О распределении энергии в спектре турбулентного потока. // Изв. АН СССР. Сер. геогр. и геофиз. Т. 32, No 1. С. 22–24. 1941.
Obukhov, A.M.: On the distribution of energy in the spectrum of turbulent flow, Izvestiya AN SSSR, Ser. Geogr. i Geofiz., V. 32., No. 1, 22–24, 1941. (in Russian)

[3] Ландау Л.Д., Лифшиц Е.М. Механика сплошных сред.// ОГИЗ Гостехиздат. 1944.
Landau L.D., Lifshitz E.M.: Mechanics of Continua. OGIZ Gostehizdat, 1944. (in Russian)

[Anderson, 2009] Anderson, P. S.: Measurement of Prandtl number as a function of Richardson number avoiding self-correlation. Boundary-Layer Meteorol., 131, 3, 345–362, 2009

[Barad, 1958] Barad M.: Project Prairie Grass, a field program in diffusion, vol 2. Technical Report Geophysical Research Papers No. 59, TR-58-235(II). Air Force Cambridge Research Center, Bedford, 1958. 209 pp

[Basu and Porté-Agel, 2006] Basu S. and Porté-Agel F.: Large-Eddy Simulation of Stably Stratified Atmospheric Boundary Layer Turbulence: A Scale-Dependent Dynamic Modeling Approach. J. Atmos. Sci. 2006, 63, 1, P. 2074–2091.

[Beare et al., 2006] Beare, R.J., MacVean, M.K., Holtslag, A.A.M., Cuxart, J., Esau, I., Golaz, J.C., Jimenez, M.A., Khairoutdinov, M., Kosovic, B., Lewellen, D., Lund, T.S., Lundquist, J.K., McCabe, A., Moene, A.F., Noh, Y., Raasch, S., Sullivan, P. : An Intercomparison of Large-Eddy Simulations of the Stable Boundary Layer. Boundary-Layer Meteorol., 118, 2, 247–272, 2006.

[Bhaganagar and Debnath, 2015] Bhaganagar K. and Debnath M.: The effects of mean atmospheric forcings of the stable atmospheric boundary layer on wind turbine wake., J. Renewable Sustainable Energy 7, 013124, 2015

[Cuxart et al., 2006] Cuxart J., Holtslag A. A. M., Beare R. J., Bazile E., Beljaars A., Cheng A., Conangla L., Ek M., Freedman F. et al.: Single-Column Model Intercomparison for a Stably Stratified Atmospheric Boundary Layer. Boundary-Layer Meteorol., 118, 2, 273–303, 2006.

[Du et al., 1995] Du S., Sawford B. L., Wilson J. D., and Wilson D. J.: A Determination of the Kolmogorov Constant (CO) for the Lagrangian Velocity Structure Function, Using a Second-Order Lagrangian Stochastic Model for Decaying Homogeneous Isotropic Turbulence, Phys. Fluids., 1, 3083–3090, 1995.

[Glazunov, 2014] Glazunov A.V.: Numerical simulation of stably stratified turbulent flows over flat and urban surfaces Isv. Atm. and Ocean. Phys. 50, 3, 236–245.

[Grachev et al., 2007] Grachev A.A., Andreas E.L, Fairall C.W., Guest P.S., Persson P.O.G.: On the turbulent Prandtl number in the stable atmospheric boundary layer. Boundary-Layer Meteorol. 125, 2, 329–341, 2007

[Grachev et al., 2013] Grachev A.A., Andreas E.L, Fairall C.W., Guest P.S., Persson P.O.G.: The Critical Richardson Number and Limits of Applicability of Local Similarity Theory in the Stable Boundary Layer. Boundary-Layer Meteorol., 147, 1, 51–82, 2013.

[Haugen, 1959] Haugen D.: Project Prairie Grass, a field program in diffusion, vol 3. Technical Report Geophysical Research Papers No. 59, TR-58-235(III). Air Force Cambridge Research Center, Bedford, 1959.

[Högström, 1996] Högström, U.: Review of Some Basic Characteristics of the Atmospheric Surface Layer, Bound.–Lay. Meteorol., 78, 215–246, 1996

[Kitamura, 2010] Kitamura Y.: Self–Consistency Validation of Subgrid Scale Parameterization Schemes in a Large–Eddy Simulation. J. of the Met. Society of Japan, 88, 5, 813–825, 2010

[Kljun et al., 2004] Kljun, N., Rotach, M. W., and Calanca, P.: A Simple Parameterisation for Flux Footprint Predictions, Bound.-Lay. Meteorol., 112, 3, 503–523, 2004.

[Kljun et al., 2015] Kljun, N., Calanca, P., Rotach, M. W. and Schmid H. P.: A simple two-dimensional parameterisation for Flux Footprint Prediction (FFP), Geosci. Model Dev., 8, 3695-3713, 2015.

[Kosoviĉ and Curry, 2000] Kosoviĉ B. and Curry J. A. A Large Eddy Simulation Study of a Quasi-Steady, Stably Stratified Atmospheric Boundary Layer. J. Atmos. Sci., 57., 8., 1052–1068, 2000.

[Leclerc et al., 1997] Leclerc, M. Y., Shen, S., Lamb, B.: Observations and large-eddy simulation modeling of footprints in the lower convective boundary layer. J. Geophys. Res. 102, 9323–9334, 1997.

[Lien and D'Asaro, 2002] Lien Ren-Chieh, D'Asaro Eric A.: The Kolmogorov constant for the Lagrangian velocity spectrum and structure function. Physics of Fluids., 14, 12, 4456–4459, 2002.

[Maronga et al., 2015] Maronga, B., Gryschka, M., Heinze, R., Hoffmann, F., Kanani-Suhring, F., Keck, M., Ketelsen, K., Letzel, M. O., Suhring, M., and Raasch, S.: The Parallelized Large-Eddy Simulation Model (PALM) version 4.0 for atmospheric and oceanic flows: model formulation, recent developments, and future perspectives, Geosci. Model Dev., 8, 2515-2551, 2015.

[Obukhov A. M., 1959] Obukhov A. M. Description of turbulence in terms of Lagrangean variables. Adv. in Geophys., 6., 113–115, 1959.

[Poggi et al., 2008] Poggi D., Katul G. G. and Cassiani M. On the anomalous behavior of the Lagrangian structure function similarity constant inside dense canopies. Atmospheric Environment, 42, 4212–4231.

[Rizza et al., 2010] Rizza U., Degrazia G. A., Mangia C., Pereira E. and Filho E. Estimation of the Kolmogorov constant for the Lagrangian velocity spectrum and structure function

[Rotach et al., 1996] Rotach M.W., Gryning S.E. and Tassone C.: A two-dimensional Lagrangian stochastic dispersion model for daytime conditions. Q. J. R. Meteorol. Soc., 122, 367–389, 1996.

[Steinfeld et al., 2008] Steinfeld G., Raasch S. and Markkanen T.: Footprints in Homogeneously and Heterogeneously Driven Boundary Layers Derived from a Lagrangian Stochastic Particle Model Embedded into Large-Eddy Simulation. Boundary-Layer Meteorol., 114, 3, 503–523, 2008.

[Thomson, 1987] Thomson D.: Criteria for the selection of stochastic models of particle trajectories in turbulent flows. J

Fluid Mech., 180, 529–556, 1987.

[Willis and Deardorff, 1976] Willis, G. E., and J. W. Deardorff: A laboratory model of diffusion into the convective planetary boundary layer. Quart. J. Roy. Meteor. Soc., 102, 427–445, 1976.

[Wilson et al., 1981] Wilson J., Thurtell G, Kidd G. Numerical simulation of particle trajectories in inhomogeneous turbulence. III. Comparison of predictions with experimental data for the atmospheric surface layer. Boundary-Layer Meteorol., 21, 4, 443–463, 1981.

[Wilson, 2015] Wilson J. D.: Computing the Flux Footprint. Boundary-Layer Meteorol., 156, 1, 1-14, 2015.

[Zhou and Chow, 2011] Zhou, B. and Chow. F.K.: Large-eddy simulation of the stable boundary layer with explicit filtering and reconstruction turbulence modeling. Journal of the Atmospheric Sciences 68, 9, 2142–2155, 2011.

[Zhou and Chow, 2012] Zhou, B. and Chow. F.K.: Turbulence Modeling for the Stable Atmospheric Boundary Layer and Implications for Wind Energy. Flow Turbulence Combust 88, 255–277, 2012

[Zilitinkevich et al., 2013] Zilitinkevich S. S., Elperin T., Kleeorin N., Rogachevskii I., Esau I.: A Hierarchy of Energy- and Flux-Budget (EFB) Turbulence Closure Models for Stably-Stratified Geophysical Flows., 146, 3, 341–373, 2013.

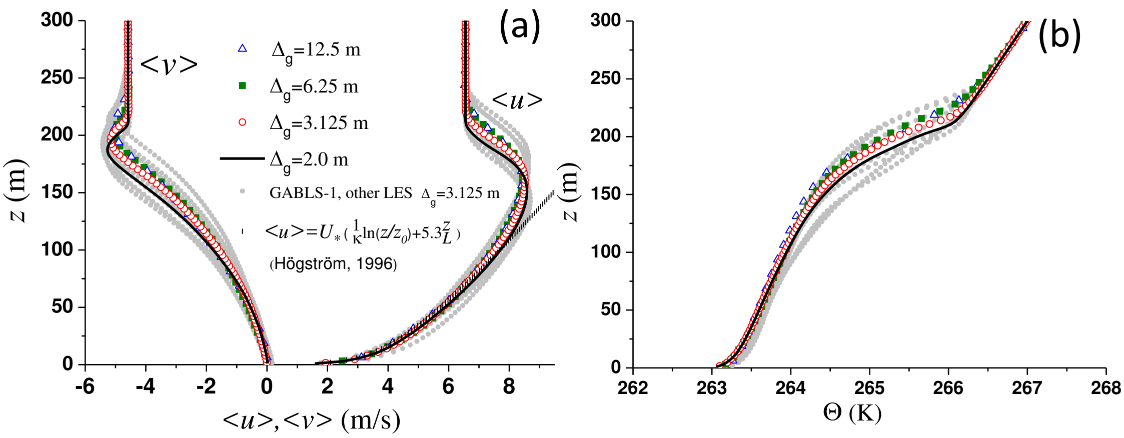

Figure AR1: **(Fig.1 from the original version and Fig.2 from the revised paper)** Mean wind velocity $\langle \vec{u} \rangle$ (a) and temperature $\langle \Theta \rangle$ (b) in runs with different grid steps (spatial step is pointed in legend). Gray dots are the data from other LES models obtained in [Beare et al., 2006] (wind velocity is rotated 35^o clockwise). 'Standard' wind profile for stable conditions in accordance with [Högström, 1996] is shown by the vertical dashes.

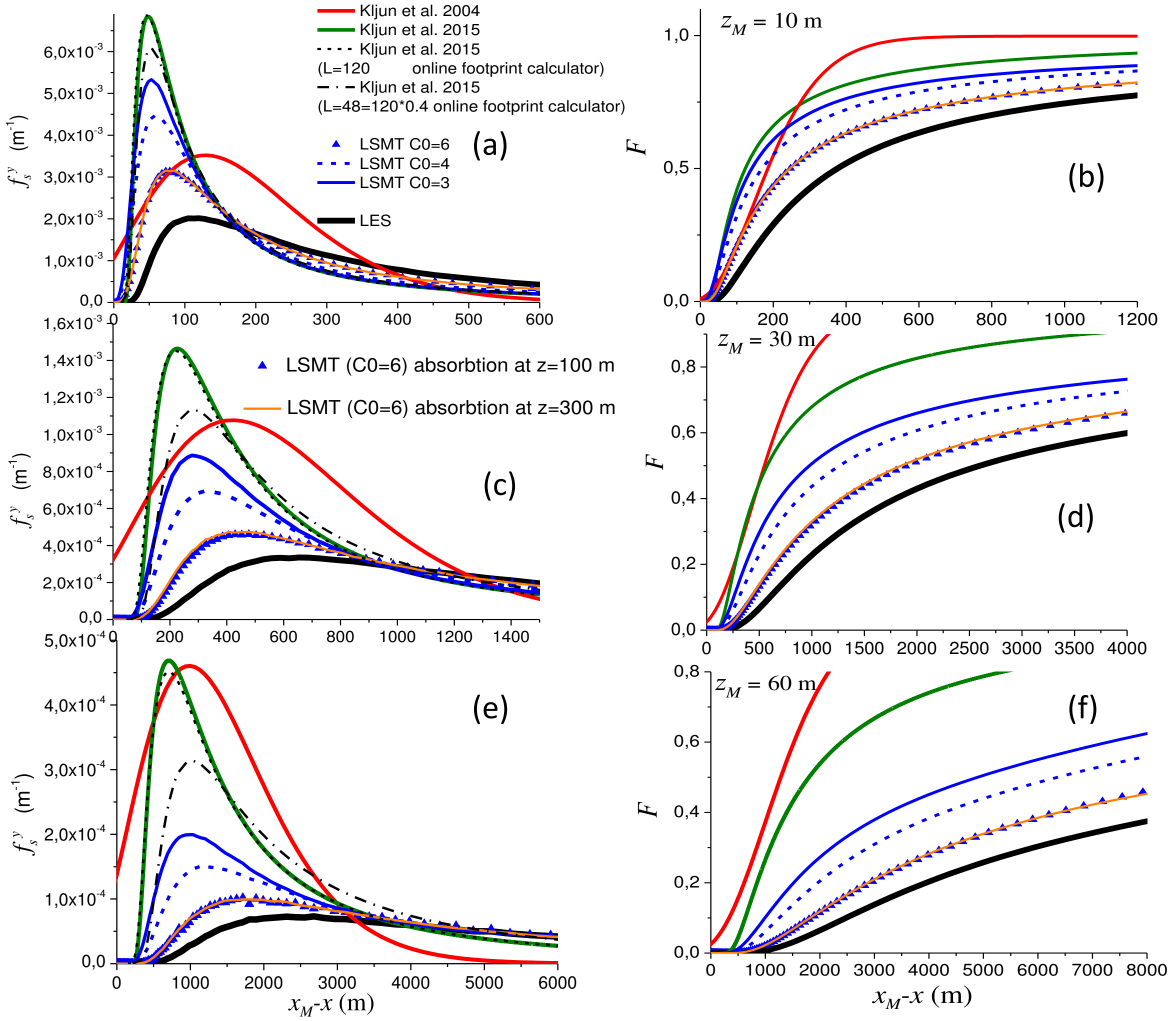

Figure AR2: **(Fig.11 from the original version and Fig.13 from the revised paper)** Crosswind-integrated footprints f_s^y (a,c,e) and cumulative footprints F (b,d,f) for sensor height $z_M = 10$ m (a,b), $z_M = 30$ m (c,d) and $z_M = 60$ m (e,f). Solid lines - LES with grid steps Δ_g=2.0 m. Triangles - LSMT ([Thomson, 1987] model), $C_0 = 6$, absorbtion at z=100 m. Orange curves LSMT, $C_0 = 6$, absorbtion at z=300 m. Dashed blue lines - LSMT, $C_0 = 4$. Solid blue lines - LSMT, $C_0 = 3$. Red lines - parameterisation [Kljun et al., 2004]. Green lines - parameterisation [Kljun et al., 2015]. Dashed lines online FPP calculator with L=120. Dash-dot lines FPP calculator with L=48.

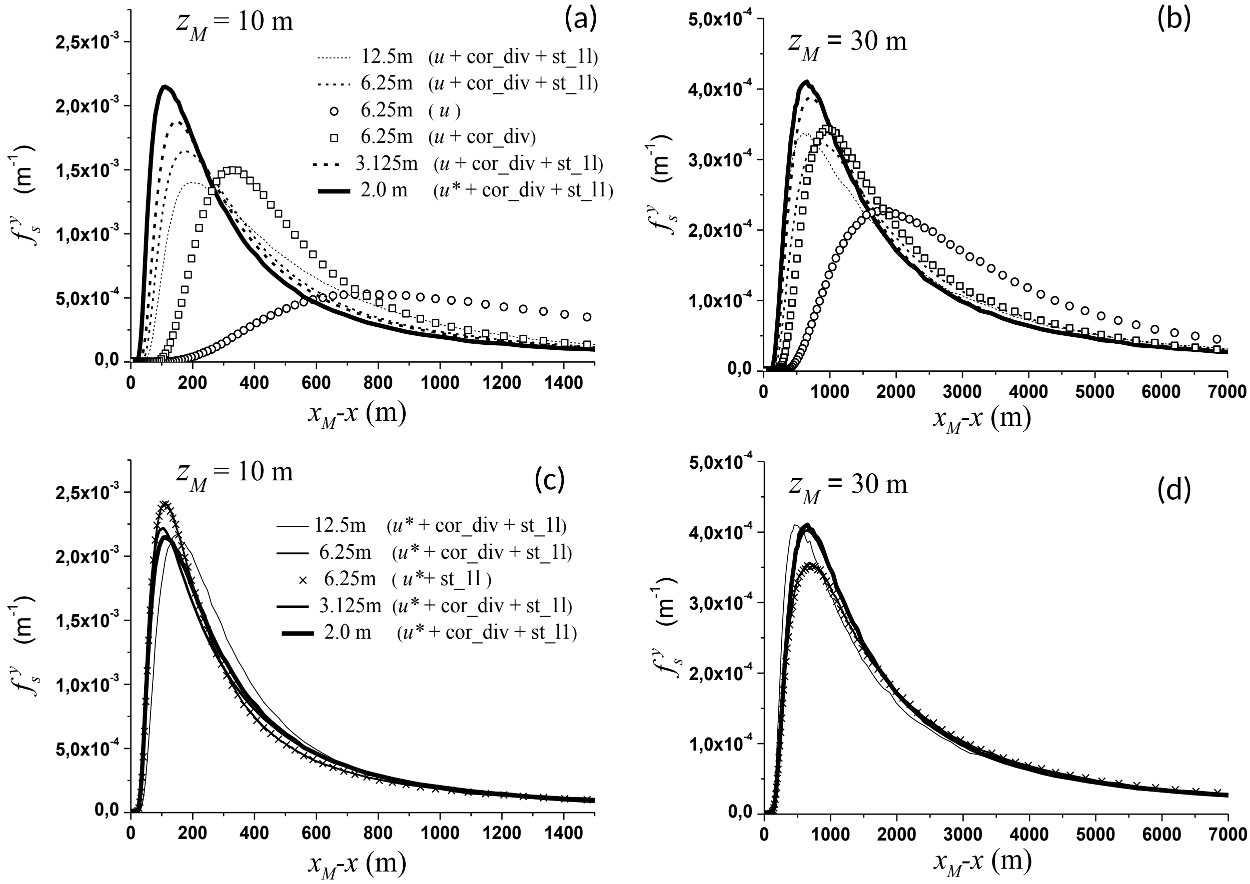

Figure AR3: (Fig.3 from the original paper,**with normalization**) Crosswind-integrated scalar flux footprints f_s^y in stable ABL, computed by the different methods and with different grid steps; (a,c) sensor height z_M=10 m, (b,d) z_M=30 m. Grid steps and methods are indicated in the legend: u - particles are transported by a filtered LES velocity $\overline{\overline{u}}$; u^* - particles are transported by recovered velocity $\vec{u}^* = F^{-1}\overline{\overline{u}}$; cor_div - the additional correction of velocity (Eqs. 33, 34); st_1l - stochastic subgrid model (Eq. 28) is applied for the particles within the first computational grid layer.

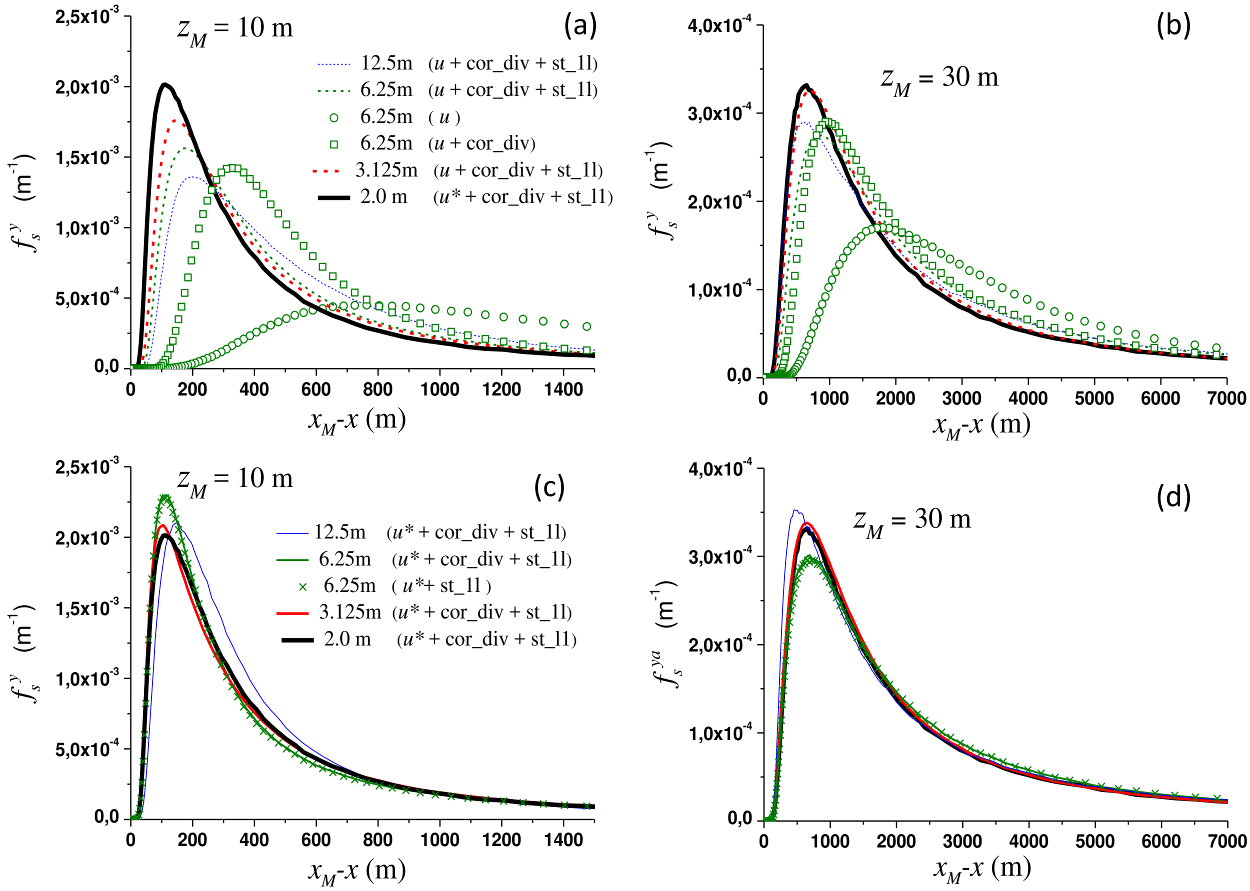

Figure AR4: (Fig.4 from the revised paper,**without normalization**) Crosswind-integrated scalar flux footprints f_s^y in stable ABL, computed by the different methods and with different grid steps; (a,c) sensor height z_M=10 m, (b,d) z_M=30 m. Grid steps and methods are indicated in the legend: u - particles are transported by a filtered LES velocity $\overline{\vec{u}}$; u^* - particles are transported by recovered velocity $\vec{u}^* = F^{-1}\overline{\vec{u}}$; cor_div - the additional correction of velocity (Eqs. 34, 35); st_1l - stochastic subgrid model (Eq. 28) is applied for the particles within the first computational grid layer.

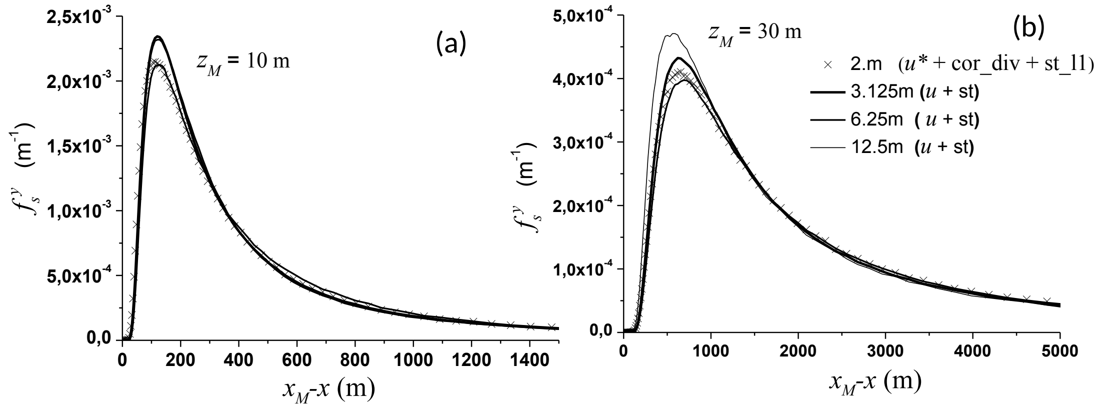

Figure AR5: (Fig.5 from the original paper,**with normalization**) Crosswind-integrated scalar flux footprints f_s^y, computed using stochastic subgrid model (Eq. 28-32); (a) sensor height z_M=10 m, (b) z_M=30 m. Grid steps are given in the legend. Crosses denote footprints computed with subgrid LSM applied for the particles within the first grid layer only.

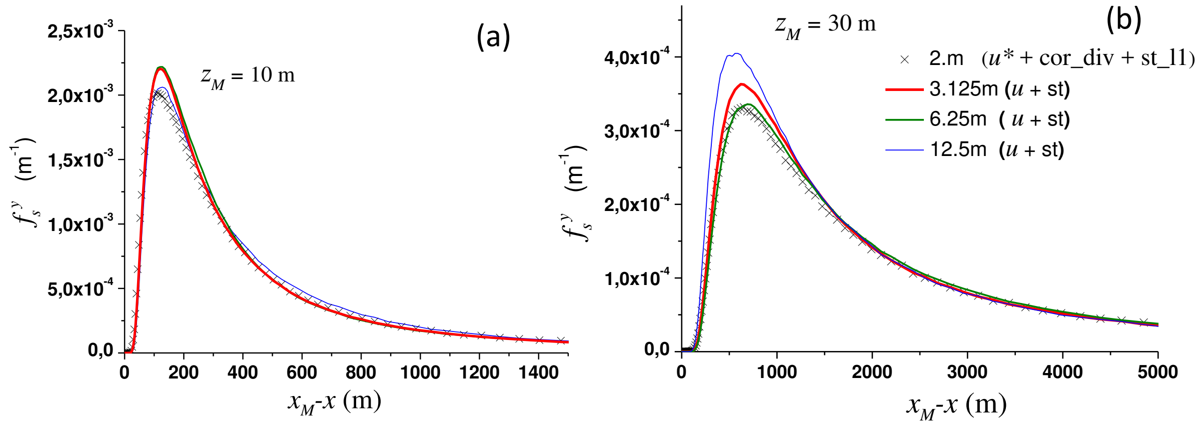

Figure AR6: (Fig.6 from the revised paper,**without normalization**) Crosswind-integrated scalar flux footprints f_s^y, computed using stochastic subgrid model (Eq. 28-32); (a) sensor height z_M=10 m, (b) z_M=30 m. Grid steps are given in the legend. Crosses denote footprints computed with subgrid LSM applied for the particles within the first grid layer only.

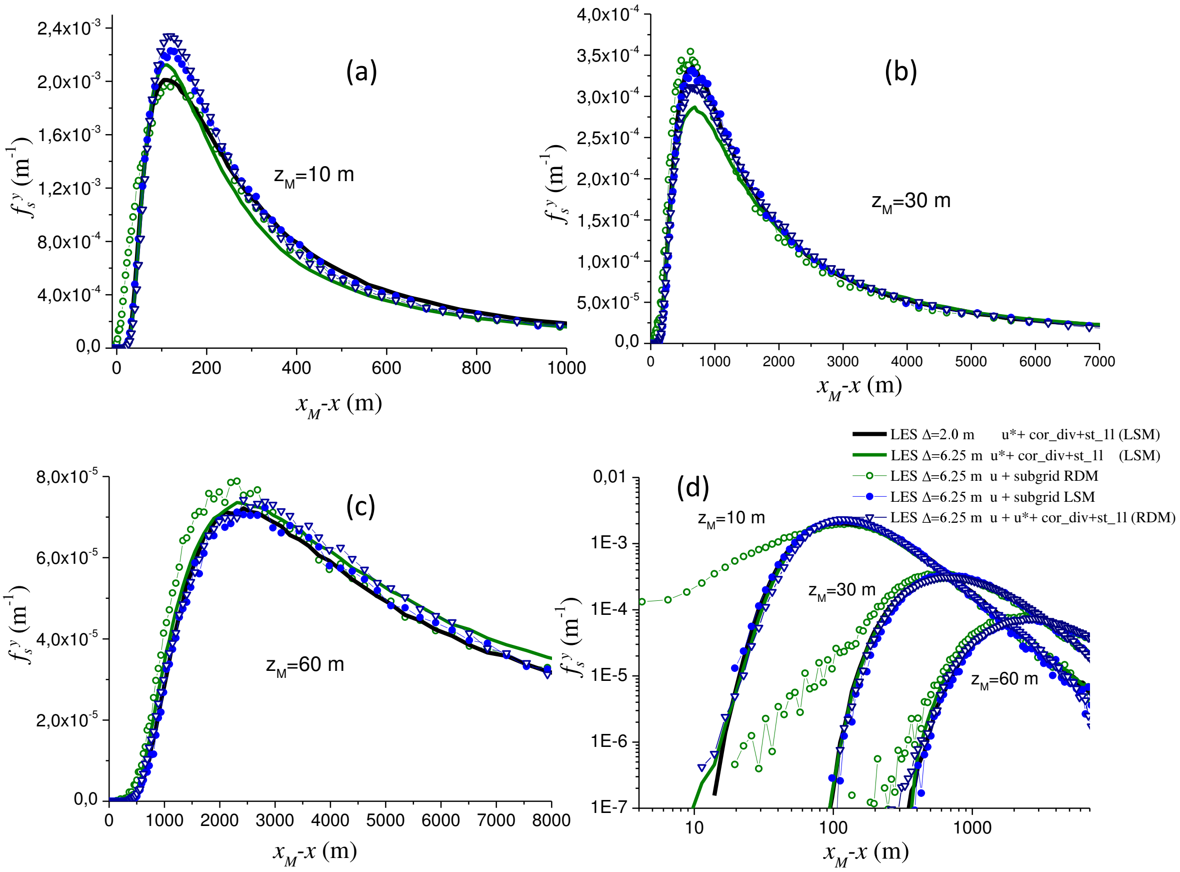

Figure AR7: **(Fig.7 from the revised paper)** Crosswind-integrated scalar flux footprints f_s^y, obtained in LES with $\Delta_g = 6.25$ m using different stochastic Lagrangian subgrid models RDM (Eq. 33) and LSM (Eqs. 28-32); The results obtained with these subgrid models applied within the first computational grid layer in combination with velocity recovering $\vec{u}^* = F^{-1}\overline{\vec{u}}$ and correction of velocity (Eqs. 34, 35) are also shown. Black lines are the footprints in LES with $\Delta_g = 2.0$ m.

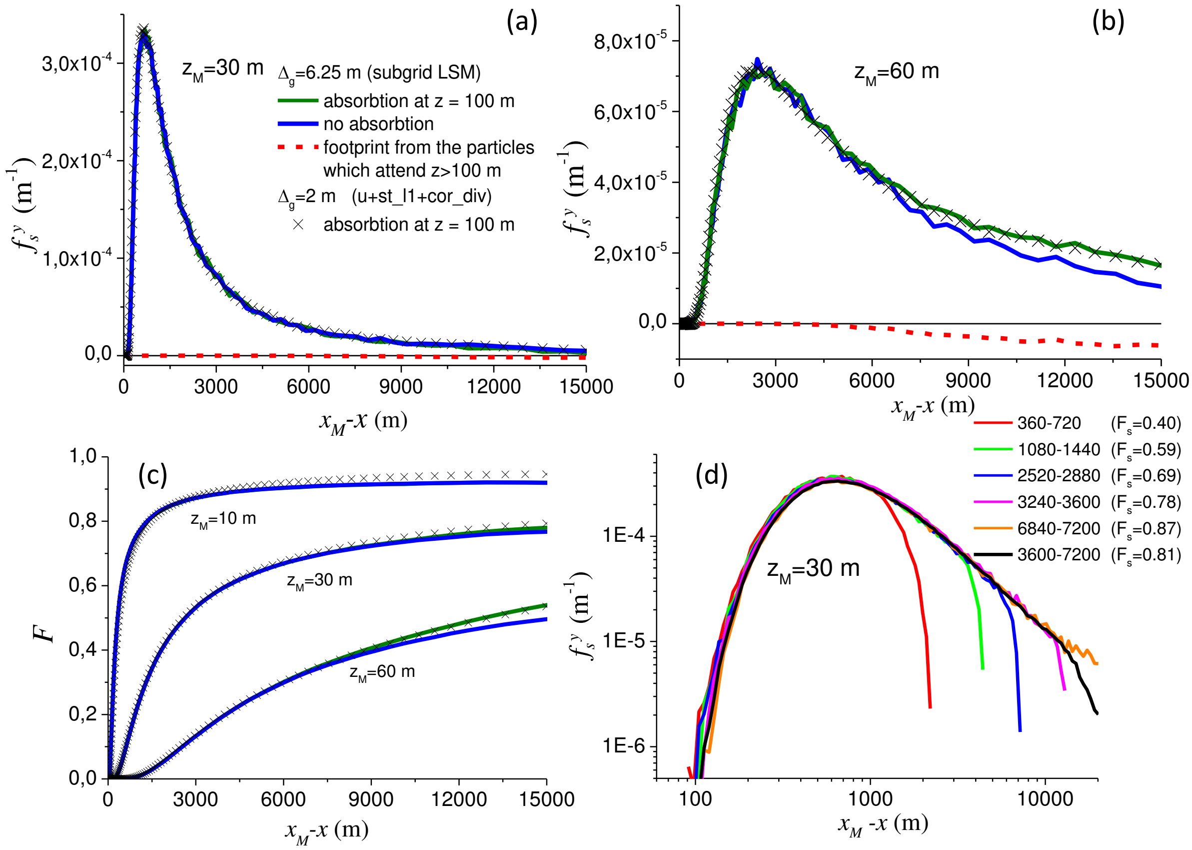

Figure AR8: **(Fig.A1 from the revised paper)** The footprint functions f_s^y (a,b) and the cumulative footprints F (c) obtained without the prescribed absorbtion (blue lines) in comparison with the results of simulation where the absorbtion is imposed at the level $z = 100$ m (green lines). Red dashed lines are the footprints from the particles which attained the level $z = 100$ m. (d) - Footprints obtained with the different intervals of averaging $[t_1, t_2]$ (shown in seconds in the legend), the normalized vertical concentration fluxes $\langle F_s(z_M)/F_s(0)\rangle_{[t_1,t_2]}$ are shown in brackets.

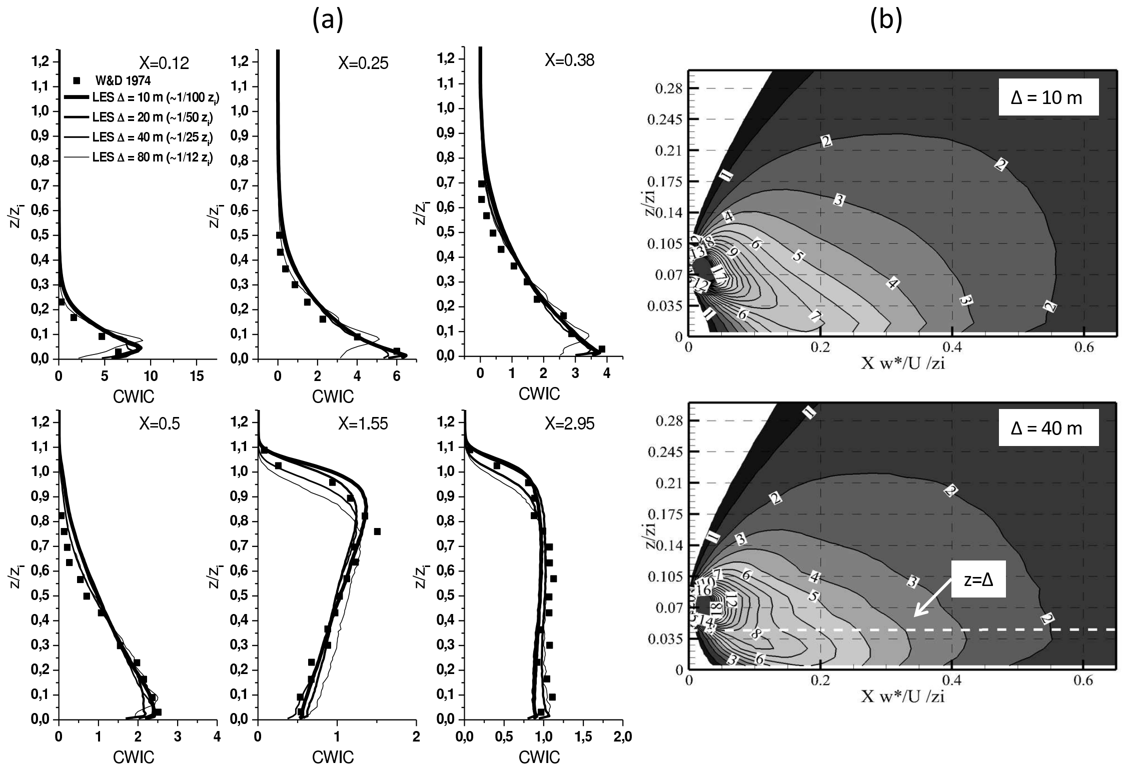

Figure AR9: **(Fig.S1.1 from the Supplements to the paper)** Crosswind integrated concentration $\tilde{C}^y = C^y U z_i/Q$ depending on normalized height z/z_i and non-dimensional distance from the source $X = xw^*/(Uz_i)$. (a) CWIC profiles $\tilde{C}^y$ computed in LES with different resolution (solid lines) in comparison with laboratory data (squares). (b) CWIC isolines computed with grid steps $\Delta_g = 10$ m$\approx z_i/100$ and $\Delta_g = 40$ m$\approx z_i/25$ (dashed line - first computational level $z = \Delta_g$).

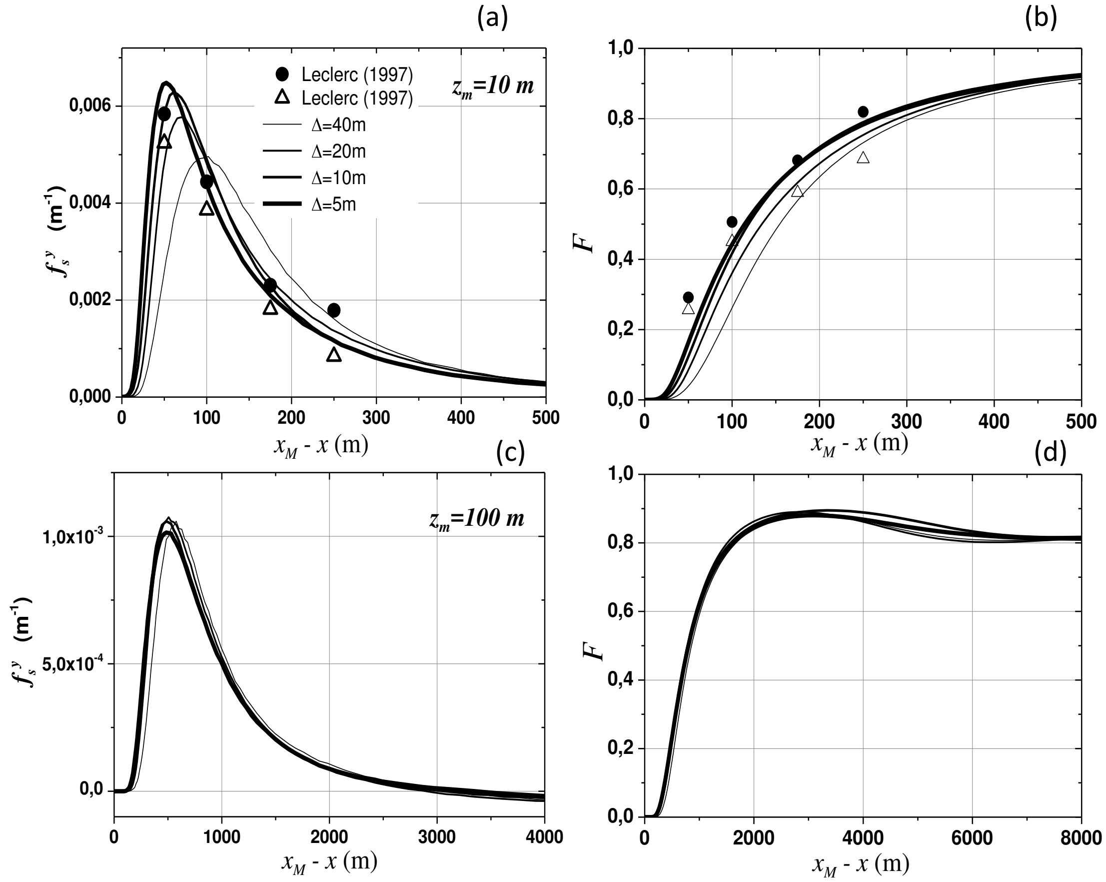

Figure AR10: **(Fig.S1.3 from the Supplements to the paper)** Footprints f_s^y (a,b) and cumulative footprints F (c,d) for the sensor heights z_M=10m (a,b) and z_M=100m (c,d), computed with the different spatial resolution in LES. Symbols - observational data [Leclerc et al., 1997]

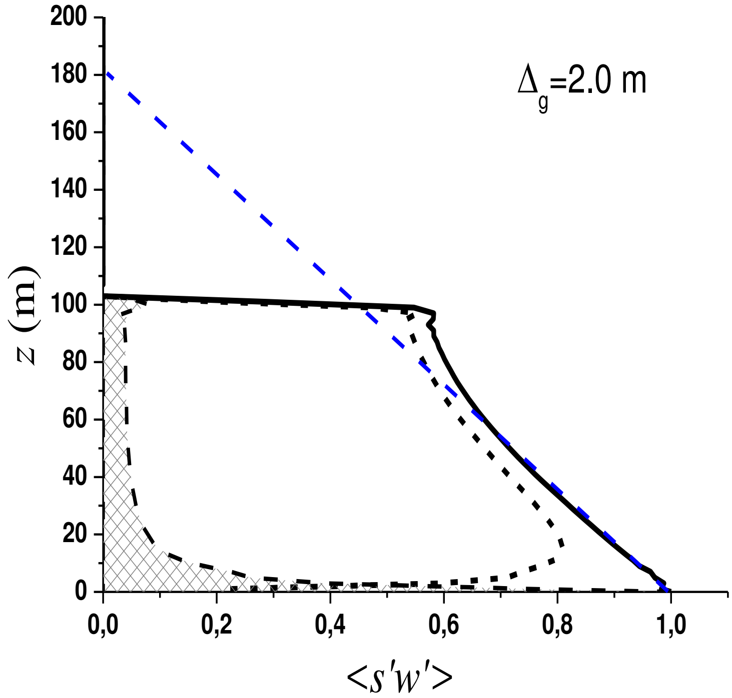

Figure AR11: Modified Fig.3. Concentration vertical flux profile obtained in LES with the absorbtion condition applied at z=100 m and the liner flux profile as it was predicted by Stull, 1988 or Beare et al., 2006 (blue dashed straight line)

Large-eddy simulation and stochastic modelling of Lagrangian particles for footprint determination in stable boundary layer

Andrey Glazunov[1], Üllar Rannik[2], Victor Stepanenko[3], Vasily Lykosov[1,3], Mikko Auvinen[2], Timo Vesala[2], and Ivan Mammarella[2]

[1]Institute of Numerical Mathematics RAS , GSP-1, 119991, Gubkina str., 8, Moscow, Russia
[2]Department of Physics, P.O. Box 64, University of Helsinki, 00014 Helsinki, Finland
[3]Moscow State University, Research Computing Center, GSP-1, 119234, Leninskie Gory, 1, bld. 4, Moscow, Russia

Correspondence to: A. Glazunov (and.glas@gmail.com)

Abstract. Large-eddy simulation (LES) and Lagrangian stochastic modelling of passive particle dispersion were applied to the scalar flux footprint determination in stable atmospheric boundary layer. The sensitivity of the LES results to the spatial resolution and to the parameterizations of small-scale turbulence was investigated. It was shown that the resolved and partially resolved ~~"~~('subfilter-scale~~"~~') eddies are mainly responsible for particle dispersion in LES, implying that substantial improvement may be achieved by using recovery of small-scale velocity fluctuations. In LES with the explicit filtering this recovering consists of application of the known inverse filter operator. The footprint functions obtained in LES were compared with the functions calculated with the use of first-order single particle Lagrangian stochastic models (LSM), zeroth-order Lagrangian stochastic models - the random displacement models (RDM) ~~, and analytical~~ and footprint parameterisations. ~~It was observed that the value of the Kolmogorov constant $C_0 = 6$ provided the best agreement of the one-dimensional LSMs results with LES, however, also that different LSMs can produce quite different footprint predictions.~~ According to presented LES the source area and footprints in stable boundary layer can be substantially more extended than those predicted by the modern ~~analytical~~ footprint parameterizations and LSMs.

1 Introduction

Micrometeorological measurements of vertical turbulent scalar fluxes in the atmospheric boundary layer (ABL) are usually carried out at altitudes $z_M \geq 1.5$ m due to technological limitations of the eddy covariance method. The measurement results are often attributed to the exchange of heat, moisture and gases at the surface. This procedure is not justified for inhomogeneous surfaces because of large area contributing to the flux, and because of variability of the second moments with height. The relationship between the ~~near-surface~~ surface flux $F_s(x,y,0)$ and the flux ~~$F_s(\boldsymbol{x}_M) = \langle w's' \rangle$, with angle brackets denoting the ensemble averaging,~~ $F_s(x_M,y_M,z_M)$, measured in point ~~$\boldsymbol{x}_M$ at some distance from the ground~~ $\boldsymbol{x}_M = (x_M,y_M,z_M)$, can be formalized via the footprint function ~~$f_s(x,y,\boldsymbol{x}_M)$:~~ f_s:

$$F_s(x_M,y_M,z_M) = \int\limits_{-\infty}^{\infty}\int\limits_{-\infty}^{\infty} f_s(x,y,x_M,y_M,z_M)F_s(x,y,0)\,dx\,dy. \qquad (1)$$

Traditionally, footprint functions $f_s^d(x^d, y^d, \boldsymbol{x}_M) = f_s(x, y, \boldsymbol{x}_M)$ are expressed in local coordinate system with the origin which coincides with the sensor position (here, $x^d = x_M - x$ is the positive upwind distance from the sensor and $y^d = y_M - y$ is the crosswind distance, see Fig. 1a). In horizontally homogenous case these functions do not depend on x_M and y_M. In ABL the surface area contributing to the flux is elongated in wind direction, therefore the crosswind-integrated footprint function f_s^y defined as

$$f_s^y(x^d, z_M) = \int\limits_{-\infty}^{\infty} f_s^d(x^d, y^d, z_M)\, dy^d, \tag{2}$$

is one of the most required characteristics for the practical use.

The measurements of the ~~function f_s~~ scalar flux footprint functions in natural environment are restricted (e.g., Finn et al., 1996; Leclerc et al., 1997, 2003; Nicolini et al., 2015) due to the necessity to conduct the emission and detection of artificial tracers. Besides, such measurements are not available for the stably stratified ABL, where the area of the surface influencing the point of measurements increases.

~~Stochastic models, used for a footprint calculation~~ Modelling approaches used for footprint calculation include stochastic models, such as single particle such as single particle first-order Lagrangian stochastic models based on generalized Langevin equation (LSM) and zeroth-order stochastic models (also known as the random displacement models, RDM) (see the reviews listed in the papers (Wilson and Sawford, 1996), (Wilson, 2015) and the monograph (Thomson and Wilson, 2013))~~, as well as analytical models (e.g., Horst and Weil, 1992; Kormann and Meixner, 2001; Kljun et al., 2004, 2015).~~. Besides, one can use the analytical models (e.g., Horst and Weil, 1992; Kormann and Meixner, 2001) and the parameterizations based on the scaling approach (Kljun et al., 2004, 2015). All of these models should be calibrated against the data considered to be representative of real processes. ~~Results of these models~~ Their results depend on the choice of universal functions in the ABL or in the surface layer (non-dimensional velocity and scalar gradients, non-dimensional dissipation, dispersion of the velocity components etc.). Commonly, the applicability of ~~these~~ the analytical models is limited by a "constant flux layer" simplification, assuming that the measurement height z_M is much less than the thickness of the ABL z_i. However, under the strongly stable stratification the thickness z_i may be several meters, therefore, the vertical gradients of momentum and scalars fluxes near the surface can be large. It can lead to incorrect functioning of the models designer for, and tested on the data gathered under different conditions.

Large eddy simulation (LES), employing Eulerian approach for the transport of scalars, was first time applied for a footprint calculation in (Leclerc et al., 1997). Modern computational technologies allow to combine Eulerian and Lagrangian methods for turbulence simulation and ~~particles~~ particle transport (e.g., Weil et al., 2004; Steinfeld et al., 2008; Cai et al., 2010; Hellsten et al., 2015) and to perform detailed calculations of averaged two-dimensional footprints under different types of stratifications in ABL and footprints $f_s(x, y, \boldsymbol{x}_M)$ over heterogeneous surfaces (for example, urban surface and surfaces with alternating types of vegetation). Some examples of such calculations are given in (Steinfeld et al., 2008; Hellsten et al., 2015).

Lagrangian transport in LES is complicated by the problem of description of small-scale (unresolved) fluctuations of the particle velocity, which is similar to the problem of subgrid modelling of Eulerian dynamics. A common approach for Lagrangian subgrid modelling in LES is the application of subgrid LSMs (e.g., Weil et al., 2004; Steinfeld et al., 2008; Cai et al., 2010;

Shotorban and Mashayek, 2006). This approach requires a number of additional calculations for each particle (e.g., interpolations of subfilter stresses τ_{ij} and subgrid dissipation ϵ into the particle position $\boldsymbol{x}^p$). In addition, it is necessary to generate a three-component random noise for each particle, that is a time-consuming computational operation. Numerically stable solution to the generalized Langevin equation (see Sect. 2.3, Eq. (9)) in LES requires a smaller time steps than the steps to solution of Eulerian equations, because local Lagrangian decorrelation time $T_L(\boldsymbol{x}^p, t)$ can be very small.

The statistics of simulated turbulence in LES may significantly differ from the statistics of real turbulence. For example, the use of dissipative numerical schemes or low-order finite-difference schemes usually results in a suppression of fluctuations over almost the entire resolved spectral ranges of discrete models (see e.g., Fig. 16 in Piotrowski et al., 2009). Turbulent fluxes (in the Eulerian representation) associated with these fluctuations are restored by subgrid closure. However, in terms of the Lagrangian transport the effects of distortion of small-scale part of the spectrum are most often not considered.

Numerical simulations of Lagrangian transport in LES are also limited by the low scalability of parallel algorithms. This is due to the impossibility of uniform loading of processors in a joint solution to the Euler and Lagrangian equations, a large number of interprocessor exchanges and unstructured distribution of characteristics required for Lagrangian advection in the computer RAM memory.

Thus, all methods of numerical and analytical determination of the functions f_s have individual drawbacks. At the same time, due to the lack of sufficient amount of experimental data and due to their low accuracy, there are no clear criteria for evaluation of different models.

According to the need of computational cost reduction, one of the objectives of this study is to establish the role of stochastic subgrid modelling in the correct description of the ~~particles~~ particle dispersion in LES. Is it possible to simplify the calculation and to avoid the introduction of stochastic terms without the loss of accuracy in some integral characteristics, such as the footprints or the concentration of pollutants emitted from the point sources? The role of subgrid fluctuations is reduced with an increase of spatial LES resolution. Therefore, the independence of results from the mesh size is used as a criterion for checking the quality of Lagrangian transport procedures in LES. It will be demonstrated that the subgrid stochastic modelling in LES can be omitted in most cases. Instead, we propose ~~"computationally cheap"~~ 'computationally cheap' procedure of inverse filtering supplemented by divergent correction of Eulerian velocity to replace the subgrid stochastic modelling in LES (see description below).

Subgrid transport is especially significant near the surface and/or under ~~the~~ stable stratification – all are the cases associated with small eddies size. That is why the stable ABL was selected as the key test scenario in this study. We slightly modified the setup of the numerical experiment GABLS (Beare et al., 2006) for this purpose.

LES results are used as the input data for the stochastic models (LSMs and RDMs). These data are pre-adjusted using known universal dependencies and taking into account an incomplete representation of turbulent energy in LES. The comparison of results of different stochastic models and the results from LES allows to specify the parameters for the LSMs and permits to identify the differences between LSMs and RDMs under the conditions which have not been tested previously.

The paper is organized as follows. Section 2 contains the description of some common features of approaches: the implemented numerical algorithm for footprint estimation in LES and LS models (Sect. 2.1); LES governing equations and the definitions of some terminology used for the small-scale modelling description and for the testing of ~~particles~~ particle transport (Sect. 2.2); the definitions of stochastic models (LSMs and RDMs) and pointing to some problems connected with uncertainty of the choice of turbulent statistics for them (Sect. 2.3 and 2.4). Section 3 contains short description of the numerical algorithms~~and~~ , the turbulent closure for LES model used in this study (Sect. 3.1) and the description of the different approaches for the Lagrangian particles transport in LES tested here (Sect. 3.2). Sect. 4 is mainly devoted to the testing of ability of LES model with rough spatial resolution to reproduce particle dispersion correctly. For this sake, we implemented special setup of the numerical experiment (see Sect. 4.1) permitting to compare Lagrangian and Eulerian statistics (see Sect. 4.2.2). The focus was made on the approaches with the limited use of subgrid stochastic modelling (see Sect. 4.2.1 where the sensitivity of the computed footprints to the spatial resolution was investigated). The footprints computed with LES model with simple subgrid LSM and RDM (traditional approach) are presented in Sect. 4.2.3 ~~.~~ and Sect. 4.2.4. Two-dimensional footprints are shown in Sect. 4.3. Due to large sensitivity of LSMs to the turbulent statistics we emphasize data preparation for them using LES results, measurements data and similarity laws in Sect. 5.1. Section 5 contains the results of footprint modelling with the use of the set of different RDMs and LSMs (specified in Sect. 5.2) in comparison with LES results (see Sect. 5.3). Section 6 is devoted to the comparison of footprints, computed in LES with the ~~analytical~~ footprint parameterisations based on a scaling approach by Kljun et al. (2004, 2015). Section 7 summarises the results.

In addition to the basic calculation, we carried out a series of tests (see Supplement Sect. S1) under unstable stratification in ABL with ~~the~~ different grid steps in LES model. This allows to compare the results presented here with ~~the~~ similar results obtained in previous studies (e.g., Steinfeld et al., 2008; Weil et al., 2004) and to verify the performance of our LES model in footprint evaluation. Furthermore, we demonstrate the results of footprint calculations above the inhomogeneous surface (Supplement Sect. S2), ~~which imitates the lake of a small size, surrounded by forest~~with a huge number of particles involved in calculations simultaneously. Computational aspects of technology are discussed as well.

2 Modelling approaches

2.1 Numerical evaluation of footprints

Computational methods for determination of footprints often reduce to the implementation of Lagrangian transport of marked particles. Each particle can contain a number of attributes, including its initial coordinate $\boldsymbol{x}_0^p$ and time t_0^p. Choose two small horizontal plates δ_S and δ_M for averaging in the neighborhood of zero with the areas S_S and S_M, respectively. Define the time interval $T_p = [t_0, t_2]$, during which new particles are ejected near the ground with the intensity H (here H is the mathematical expectation of the new ~~particles~~ particle number emitted per unit area per unit time) and the interval $T_a = [t_1, t_2]$ $(t_1 > t_0)$, when particles are detected near the point of measurement. If t_1 is sufficiently large for the ensemble averaged flux to attain constant value in time, and T_a is quite large for statistically significant averaging, then the footprint f_s can be evaluated by the formula

$$f_s(x_S, y_S, x_M, y_M, z_M) \approx$$
$$\approx \frac{1}{S_M}\frac{1}{T_a}\sum_{p=1}^{n_{SM}}\left(\int_{\delta_S} H(x_0^p + x', y_0^p + y', t_0^p)dx'dy'\right)^{-1}\frac{w^p}{|w^p|}I_{SM}^p, \qquad (3)$$

where n_{SM} is the number of ~~particles, the trajectories of which at least once crossed~~ intersections of the plane $z = z_M$ by the particle trajectories at horizontal coordinates $\boldsymbol{x}_1^p : (x_1^p - x_M, y_1^p - y_M) \in \delta_M$ in time interval T_a, $I_{SM}^p = 1$ if the initial coordinates $\boldsymbol{x}_0^p$ of such particle satisfy the condition $((x_1^p - x_0^p) - (x_M - x_S), (y_1^p - y_0^p) - (y_M - y_S)) \in \delta_S$ and $I_{SM}^p = 0$ otherwise. Here, w^p is the vertical component of the particle velocity at the moment of crossing the plane $z = z_M$. ~~In the~~ Schematic representation of the algorithm for the footprint function determination in LES is shown in Fig. 1. In accordance with Eq. (3) and the description above, the particle crossing the test area δ_M brings the impact into the value $f_s(x_S, y_S, \boldsymbol{x}_M)$, then the beginning of its modified trajectory shifted in a such way to superpose the point $\boldsymbol{x}_1^p$ with sensor position $\boldsymbol{x}_M$ belongs to the test area δ_S. For example (see, Fig. 1b), when the footprint value is calculated at the point (x_S, y_S) only the red particle is counted, but not the blue particle. Such algorithm of averaging was selected because it permits to refine the footprint resolution on the vicinity of sensor independently on the area of δ_M using the assumption of some spatial homogeneity.

In the horizontally homogeneous case one can calculate footprint $\cancel{f_s(x^d, y^d, z_M)}$ $f_s^d(x^d, y^d, z_M)$ performing averaging over statistically equivalent coordinates of sensor position~~(here $\boldsymbol{x}^d = (x_M - x, y_M - y, z)$)~~. For this averaging in LES with periodic domain one can prescribe the coordinates (x_M, y_M) to the domain center and select the area δ_S to be equal to whole domain size. Analogical methods can be applied when using LSMs or RDMs, whereas in the case of RDMs particle displacement should be used in the Eq. ~~3~~ (3) instead of velocity.

Nonuniform Cartesian grid $\boldsymbol{x}_{ij}^d = (x_i^d, y_j^d)$ (where, $-20 \leq i \leq 160$; $-120 \leq j \leq 120$), stretched with the distance from the sensor position, was selected for the footprint functions accumulation in the following sections of this paper. Grid was prescribed as: $(x_0^d, y_0^d) = (0, 0)$; $x_i^d = \Delta_{x0}\gamma_x^{|i|} i/|i|$ and $y_i^d = \Delta_{y0}\gamma_y^{|j|} j/|j|$ if $i \neq 0$ and $j \neq 0$; $\Delta_{x0} = \Delta_{y0} = 2$ m; $\gamma_x = \gamma_y = 1.05$. This grid is independent of the LES model resolution and coincides with the footprint grids selected for all runs with LSMs and RDMs.

2.2 Lagrangian particles embedded into LES

Lagrangian particle velocity $\boldsymbol{u}^p$ and the particle position $\boldsymbol{x}^p$ can be computed in LES models as follows:

$$u_i^p = \overline{u}_i^{(p)} + u''^p_i, \qquad dx_i^p = u_i^p dt. \qquad (4)$$

Here $\overline{u}_i^{(p)}$ is the interpolation of the resolved Eulerian velocity into the particle position; u''^p_i are the small-scale unresolved Lagrangian velocity fluctuations associated with Eulerian velocity fluctuations belonging to "subgrid" and "subfilter" scales. Here and later we shall use the designation "subfilter" to denote the fluctuations which belong to the resolved spectral range of the discrete model, but are not reproduced numerically, and the designation "subgrid" for the fluctuations which can not be represented on the grid due to smallness of the scales. LES governing equations for filtered velocity $\overline{\boldsymbol{u}}$ are:

$$\frac{\partial \overline{u}_i}{\partial t} = -\frac{\partial \overline{u}_i \overline{u}_j}{\partial x_j} - \frac{\partial \tau_{ij}}{\partial x_j} - \frac{\partial \overline{p}}{\partial x_i} + \overline{F_i^e}, \qquad \frac{\partial \overline{u}_i}{\partial x_i} = 0, \tag{5}$$

where F_i^e comprises Coriolis and buoyancy forces~~; –~~, $\overline{p}$ is normalized pressure and $\tau_{ij} = \overline{u_i u_j} - \overline{u_i}\;\overline{u_j}$ denotes the modeled "subgrid/subfilter" ~~–~~stress tensor. System of equations (5) can be supplemented by the Eulerian equations of scalars transport:

$$\frac{\partial \overline{s}}{\partial t} = -\overline{u}_i \frac{\partial \overline{s}}{\partial x_i} - \frac{\partial \vartheta_i^s}{\partial x_i} + \overline{Q_s}, \tag{6}$$

where $\overline{Q_s}$ denotes sources intensity; $\vartheta_i^s = \overline{s u_i} - \overline{u_i}\;\overline{s}$ are the parameterized "subgrid/subfilter" fluxes. Usually, the fluctuations $\boldsymbol{u}''^p$ are defined to be dependent on some random function ξ, introduced in order to provide the missing part of mixing. The particular approaches for computing ~~of~~ the unresolved part of particle velocity will be discussed and tested in the following sections.

There is a great practical interest in the calculation of footprints, as well as of spatial and temporal characteristics of pollution transport from localized sources above heterogeneous surfaces and in the areas with complex geometry (in the urban environment, over the surfaces with complex terrain or over the alternating types of vegetation). LES of such flows becomes a routine procedure with increasing performance of computers. However, the calculation of statistical characteristics of Lagrangian trajectories is complicated in this case by the need of transport of huge number of tracers (e.g., Hellsten et al., 2015). For example, it is necessary to calculate the trajectories of about 10^9 particles (see Supplement Sect. S2) to obtain the footprints above the ~~"lake" –~~ inhomogeneous surface with the explicitly prescribed obstacles (the task similar to that presented in (Glazunov and Stepanenko, 2015)).

On the other hand, a large number of particles (see, e.g., Supplement Fig.S2.1b) allows to estimate the local instantaneous spatially filtered concentration of the scalar:

$$s_P(\boldsymbol{x}, t) = \sum_{p=1,N} G(\boldsymbol{x} - \boldsymbol{x}^p(t)), \tag{7}$$

where G is the function which coincides with the convolution kernel of LES filter operator and N is the total number of particles in the domain. If the mathematical expectation Q_p of a number of new particles ~~appearing~~ ejected in a unit volume during unit time interval is proportional to the Eulerian concentration source strength $Q_p(\boldsymbol{x},t) = C\overline{Q}_s(\boldsymbol{x},t)$, then ~~$s_p(\boldsymbol{x},t) \approx C\overline{s}(\boldsymbol{x},t)$~~ $s_P(\boldsymbol{x},t) \approx C\overline{s}(\boldsymbol{x},t)$. One can perform the same operations with the "Lagrangian" concentration ~~$s_p(\boldsymbol{x},t)$~~ $s_P(\boldsymbol{x},t)$ as the operations with the Eulerian scalar $\overline{s}$. Below, we will compare the averaged values of ~~s_p~~ s_P and $\overline{s}$ and their spatial variability. Besides, we will use the estimation of concentration ~~$s_p(\boldsymbol{x},t)$~~ $s_P(\boldsymbol{x},t)$ for correcting the ~~particles~~ particle velocities (see, Sect. 3.2.1, Eqs. (34),(35)), in order to approximate the effect of subgrid turbulence.

2.3 Single particle first-order Lagrangian stochastic models (LSM)

Another approach (more widespread due to a lower computational cost) is the replacement of the entire turbulent component of velocity by a random process (Lagrangian stochastic models (LSM)):

$$u_i^p = \left\langle u_i^{(p)} \right\rangle + u_i'^p, \qquad dx_i^p = u_i^p dt. \tag{8}$$

Here $\left\langle u_i^{(p)} \right\rangle$ is the ensemble averaged Eulerian velocity at point $\boldsymbol{x}^p$. ~~In the single~~ Note, that LSMs are assumed to be also applicable under the temporal evolution of turbulence statistics. In this paper we shall consider ABL as it approaches a quasi-steady state. Therefore, due to assumption of ergodicity, ensemble averaging can be replaced by averaging in time and in the directions of spatial homogeneity: $\langle\varphi\rangle \approx \langle\varphi\rangle_{x,y,t}$.

Single particle first-order LSM ~~velocity~~ is formulated as follows. Velocity $u_i'^p$ is ~~defined as a Markovian process and is the solution of generalized Langevin~~ described by the stochastic differential equation:

$$du'^p_i = a_i(\boldsymbol{x}^p, \boldsymbol{u}^p, t)dt + b_{ij}(\boldsymbol{x}^p, \boldsymbol{u}^p, t)\xi_i^p, \tag{9}$$

where ξ stays for the delta-correlated (usually Gaussian) random noise with the variance dt

$$\left\langle \xi_i^p(t)\xi_j^h(t+t') \right\rangle = \delta_{ij}\delta_{ph}\delta(t')dt \tag{10}$$

and with the zero average $\langle \xi_i^p \rangle = 0$; a_i, b_{ij} are the functions depending on the Eulerian characteristics of turbulence and on the Lagrangian velocity of the particle. Typically b_{ij} is calculated by the formula

$$b_{ij} = \delta_{ij}\sqrt{C_0\epsilon}, \tag{11}$$

where, ϵ denotes the energy dissipation rate, averaged for a fixed coordinate, C_0 is the Kolmogorov constant. This kind of random term (arguments are given in (Thomson, 1987) and (Sawford, 1993)) is defined by Lagrangian velocity structure function in the inertial range (see Monin and Yaglom, 1975):

$$D_{ij}(t') = \langle (u_i(t+t') - u_i(t))(u_j(t+t') - u_j(t)) \rangle = \delta_{ij}C_0\epsilon t' \tag{12}$$

if $\tau_\eta \ll t' \ll T_E$ ($\tau_\eta = (\nu/\epsilon)^{1/2}$ is the Kolmogorov microscale, $T_E = E^2/\epsilon$ is the energy containing turbulent time scale ~~,~~ and E is the turbulent kinetic energy~~)~~.

The function a_i (drift term) determines the behavior of particles at large times $t \sim T_L \sim T_E$ (here T_L is the Lagrangian decorrelation time scale). For spatially inhomogeneous and statistically non-stationary turbulent flows, including ABL, the choice of a_i is usually done according to the well mixed condition (WMC; Thomson, 1987). In general WMC does not lead to a unique solution for a_i. Different LSMs are constructed by introducing the additional physical assumptions and can lead to inequivalent results.

Lagrangian models are very sensitive to the choice of universal functions that define the normalized RMS of the vertical velocity $\tilde{\sigma}_w = \left\langle w'^2 \right\rangle^{1/2} / U_*$ and non-dimensional dissipation $\tilde{\epsilon} = \epsilon z / U_*^3$ (here U_* is the friction velocity). Besides, the simulation results are affected by the choice of ~~a "universal constant"~~ value of C_0. It can be shown (e.g., Durbin, 1984; Wilson and Yee, 2007) that for one-dimensional LSM, these parameters determine the eddy diffusivity K_s for the scalar in the diffusion limit (when $t \gg T_L$, i.e. at large distances from the source):

$$K_s = \frac{2\sigma_w^4}{C_0\epsilon} = \frac{2\tilde{\sigma}_w^4}{C_0\tilde{\epsilon}} U_* z. \tag{13}$$

The data of measurements in the ABL demonstrate large variation. For example, the values of $\tilde{\sigma}_w^2$ range from 1.0 to 3.1 (see Table 1 in Banta et al., 2006). According to Eq. (13) it implies the change of K_s by more than nine times.

There is no consensus on the value of C_0 as well. Formally, C_0 has the meaning of a universal Kolmogorov constant in Eq. (11). The estimation of this constant for an isotropic turbulence using the data of laboratory measurements and DNS provides an interval $C_0 = 6. \pm 0.5$ (see, Lien and D'Asaro (2002)). However, the values $C_0 \sim 3-4$ are often used for LSM of particle transport in ABL ~~.~~ independently from the type of the stratification. These values have been obtained by the different methods. For instance, the value ~~$C_0 = 3.1$~~ C_0 = 3.1 for a one-dimensional LSM corresponds to a calibration performed in Wilson et al. (1981) according to observation data ~~(Barad, 1958; Haugen, 1959)~~Barad (1958); Haugen (1959). This calibration ~~(see Wilson, 2015)~~ (see, Wilson (2015)) assumes that the turbulent Schmidt number $Sc = K_m/K_s = 0.64$ near the surface (here ~~K_m~~ K_m is the eddy viscosity). It is known that determination of the turbulent Prandtl number $Pr = K_m/K_h$ (K_h - heat transfer eddy diffusivity) and Schmidt number based on observation data is complicated by large statistical errors associated with the problem of self-correlation (Anderson, 2009; Grachev et al., 2007). Therefore, ~~the existing estimation of C_0 can not~~ this method of estimation of C_0 cannot be considered as final and should be confirmed by future studies. In Rizza et al. (2010) the values of C_0 were determined using the LES-based evaluations of the velocity structure functions and the Lagrangian spectra in convective and neutrally-stratified ABLs. In this study the LES model had relatively low resolution, which can be insufficient for accurate determination of this constant in the inertial subrange (see discussion on the resolution requirements in Lien and D'Asaro (2002)). Nevertheless, the value $C_0 \sim 3$, in the paper by Rizza et al. (2010) is relevant for LSMs applied to the convective ABL, in that case the constant is also responsible for the energy containing time scales which are well resolved in LES. The detailed overview of the methods of determination of the constant C_0 can be found in Poggi et al. (2008), where the discussion on the disagreements of the different approaches is also included. The results of the LSMs are very sensitive to the choice for C_0 as it was shown earlier by Du et al. (1995), Rotach et al. (1996), Wilson (2015) and many others. Below we show that the ~~value of C_0 significantly affects the results of footprint calculations~~commonly used value of $C_0 \sim 3-4$ can be greatly underestimated for the use as a parameter in LSMs applied to the stably stratified ABL.

2.4 Zeroth-order Lagrangian stochastic models or random displacement models (RDM)

A simplest approach for development of the models of particle dispersion entails replacement of Eulerian advection-diffusion equation

$$\frac{\partial \langle s \rangle}{\partial t} + \langle u_i \rangle \frac{\partial \langle s \rangle}{\partial x_i} = \frac{\partial}{\partial x_i} K_s \frac{\partial \langle s \rangle}{\partial x_i} + Q_s \tag{14}$$

by the stochastic equation for particle position (random displacement models (RDM)):

$$dx_i^p = \langle u_i \rangle dt + \frac{\partial K_s}{\partial x_i} dt + \sqrt{2K_s}\xi_i^p. \tag{15}$$

Probability density of particle position P is connected with scalar field concentration $\langle s \rangle$ as follows:

$$\langle s(\boldsymbol{x},t) \rangle = \int\limits_{R^3} \int\limits_{-\infty}^{t} Q_s(\boldsymbol{x}_0,t_0) P(\boldsymbol{x},t|\boldsymbol{x}_0,t_0) d^3\boldsymbol{x}_0 dt_0. \tag{16}$$

Using the Fokker-Planck equation it can be shown that the Eq. (15) is equivalent to the Eq. (14) from the point of view of concentration transport when the time step dt tends to zero (Durbin, 1983; Boughton et al., 1987).

RDM has some major disadvantages. First, it shares the limitation of Eulerian eddy-diffusion treatment of turbulent dispersion, i.e. "K-theory". Correspondingly, it is not able to describe the non-diffusive near field of a source. Also, RDM can not be applied for the convective ABL, where the counter-gradient transport is observed. Besides, it requires the exact values of diffusion coefficient K_s, which can not be measured directly.

3 Details of LES model used in this study

3.1 Numerical algorithms and turbulent closure

System of equations (5 - 6) is discretized using explicit finite-difference scheme with the second-order temporal approximation (Adams-Bashforth method) and fourth-order (fully-conserved for advective terms) spatial approximation of velocity and scalars on staggered grid (Morinishi et al., 1998).

Mixed model (Bardina et al., 1980), expressed as the sum of the Smagorinsky and scale-similarity models, is used for calculation of turbulent stress tensor:

$$\tau_{ij}^{mix} = \tau_{ij}^{smag} + \tau_{ij}^{ssm} = -2(C_s\overline{\Delta})^2|\overline{S}|\overline{S}_{ij} + (\overline{\overline{u}_i\,\overline{u}_j} - \overline{\overline{u}}_i\,\overline{\overline{u}}_j), \tag{17}$$

where $\overline{S}_{ij}$ is the filtered strain rate tensor, C_s is the dynamically determined (Germano et al., 1991) dimensionless coefficient which depends on time and spatial coordinates. The a priori tests using the data of laboratory measurements show that scale-similarity models with Gaussian or box filters provide correlation typically as high as 80% between real and modeled stresses (see overview in Meneveau and Katz, 2000). The significant part of this correlation can be attributed to non-ideality of the spatial filter and use of common information for computing both the real and modeled stresses (Liu et al., 1994). The discrete spatial filter used in this study has a smooth transfer function in spectral space, so it can be supposed that the scale-similarity part of Eq. (17) is mainly responsible for the influence of velocity fluctuations belonging to "subfilter" scales.

The procedure of calculation of the coefficients $X(\boldsymbol{x},t) = (C_s\overline{\Delta})^2$ reduces to minimization of the ~~Euclidean norm $(\varepsilon_{ij}, \varepsilon_{ij})$ of the~~ functional $\Psi(X) = \int_\Omega \varepsilon_{ij}(\boldsymbol{x})\,\varepsilon_{ij}(\boldsymbol{x})d\boldsymbol{x}$ where Ω is the model domain and $\varepsilon_{ij}(\boldsymbol{x})$ is the the residual of the overdefined system of equations

$$\widehat{(X M_{ij}^{\tau})} - \alpha^2 X(M_{ij}^{T}) = L_{ij} - H_{ij} + \varepsilon_{ij}, \tag{18}$$

obtained by substitution of mixed model (Eq. 17) into the Germano identity as

$$T_{ij} - \widehat{\tau_{ij}} = \widehat{\overline{u}_i\,\overline{u}_j} - \widehat{\overline{u}}_i\,\widehat{\overline{u}}_j. \tag{19}$$

Here T_{ij} are subgrid/subfilter stresses for the smoothed velocity $\widehat{\overline{\mathbf{u}}}$, obtained by successive application of basic $F_{\overline{\Delta}}$ and test $F_{\widehat{\Delta}}$ spatial filters, $\alpha = \widehat{\overline{\Delta}}/\overline{\Delta}$ is the ratio of the filters widths. Tensors M_{ij}^{T}, M_{ij}^{τ}, L_{ij} and H_{ij} are calculated as follows:

$$\begin{aligned} &M_{ij}^{T} = 2\left|\widehat{\overline{S}}\right|\widehat{\overline{S}}_{ij}, \quad M_{ij}^{\tau} = 2|\overline{S}|\overline{S}_{ij}, \\ &L_{ij} = \widehat{\overline{u}_i\,\overline{u}_j} - \widehat{\overline{u}}_i\,\widehat{\overline{u}}_j, \quad H_{ij} = \left(\widehat{\overline{\widehat{\overline{u}}_i\,\widehat{\overline{u}}_j}} - \widehat{\overline{\widehat{\overline{u}}}}_i\,\widehat{\overline{\widehat{\overline{u}}}}_j\right) - \left(\widehat{\overline{\overline{u}_i\,\overline{u}_j}} - \widehat{\overline{\overline{u}}}_i\,\widehat{\overline{\overline{u}}}_j\right). \end{aligned} \tag{20}$$

The generalized solution to the discrete analogue of Eq. (18) is searched using the iterative conjugate gradients (CG) method with diagonal preconditioner. To do this, the problem is reduced to a linear system of equations

$$A^*_\Delta A_\Delta X_\Delta = A^*_\Delta R_\Delta, \tag{21}$$

where X_Δ is the the desired solution (a vector of dimension $N = N_x N_y N_z$ with the values defined in the center of grid cells); A_Δ and $R_\Delta = L_\Delta - H_\Delta$ are the discrete analogues of the operator and the right hand side of Eq. (18) correspondingly; A^*_Δ is the transpose matrix. The diagonal preconditioner P_Δ for CG method was selected as follows:

$$P_\Delta = \left(\alpha^4 M^T_\Delta M^{T*}_\Delta + \mu(M^\tau_\Delta M^{\tau*}_\Delta - 2\alpha^2 M^T_\Delta M^{\tau*}_\Delta)\right)^{-1}, \tag{22}$$

where $\mu = const \sim 1$ is the empirical coefficient independent on time and spatial position. The solution X_Δ contains negative values (unconditional minimization of the functional is used), however, mixed model (Eq. 17) reduces their relative number compared with the dynamic Smagorinsky model. In the algorithm, negative values are replaced by zeroes. In fact, this dynamic procedure is close to approach proposed in (Ghosal et al., 1995), with the difference that the mixed model was applied here and iterative method was replaced by a faster CG method.

Eddy diffusion models are used for subgrid heat and concentration transfer:

$$\vartheta^s_i = -{K_h}^{subgr}\frac{\partial \overline{s}}{\partial x_i}, \tag{23}$$

here ${K_h}^{subgr} = (1/Sc^{subgr})(C_s\overline{\Delta})^2|\overline{S}|$ is the eddy diffusivity, which is independent on the type of scalar. Subgrid turbulent Schmidt and Prandtl numbers are fixed $Sc^{subgr} = Pr^{subgr} = 0.8$.

A distinctive feature of this model is that the discrete spatial filter operator $F_{\overline{\Delta}} = F_x F_y F_z$ is explicitly involved in calculation of stresses. The following discrete basic filter is selected:

$$F_x(\varphi)_{i,j,k} = (1/8)\varphi_{i-1,j,k} + (3/4)\varphi_{i,j,k} + (1/8)\varphi_{i+1,j,k}, \tag{24}$$

here i,j,k denote a grid cell number, φ is any variable. Similar filtering is applied along the coordinates y and z. It is reasonable to expect that we get the velocity $\overline{\boldsymbol{u}}$, smoothed according to specified filtering operator as a solution to Eq. (5) supplemented by the mixed closure (Eqs. 17 - 21). Since the discrete filtering operator is invertible, we can find the following velocity at any point and time:

$${u_i}^* = F^{-1}_{\overline{\Delta}}\overline{u}_i, \tag{25}$$

which better reflects the small-scale spatial variability. Approximate inverse filter is calculated as a series (Van Cittert, 1931):

$$F^{-1}_{\overline{\Delta}} \approx F^{-1}_n = \sum_{k=0}^{n}(I - F_{\overline{\Delta}})^k, \tag{26}$$

where I is a unity operator; in the calculations presented below we used $n = 5$. Spatial spectra of "defiltered" ~~–~~velocity $\boldsymbol{u}^*$ under the neutral, unstable and stable stratification were obtained earlier (Glazunov, 2009; Glazunov and Dymnikov, 2013; Glazunov, 2014). It was found in all cases that this procedure improves the small-scale parts of the spectra according to dependence $S \sim k^{-5/3}$, ~~leads to better coincidence~~ provides better agreement of spectra calculated with the different spatial resolution and improves convergence of non-dimensional spectra if proper length scales are used for normalization.

3.2 Methods for Lagrangian particle transport in LES

3.2.1 Subgrid and subfiler modelling

Below, the subgrid and subfilter modelling methods used for the simulations in the current study are listed. These methods will be used also in combinations as defined in Sect. 4.2.

(1) Improvement of Lagrangian transport using inverse filtering of Eulerian velocity field

First, we will use the recovery of "subfilter" fluctuations (Eqs. 25, 26) in order to transport Lagrangian particles more precisely:

$$\boldsymbol{u}^p = \boldsymbol{u}^{*(p)} \tag{27}$$

Note, that for the use of such a procedure, LES models should exhibit the properties of model with an explicit filtering. Similar approach was recently applied by Michalek et al. (2013) in LES with approximate deconvolution subgrid model ~~(ADM, see, Stolz et al., 2001)~~ (ADM, see Stolz et al., 2001), which can be also considered as the model with explicit filtering. In most cases, the suppression of small-scale fluctuations in LES (particularly in those that use a low-order numerical schemes) occurs as a result of combined effect of approximation errors and the subgrid closure. Therefore, the shapes of effective spatial filters of most models can only be determined by aposteriori analysis of the calculation results.

(2) Lagrangian stochastic subgrid/subfilter model

Second, we will apply the subgrid stochastic model proposed in (Shotorban and Mashayek, 2006):

$$du_i^p = \left(-\frac{\partial \overline{p}}{\partial x_i} - \frac{1}{T_L}(u_i^p - \overline{u}_i^{(p)})\right) dt + \sqrt{C_0 \epsilon}\xi_i^p. \tag{28}$$

The parameter C_0 was specified to be equal to 6, because the stochastic part of the model (Eq. 28) is mainly responsible for spatial and time scales in an isotropic inertial subrange of the turbulence. When using dynamic mixed model (Eqs. 17 - 21), a value of ϵ is not calculated directly, and then it is assumed that the dissipation is locally balanced by shear production and buoyancy production or sink. In addition, since this model can produce a local generation of kinetic energy, the averaging in a horizontal plane was performed to avoid negative values of dissipation:

$$\epsilon = \left\langle -\overline{S}_{ij}\tau_{ij} \right\rangle_{xy} + \frac{g}{\Theta_0}\left\langle \vartheta_3^{\Theta} \right\rangle_{xy}, \tag{29}$$

where ϑ_3^{Θ} is the vertical subgrid flux of potential temperature and g/Θ_0 is the buoyancy parameter. Time scale T_L was evaluated as:

$$T_L = (E^{subgr} + E^{subf}) / \left(\frac{1}{2} + \frac{3}{4}C_0\right)\epsilon. \tag{30}$$

Thus, the total unresolved kinetic energy was calculated as the sum of "subfilter" energy

$$E^{subf} = \frac{1}{2}\left\langle (u_i^* - \overline{u}_i)^2 \right\rangle_{xy} \tag{31}$$

and "subgrid" energy:

$$E^{subgr} \approx \frac{1}{2}\int\limits_{kmin_i}^{\infty} S_i(k_i)dk_i \approx \frac{3}{4}C_K'\epsilon^{2/3}\sum_{i=1,3}\left(\frac{\pi}{\Delta_{gi}}\right)^{-2/3}. \tag{32}$$

To evaluate the value E^{subgr} it was supposed that "subgrid" fluctuations belong to quite a wide inertial range with the ~~spectrum $E(k) = C_K\epsilon^{2/3}k^{-5/3}$~~component-wise velocity spectra $S_i(k_i) = C_K'\epsilon^{2/3}k_i^{-5/3}$, and that the minimal ~~wavenumber~~ wavenumbers for these fluctuations ~~$k_{min} = \pi/\Delta_g$ corresponds to a wavelength~~ $kmin_i = \pi/\Delta_{gi}$ correspond to wavelengths in two grid steps. Here, Δ_{gi} is the grid step in the appropriate direction and $C_K' = \frac{18}{55}C_K = 0.5$ is the Kolmogorov constant (here, $C_K \approx 1.5$ is the Kolmogorov constant associated with three-dimensional wavenumbers).

All the values required for a application of this model were linearly interpolated into the particle position everywhere except at heights $z < \Delta_g/2$, where we use the constant values $T_L(\Delta_g/2)$ and $\epsilon(\Delta_g/2)$. This procedure is rather arbitrary, but it does not have large impact on the results due to the small decorrelation time $T_L(\Delta_g/2)$. Besides, there are no physically grounded reasons for the justification of such interpolations in LES because the resolved velocity in the vicinity of surface is greatly corrupted by the approximation errors. Such procedures should be considered as an adjustments depending on the numerical scheme and on the subgrid closure.

(3) ~~Divergent correction of the Eulerian velocity field~~Random displacement subgrid/subfilter model

~~Third, in~~ Third, the RDM specified in Sect. 2.4 will be adopted for the Lagrangian particles subgrid dispersion. In this case we shall use the same subgrid diffusivity $K_h{}^{subgr}$ both for the Eulerian scalars (Eq. 23) and for the particles displacement calculations:

$$dx_i^p = \overline{u}_i^{(p)}dt + \frac{\partial K_s^{subgr(p)}}{\partial x_i}dt + \sqrt{2K_s^{subgr(p)}}\xi_i^p. \tag{33}$$

This model does not contains the arbitrary specified parameters except those which were already used in the Eulerian LES. The coefficient K_s^{subgr} was linearly interpolated into the particle positions at heights $z \geq z_0$ with the assumption that $K_s^{subgr}(x,y,0) = 0$. A constant value $K_s^{subgr}(x,y,z) = K_s^{subgr}(x,y,z_0)$ was used for $z < z_0$.

(4) Divergent correction of the Eulerian velocity field

Finally, in order to find out whether the subgrid mixing is one of the key processes in the dispersion of Lagrangian tracers, we introduced an additional correction to the particle velocities:

$$\boldsymbol{u}_{cor\_div}^{(p)} = \overline{\boldsymbol{u}}^{(p)} + \overline{\boldsymbol{u}}_{div}^{(p)}, \tag{34}$$

where $\overline{\boldsymbol{u}}_{div}$ is the deterministic divergent additive to the velocity field $\overline{\boldsymbol{u}}$:

$$\overline{u}_{div,i} = \frac{\vartheta_i^{sp}}{s_{\cancel{p}}P} \tag{35}$$

with the imposed restriction $\overline{u}_{div,i} = 0$ if ~~$s_p = 0$~~$s_P = 0$. Here, the "subgrid" flux ϑ_i^{sp} is calculated using the same closure as the closure for Eulerian scalars $\overline{s}$, with the only difference that the concentration ~~s_p~~s_P, estimated by the number of particles in a grid cell, is used in ~~formula~~ Eq. (23).The applicability of this procedure ~~is determined by~~ justified because of the large number of particles involved in simulation (in all the cases described below we have at least several dozens of particles in each grid cell).

Correction given by Eqs. (34), (35) does not provide true small-scale mixing, but only introduces an additional "stretching" or "compression" of the small volumes filled with particles and provides concentration fluxes across the borders of grid cells close to "subgrid" fluxes in Eulerian model. Using this correction, we are guaranteed to get a high correlation between the "Eulerian" and "Lagrangian" concentrations (in all our preliminary tests $\left\langle \overline{s}' s'_p \right\rangle_{xy} / \sqrt{\left\langle \overline{s}'^2 \right\rangle \left\langle s'^2_p \right\rangle} \approx 0.9$).

The idea of such a correction was based on the assumption that details of the mechanism of subgrid mixing have a little influence on the statistics of trajectories at sufficiently large distances from the source and at ~~the big~~ long enough time t. It was assumed that the quick mixing on small spatial scales can be implicitly substituted by the approximation errors arising in the procedures of interpolation and by the errors of discrete solution to the advection equation. Correction brings an additional systematic effect to reduce incorrect particle transport by the large eddies.

3.2.2 Simplified velocity interpolation

In preliminary tests it became clear, that trilinear interpolation of each velocity component provides no advantages for footprint calculation in comparison with the following simplified linear interpolation on a staggered grid:

$$
\begin{aligned}
u^{(p)} &= \overline{u}_{i-1/2,j,k} \frac{x_{i+1/2,j,k} - x^p}{\Delta x} + \overline{u}_{i+1/2,j,k} \frac{x^p - x_{i-1/2,j,k}}{\Delta x}, \\
v^{(p)} &= \overline{v}_{i,j-1/2,k} \frac{y_{i,j+1/2,k} - y^p}{\Delta y} + \overline{v}_{i,j+1/2,k} \frac{y^p - y_{i,j-1/2,k}}{\Delta y}, \\
w^{(p)} &= \overline{w}_{i,j,k-1/2} \frac{z_{i,j,k+1/2} - z^p}{\Delta z} + \overline{w}_{i,j,k+1/2} \frac{z^p - z_{i,j,k-1/2}}{\Delta z},
\end{aligned}
\tag{36}
$$

where position (i, j, k) is the center of a grid cell containing the particle. Trilinear interpolation and interpolation given by Eq. (36) provide nearly the same concentration fluxes across the borders of a grid cell, but the latter does not result in additional substantial smoothing of velocity. An exception was made for the grid layer closest to the surface ($z^p < \Delta_g$) where the mean velocity components were adjusted according to the Monin-Obukhov similarity theory with the dimensionless functions taken from (Businger et al., 1971).

4 LES of stable ABL and footprint calculations

4.1 The setup of numerical experiment

Stable boundary layer at the latitude 73° N in ~~close to the~~ almost steady state conditions was considered. The calculations were carried out according to the GABLS scenario (Beare et al., 2006), with the difference that the geostrophic wind $\boldsymbol{U}_g$ has been rotated 35~~^{o}~~° clockwise such that the wind direction near the surface approximately coincides with the axis x. The duration of runs is 9 hours. The initial wind velocity coincides with geostrophic velocity $|\boldsymbol{U}_g|$ = 8 m/s. The initial potential temperature $\overline{\Theta}$ is equal to the surface temperature $\Theta_s|_{t=0} = 265$ K up to the height 100 m and increases linearly with the rate $d\Theta/dz = 0.05$ K/m if $z > 100$ m. During the calculations, the surface temperature decreases linearly with time: $d\Theta_s/dt = -0.25$ K/hour. Dynamical and thermal roughness parameters z_0 and $z_{0\Theta}$ are set to 0.1 m. The calculations were performed at the equidistant grids with steps $\Delta_g = 2.0$ m, 3.125 m, 6.25 m and 12.5 m. The size of the horizontally periodic computational domain was equal to $400 \times 400 \times 400$ m^3. The last hour of numerical experiments was used for averaging ~~of~~ the results and subsequent analysis.

This setup is based on the observation data (see, Kosoviĉ and Curry (2000)). As it was shown in (Beare et al., 2006), the LES results obtained under the same conditions with the different models converged with the higher grid resolutions. Later, this case was used for testing the LES models e.g. in (Maronga et al., 2015; Zhou and Chow, 2012; Bhaganagar and Debnath, 2015) and many others and for the improvement of subgrid modelling e.g. in (Basu and Porté-Agel, 2006; Zhou and Chow, 2011; Kitamura, 2010). The LES model presented here was tested earlier under the non-modified setup of GABLS in (Glazunov, 2014), where the turbulent statistics above a flat surface and above an urban-like surface were investigated. In all of these studies, LES results were in agreement with the known similarity relationships for the stable ABL. This allows to consider the LES data for GABLS as a reference case for testing of the approaches utilizing the statistical averaging of the turbulence (e.g., see Cuxart et al. (2006), where the intercomparison of single-column models was performed). Several of nondimensional relationships in stable ABL were collected and presented in (Zilitinkevich et al., 2013). Considered case is also included in the LES database for this study and fits well with the different stability regimes after the appropriate normalization. Therefore, the results obtained in this particular case can be generalized for many cases due to similarity of the stable ABLs. Besides, the presented simulations are easily reproducible and they can be repeated using any LES model which contains the Lagrangian particle transport routines.

The mean wind velocity and the potential temperature, calculated with the different spatial steps Δ_g, are shown in Fig. ~~1.~~ 2 The model slightly overestimates the height of the boundary layer at coarse grids, however, the wind velocity near the surface is approximately the same in all runs. As one can see from the Fig.2, the results of simulation are in good agreement with the results from other LES presented in (Beare et al., 2006) (see, http://gabls.metoffice.com for more information). Mean wind profile computed in accordance with (Högström, 1996) is shown in Fig. 2 by the vertical dashes, in the surface layer part of the domain this "standard" profile for the stable conditions almost coincides with the longitudinal velocity obtained in LES.

Passive Lagrangian tracers were transported simultaneously with the calculations of dynamics. Each particle, when reaching a lateral boundary of domain, is returned from the opposite boundary in accordance with periodic conditions. The reflection condition is used at the ground. The particles are ejected at the height $z_0 = 0.1$ m (one particle per each grid cell adjacent to surface) with regular time intervals $\Delta t_{ej} = 1$ s. The position of the new particle within a grid cell is set randomly with uniform probability. The ejection of particles takes place continuously from the seventh to the ninth hour of the experiment.

To limit the number of the particles involved in the calculation the absorption condition is applied at the height of 100 meters within ABL. It was verified previously that the upper boundary condition does not have a large impact on the results of calculations of footprints for the heights z_M up to 60 m and for the distances $x - x_M$ considered in this paper (see Appendix A1 and the test with LSM shown by the orange curves in 12). This formulation of numerical experiment allows direct comparison of the concentration of particles $\cancel{s_p}$ s_P, estimated by Eq. (7), and the scalar concentration $\overline{s}$, calculated by the Eulerian approach (Eq. 6). For this purpose, additional scalar $\overline{s}$ is calculated from 7-th till 9-th hour with a constant surface flux $F_s = const = 1$, zero initial condition and the Dirichlet condition $\overline{s} = 0$ at the altitude 100 m.

In the last hour of simulation the averaged number of particles in each cell of the grid near the surface was approximately equal to 700-800, 350-400,180-200 and 110-130 for grids steps Δ_g=12.5 m, 6.25 m, 3.125 m and 2.0 m, respectively. Having such number of particles one can estimate the concentration $s^p(\boldsymbol{x}_{i,j,k}, t_m)$ at each time step, where $\boldsymbol{x}_{i,j,k}$ is the center of a grid cell. It was assumed, that each particle contributes to the concentration $\cancel{\tilde{s}_p(\boldsymbol{x}_{i,j,k})}$ $\tilde{s}_P(\boldsymbol{x}_{i,j,k})$ with the weight $r^p_{i,j,k} = (V^p \bigcap V_{i,j,k})/V_{i,j,k}$, where V^p is rectangular neighborhood of its position with the side Δ_g, $(V^p \bigcap V_{i,j,k})$ is the volume of intersection with grid cell, $V_{i,j,k}$ is the cell volume. This averaging is close to the filtering of Eulerian scalar (Eq. 24). The additional normalization is performed as follows: $\cancel{s_p = \tilde{s}_p \Delta t_{ej}/\Delta_z}$ $s_P = \tilde{s}_P \Delta t_{ej}/\Delta_z$. The concentration $\cancel{s_p}$ s_P corresponds to the number of particles in one cubic meter under the condition that one particle per square meter per second is ejected near the surface. Concentration $\cancel{s_p}$ s_P is numerically equal (excluding errors, determined by different methods of transport) to the concentration of the scalar field $\overline{s}$ if scalar surface flux $F_s = 1$.

Figure ~~2~~ 3 shows the resolved and the parameterized components of flux $\langle w's' \rangle$ in runs with different grid steps. It is seen that the calculation time is not large enough to reach a steady state (the total flux is not constant with the hight, so the average concentration continues to grow during the last hour). However, it was checked that the flux footprint close to the sensor is not affected by nonstationarity. Besides, we can compare the values of $\overline{s}$ and $\cancel{s_p}$ s_P, because the boundary and initial conditions are identical for them.

The unresolved fraction of the flux $F_s^{sbg} = \langle \vartheta_3^s \rangle$ is an essential part of the total flux $F_s^{tot} = \langle \overline{s}\, \overline{w} \rangle + \langle \vartheta_3^s \rangle$. Accordingly, the vertical transport of Lagrangian particles by resolved velocity $\overline{\boldsymbol{u}}$ may be significantly underestimated. Thus, we have "hard" enough test to verify Lagrangian transport in LES with poorly-resolved velocity field.

4.2 Sensitivity of LES results on methods of particle transport and spatial resolution

4.2.1 Footprint calculation with limited application of subgrid stochastic modelling in LES

Figure ~~3~~ 4 shows the scalar flux footprints averaged in crosswind direction $f_s^y(x_M - x, z_M)$ computed by different methods and with different grid steps. ~~All footprints are normalized so that~~ $\cancel{\int f_s^y(x)dx = 1.}$

In all cases, we have avoided using the subgrid scale stochastic modelling except calculating the velocity of the particles located within the first grid layer $z^p < \Delta_g$. For the curves marked "st_1l"~~-~~, the resultant velocity of the particles near the surface was calculated as follows:

$$\boldsymbol{u}^p = \boldsymbol{u}^{(p)} + r(1 - z^p/\Delta_g)\boldsymbol{u}''^p, \tag{37}$$

where the function $r(z^p)$ is defined as $r(z^p) = (1 - z^p/\Delta_g)$ if $z_p < \Delta_g$, $r(z^p) = 0$ $z_p \geq \Delta_g$ and $\boldsymbol{u}''^p$ is the random velocity component, calculated using the ~~model (~~stochastic subgrid model (Eq. 28). To take into account the memory effects in Langevin equation, the ~~model (28)~~ stochastic model was implemented inside the layer $z^p < 3\Delta_g$, so (because of the smallness of scale T_L) this procedure does not lead to significant distortions in the random component of the velocity.

If the particles are advected by the filtered velocity $\overline{\boldsymbol{u}}$ without any correction then the vertical mixing is too weak and the maxima of footprints f_s^y are strongly underestimated and shifted at the large distances from the sensor position. Divergent correction of Eulerian velocity (Eqs. 34, 35) partially improves the results (squares in Fig. ~~3~~ 4a,b). For example, maximum of footprint f_s^y for the sensor height z_M=30 m (near the fifth computational level) occurs to be close to the maxima of footprints, computed at fine grids, but it is still shifted. Thus, the correction (Eq. 34, 35) alone is not sufficient. Primarily this is due to the weak mixing below the first computational level, where the contribution of the subgrid velocity is crucial.

The inclusion of stochastics within the first layer improves the result (dashed curves in Fig. ~~3~~ 4a,b). However, it is not enough to determine footprints at altitudes comparable to the grid spacing.

The advection of particles by the velocity $\boldsymbol{u}^*$ leads to close matching of functions f_s^y, calculated with different grid steps (solid lines of different thickness in Fig. ~~3~~ 4c,d). The differences between these footprints are not significant from a practical point of view, and can be equally explained by means of the incorrect Lagrangian particles transport, as well as by means of the insufficiently accurate solution to the Eulerian equations on the coarse grid.

4.2.2 Spatial variability of scalar concentration inferred by Eulerian and Lagrangian methods

While the particles were advected by the "defiltered" ~~–~~flow we have also used the correction (Eqs. 34, 35). In this case the subgrid diffusion coefficient was reduced twice $K_h^{*subgr} = cK_h^{subgr}$, $c = 0.5$ (coefficient $c = 0.5$ was chosen because about a half of subgrid flux can be restored using "defiltering" : $\langle \overline{s} w^* \rangle - \langle \overline{s}\, \overline{w} \rangle \approx 0.5 \, \langle \vartheta_3^s \rangle$). We note that when the particles are advected by velocity $\boldsymbol{u}^{*(p)}$, then the presence or absence (crosses in Fig. ~~3~~ 4c,d) of correction has no significant effect on the function f_s^y. Nevertheless, this procedure may be useful for the following reasons.

In the inertial range of three-dimensional turbulence along with the kinetic energy the variance of a passive scalar concentration is transferred from large scales to small scales with the formation of the spatial spectrum $\cancel{S_s = K_s \epsilon_s \epsilon^{-1/3} k^{-5/3}}$ $S_s \sim \epsilon_s \epsilon^{-1/3} k^{-5/3}$ (see (Obukhov, 1949)) (here ϵ_s is the dissipation rate of the variance of concentration, caused by molecular diffusion). Lagrangian transport of particles by a divergence-free velocity field $\boldsymbol{u}^*$ with the truncated small-scale spectrum is equivalent to Eulerian advection of concentration s without any dissipation. The absence of subgrid-scale part of the velocity spectrum will lead to reduction of the forward cascade and to the accumulation of variance σ_{sp}^2 in vicinity of the smallest resolved scales.

Figure ~~4~~ 5a shows the variances of "Eulerian" concentration $\sigma_s^2(z) = \langle \overline{s}'^2 \rangle_{xyt}$ computed at different grids, and the variances of "Lagrangian" concentration $\cancel{\sigma_{sp}^2(z) = \langle s_p'^2 \rangle_{xyt}}$ $\sigma_{sp}^2(z) = \langle s_P'^2 \rangle_{xyt}$. One can see that if particles are advected by the velocity $\boldsymbol{u}^{*(p)}$ (crosses), variance σ_{sp}^2 is much larger than σ_s^2. If the velocity $\boldsymbol{u}^{*(p)} + \boldsymbol{u}_{div}^{(p)}$ is used (black circles), the values of σ_{sp}^2 and σ_s^2 become closer to each other. Besides, the correction (Eqs. 34, 35) increases the correlation corr$\cancel{(\overline{s}, s_p) = \langle \overline{s}' s_p' \rangle_{xyt} / (\sigma_{sp}\sigma_s)}$ $(\overline{s}, s_P) = \langle \overline{s}' s_P' \rangle_{xyt} / (\sigma_{sp}\sigma_s)$ of two fields calculated by means of "Eulerian" and "Lagrangian" approaches (5b).

One can expect that in more complicated cases (e.g., the turbulent flow around geometric objects and the formation of quasi-periodic eddies) the accumulation of small-scale noise in the concentration field may lead to the incorrect advection of concentration by the resolved eddies. This effect may be also important for inertial particles when the nonphysical variance of concentration can directly affect dynamics. In ~~the~~ additional tests it was found that ~~correction (34,~~ the correction given by Eqs. (34) and (35) prevents ~~particles~~ particle stagnation in zones with unresolved turbulence ~~while~~ during the modelling of urban-like environment. Thus, this correction is desirable for a number of reasons as a practical replacement of subgrid stochastics which requires large computer resources.

4.2.3 Particle advection and footprint determination in LES with subgrid LSM

One can obtain footprints close to those presented at Fig. ~~3~~ 4 by means of application of the stochastic subgrid model (Eqs. 28-32). The calculations for this model have been carried out at the grids with steps 3.125 m, 6.25 m and 12.5 m (solid lines ~~of different thickness~~ in Fig. ~~5~~ 6a,b). One can note the defect of the stochastic subgrid modelling in LES, which can not be detected by studying of the mean characteristics. In the previous subsection the recovered "subfilter" ~~-~~part of velocity $\boldsymbol{u}'' = \boldsymbol{u}^* - \overline{\boldsymbol{u}}$ and so the subfilter Lagrangian velocity $\boldsymbol{u}''^{(p)}$ were highly correlated with the resolved velocity $\overline{\boldsymbol{u}}$ in time and space. This is due to the specifics of spatial filter (Eq. 24) used for the recovering given by Eqs. (25,26). This filter has a smooth transfer function in spectral space. The analogous effects of non-ideal filters in LES which lead to the high correlations between modelled and measured turbulent stresses were obtained and discussed earlier in Liu et al. (1994) and Meneveau and Katz (2000), where the laboratory data of turbulent flows were studied. On the contrary, additional mixing in the stochastic model (Eqs. 28-32) is due to random fluctuations, which are not related to $\overline{\boldsymbol{u}}$ strictly. When one uses coarse grids, the energy of these Lagrangian fluctuations should be large enough to restore mixing in vertical direction. This is accompanied by an excessive suppression of the variability of concentration ~~s_p~~ s_P near the surface, where the contribution of subgrid mixing is large (stars in Fig. ~~4~~ 5a). The correlation between "Eulerian" ~~-concentration~~ and "Lagrangian" ~~concentarion~~ concentration is reduced simultaneously (see Fig. ~~4~~ 5b). Probably, this defect of employed Lagrangian stochastic model is connected to the horizontal averaging in evaluation of "subgrid" dissipation and energy. Nevertheless, this result shows that in some cases the stochastic subgrid modelling can prevent correct reproduction of the resolved spatial variability of particle concentration in LES along with improvement of the mean transport.

4.2.4 Footprints in LES with subgrid RDM and the comparison of different methods

In Fig. 7 footprints obtained in LES with intermediate resolution Δ_g = 6.25 m are shown. We choose this resolution because LES dynamics is still reproduced sufficiently well, but the effects from the subrgrid/subfilter Lagrangian parametrization are already clearly visible. In addition to the approaches which were already discussed above we applied the subgrid RDM (Eq. 33) and the subgrid RDM in combination with the velocity recovering (Eqs. 25,26) and the correction (Eqs. 34, 35). In the former case we restricted the activity of the subgrid RDM by the multiplying of the diffusivity coefficient $K_h^{subgr(p)}$ in (Eq. 33) on the following ramp function $r(z^p) = (1 - z^p/\Delta_g)$ if $z^p \leq \Delta_g$ and $r(z^p) = 0$ if $z^p > \Delta_g$.

Generally, results are in close agreement with the results of LES with the fine grid except of some details. One can see the intrinsic defect of the RDM when it is applied to the dispersion of particles in near field of a source. Namely, as the RDM is the approximation of the the diffusion process with the infinite speed of the signal prorogation, this model overestimates values of

f_s^y in the vicinity of the measurements point location (see Fig. 7d, where this effect is highlighted in the logarithmic scale). Nearly the same effect was obtained in Wilson (2015) (see Figs. 1-3 in its paper, where the footprints from RDM are also shifted left in comparison with the other models). It was also observed that, along with the overestimated vertical mixing, subgrid RDM leads to the propagation of some portion of the particles in the upwind direction (the function $f_s^y(x_M - x, z_M = 10)$ has the small but the positive values if $x_M - x < 0$). In LES with the intermediate resolution the mentioned overestimated mixing exceeds the similar effect in RDM standing alone (see Sect.5.3), because the coefficient K_b^{subgr} is highly variable in time and space and it can attend even larger local values then the magnitude of the averaged turbulent diffusivity K_b. At the higher levels of $z_M = 30$ m and $z_M = 60$ m, the footprints are formed as a results of averaging of the turbulent motions over the large spatial distances and over long temporal intervals, and the diffusion approximation becomes to be acceptable. As it will be shown in Sect.5.3, RDM applied alone gives a very close results to the results of LSMs in this particular case of the stable ABL.

In contrast to the subgrid LSM and to the methods of velocity correction proposed above, the advantage of the subgrid RDM consists in the absence of the arbitrary prescribed parameters and in the absence of the need to involve the additional suppositions. In terms of Eulerian statistics, this model is identical to the Eq. (6) (in the limit $dt \to 0$ and with the precision defined by the spatial approximations). From this point of view subgrid RDM can be considered as the "ideal" model, because it is determined by the coefficients which are consistent with LES dynamics of the stratified flow (the same subgrid diffusivity is used for the potential temperature which defines the buoyancy and the interchanges between the kinetic and the available potential energy). Thus, we have one more confirmation of the validity of the results, except of the invariance with respect to the grid steps.

The impact from the subgrid RDM is reduced when it is applied within the first grid layer only. In this case, the footprints are approximately the same as the footprints computed using the other approaches.

4.3 Two-dimensional footprints

The trajectories of large number of particles ($\sim 1.8 \times 10^8$) were simultaneously computed in LES with grid step 2.0 m. Accordingly, one can get statistically grounded estimation of two-dimensional footprint functions $f_s(x - x_M, y - y_M, z_M)$. These functions, computed for the sensor heights z_M=10 m and z_M=30 m are shown in the Fig. ~~6~~ 8a,b. One can see, that the area with the negative values of footprint exists. The negative values of footprints are typical (e.g., Cai et al., 2010; Steinfeld et al., 2008) for the convective boundary layer due to fast upward advection by the narrow thermal plumes and slow downward advection in the surroundings. Here, the negative values of the function f_s are connected to the Ekman spiral and to the mean transport of the particles elevated to large altitudes in the direction perpendicular to the near-surface wind. The negative values of scalar flux footprint show that the vertical turbulent transport of the scalar emitted in the relevant area is basically directed from the upper levels down to the surface. For example, the positive surface concentration flux in this area will lead to negative anomaly of the turbulent flux measured in the sensor position. This does not contradict the diffusion approximation of the turbulent mixing, because mean crosswind advection at the upper levels can produce the positive vertical concentration gradient to the right of near-surface wind.

The contribution of the negative part of the flux to the "measured" flux is significant, as shown in Fig. ~~6~~ 8c,d, where cumulative footprints, defined as

$$F(x^d, z_M) = \int\limits_{-\infty}^{x^d} f_s^y(x', z_M)dx', \tag{38}$$

are separated into positive and negative parts $F(x_M - x, z_M) = F^+ + F^-$.

5 Stochastic modelling and the comparison with LES

5.1 Preparation of turbulence data from LES for LSMs and RDMs

The LES results with grid step Δ_g=2.0 m were used for data preparation. To apply LSM (Eqs. 8, 9) the following Eulerian characteristics are required: the mean wind velocity components $\langle u \rangle$ and $\langle v \rangle$, the second moments $\langle u_i' u_j' \rangle$ and the dissipation ϵ. Stochastic models are even more sensitive to some of these characteristics than the advection of particles in LES. For example, the underestimated values of the turbulent kinetic energy in LES are the consequence of the suppression of small eddies. Nevertheless, these eddies exert relatively small influence on the mixing of scalar, because the effective eddy diffusivity associated with them $K_h^{small} \sim E_{small}^{1/2} l^{small}$ is not large due to small spatial scale. However, the turbulent energy which is substituted into LSM affects results independently of the scale and has to be evaluated with good accuracy.

5.1.1 Mean velocity

Mean wind velocity at the height $z_0 < z \leq \Delta_g$ was computed using log-linear law:

$$\langle u_i \rangle = U_* \left(\frac{1}{\kappa} ln \left(\frac{z}{z_0} \right) + C_m \frac{z}{L} \right) \times \left. \frac{\langle u_i \rangle}{|\boldsymbol{u}|} \right|_{z=\Delta_g/2}, \quad C_m = 5, \tag{39}$$

and $\langle u_i \rangle = 0$ at $z < z_0$. Here, U_* is the friction velocity, $\kappa = 0.4$ denotes the von Karman constant, L is the Obukhov length at the surface ~~(note~~

$$L = -\frac{U_*^3 \Theta_0}{g Q_s}, \tag{40}$$

where Q_s is the kinematic potential temperature flux at the surface, $g = 9.81$ m/s^2 is the acceleration of gravity and $\Theta_0 = 263.5$ K is the reference potential temperature (as it was prescribed in presented simulations and in Beare et al. (2006)). Note, that the von Karman constant is not included in the definition of the length L here and later ~~).~~ (this alternative definition of the Obukhov length is used along with the traditional one, see e.g. Zilitinkevich et al. (2013) Eq.(41)). The linear interpolation of velocity was used if $z > \Delta_g$.

5.1.2 Momentum fluxes

The fluxes $\langle u_i' u_j' \rangle = \langle \overline{u}_i' \overline{u}_j' \rangle + \tau_{ij}^{mix}$ $(i \neq j)$ were interpolated linearly and additionally smoothed everywhere in the domain. These fluxes are shown in Fig. ~~8~~ 9a.

5.1.3 Variances of velocity components

The variances of velocity components $\sigma_i^2 = \langle u_i'^2 \rangle$ were estimated by formula:

$$\sigma_i^2 = \langle (u_i^{*\prime})^2 \rangle_{x,y,t} + \frac{2}{3} E^{subg}, \tag{41}$$

where E^{subg} is the subgrid energy (Eq. 32) and $\langle (u_i^{*\prime})^2 \rangle$ are the variances of recovered velocity components. The vertical velocity variance has the greatest impact on the functions f_s^y. Figure ~~8~~ 9b shows the comparison of evaluated normalized RMS $\tilde{\sigma}_w = \sigma_w / |\tau|^{1/2}$ (solid line) with the SHEBA data (symbols; see description in (Grachev et al., 2013, fig. 15b); data kindly provided by Dr A. Grachev). The data are shown in dependence on nondimensional stability parameter $\xi = \kappa z / \Lambda$, where

$$\Lambda(z) = -\frac{|\tau|^{3/2} \Theta_0}{gQ} \tag{42}$$

is the local Obukhov length, determined using values of fluxes of momentum $|\tau|$ and temperature Q at the given height z (local scaling in stable ABL (Nieuwstadt, 1984)). The measurements suggest that the mean value of normalized RMS $\tilde{\sigma}_w \approx 1.33$ if value ξ is small. Figure ~~8~~ 9b shows, that our estimation of RMS is slightly less than the measured values in the interval $0.03 < \xi < 0.2$. Respectively, the final values of vertical velocity variance designed for the substitution in stochastic models were corrected as follows: $\sigma_w^2 = 1.33^2 |\tau|$ if $\xi < 1$. At the higher levels the estimation (Eq. 41) was applied.

The final estimations of the variances of velocity components are shown in Fig. ~~8~~ 9c by the solid lines. Dashed lines are the filtered resolved velocity $\overline{u}_i$ variances. The estimation of the variance σ_w^2 using ~~formula~~ Eq. (41) is shown by the circles. One can see that significant parts of variances were not reproduced explicitly in LES and were recovered using ~~abovementioned~~ above mentioned assumptions.

5.1.4 Turbulent energy dissipation rate

Usual interpolation is not applicable to the calculation of dissipation rate near the surface, where $\epsilon \sim 1/z$. Besides, the values of dissipation $\epsilon_{\Delta k}$ computed in LES at the levels $z_k = (k - 1/2)\Delta_g$ are approximately equal to the averaged values inside the layers $(k-1)\Delta_g < z \leq k\Delta_g$, but not to the physical dissipation at given altitudes. Under the assumption that $|\tau|$ is constant with height and neglecting the stratification inside first layer, one can get the following corrected value of ϵ at the height $z = \Delta_g/2$:

$$\epsilon|_{z=\Delta_g/2} \approx 2\epsilon_{\Delta 1} / ln(\Delta_g / z_0) \tag{43}$$

Additional analysis showed that, if $z < 0.25 z_i$, then the local balance of turbulent ~~energy~~ kinetic energy (TKE) is well satisfied: $\epsilon \approx S + B$, where S and B are shear and buoyancy production. Therefore, the nondimensional dissipation can be approximated by a formula

$$\tilde{\epsilon} = \frac{\epsilon z}{|\tau|^{3/2}} = \phi_m\left(\frac{z}{\Lambda}\right) - \frac{z}{\Lambda} = \frac{1}{\kappa} + (C_m^\Lambda - 1)\frac{z}{\Lambda}, \tag{44}$$

where

$$\phi_m = \left|\frac{\partial\langle\boldsymbol{u}\rangle}{\partial z}\right| \frac{z}{|\tau|^{1/2}} = \frac{1}{\kappa} + C_m^\Lambda \frac{z}{\Lambda} \tag{45}$$

is the nondimensional velocity gradient; $C_m^\Lambda = 5$, according to the observation data (e.g., Grachev et al., 2013) and LES results (e.g., Glazunov, 2014). Here, the assumption is used that the shear $\partial\langle\boldsymbol{u}\rangle/\partial z$ and the stress τ are collinear. Previous LES studies of stable ABL (e.g., Beare et al., 2006) also give neglectfully small values of the transport terms in TKE balance. The experimental confirmation of the validity of Eq. (44) can be found in (Grachev et al., 2015), where the dissipation in stable ABL was estimated using the spectral analysis of longitudinal velocity in inertial range. In accordance with this paper: $\tilde{\epsilon} \approx \phi_m$, that is almost indistinguishable from Eq. (44) within the accuracy of the experimental data and the ambiguity of the method of dissipation evaluation.

Discrete values of nondimensional dissipation $\epsilon_{\Delta k} z_k/|\tau|^{3/2}$ are shown in Fig. ~~9~~ 10a by circles. Dashed straight line is the universal function (Eq. 44). One can see, that the correction (Eq. 43) makes the dissipation values closer to the function (Eq. 44). Finally, the profile of dissipation $\epsilon_{cf}(z)$ for LSM was corrected as follows (see Fig. ~~9~~ 10b). The dissipation was set to be constant below some height z_e, and was replaced by universal function $\epsilon = \tilde{\epsilon}|\tau|^{3/2}/z$ up to the level with $z/\Lambda = 1$. The height z_e was chosen in a such way to equalize values of the dissipation averaged in a layer $0 \le z \le \Delta_g$ and the dissipation $\epsilon_{\Delta 1}$. Figure ~~9~~ 10b shows that the corrected dissipation ϵ_{cf} (solid line) is very close to "discrete" dissipation $\epsilon_{\Delta k}$ (circles), except for the first computational level.

5.1.5 Diffusion coefficients

Random ~~displacements~~ displacement model (Eq. 15) requires the estimation of eddy diffusion coefficient K_s. Note, that due to anisotropy, one should use tensor diffusivity K_s^{ij} in a general case. Neglecting this fact, let us assume that the principal axes of the tensor K_s^{ij} are aligned with the coordinate axes. The correspondent coefficients K_s^{ww}, K_s^{uu} and K_s^{vv} (see Fig. ~~8~~ 9d) can be calculated as follows:

$$K_s^{ww} = -\langle w's'\rangle / \left(\frac{\partial\langle\overline{s}\rangle}{\partial z}\right), \tag{46}$$

$$K_s^{uu} = \frac{\sigma_u^4}{\sigma_w^4} K_s^{ww}, \quad K_s^{vv} = \frac{\sigma_v^4}{\sigma_w^4} K_s^{ww}. \tag{47}$$

The horizontal eddy diffusivities K_s^{uu} and K_s^{vv} are estimated taking into account the expression (13).

One can see that the formula (Eq. 13) provides a good approximation for the coefficient K_s^{ww} if one sets the value $C_0 = 6$. We note, that the data of LES were substantially corrected to get this estimation. Very fine ~~grids~~ grid simulations are needed to verify and ~~to~~ justify the given value. There is no guarantee that this constant is actually universal under different stratification in the ABL.

5.2 Specification of LSMs and RDMs tested against LES

The following stochastic models were tested using the data prepared as described above.

(1) RDM0 is the random displacements model with uncorrelated components. Particle position is computed by the formula similar to Eq. (15) but with direction-dependent coefficients (see, Eqs. (46), (47) and Fig. ~~8~~ 9d). The components of the Gaussian random noise satisfy the ~~condition~~ Eq. (10).

(2) RDM1 differs from RDM0 by using the noise with inter-component correlations:

$$\left\langle \xi_i^p(t)\xi_j^h(t+t')\right\rangle = \frac{\left\langle u_i' u_j'\right\rangle}{\sigma_i\sigma_j}\delta_{ph}\delta(t')dt, \tag{48}$$

where $\sigma_i = \left\langle {u'}_i^2\right\rangle^{1/2}$.

(3) LSM0 is the Lagrangian stochastic model without WMC:

$$d{u'}_i^p = -\frac{{u'}_i^p}{T_L^i}dt + \sqrt{C_0\epsilon}\xi_i^p, \quad T_L^i = \frac{2\sigma_i^2}{C_0\epsilon}. \tag{49}$$

(4) LSM1 is based on the one-dimensional well-mixed model:

$$dw^p = \left(-\frac{w^p}{T_L^w} + \frac{1}{2}\frac{\partial\sigma_w^2}{\partial z}\left(1+\frac{(w^p)^2}{\sigma_w^2}\right)\right)dt + \sqrt{C_0\epsilon}\xi_3^p, \quad T_L^w = \frac{2\sigma_w^2}{C_0\epsilon}, \tag{50}$$

supplemented by uncorrelated horizontal mixing similar to Eq. (49) with the appropriate variances σ_u^2 and σ_v^2 .

(5) LSMT is three-dimensional Lagrangian stochastic model satisfying WMC, which is proposed by Thomson (1987). For the incompressible turbulent fluid in a steady state and under the condition of zero mean vertical velocity this model (Thomson, 1987, formula (32)) reads:

$$\begin{aligned} a_i^p &= -\frac{1}{2}\delta_{ij}C_0\epsilon(\tau^{-1})_{ik}{u'}_k^p + \frac{1}{2}\frac{\partial\tau_{il}}{\partial x_l} + \frac{\partial\left\langle u_i^{(p)}\right\rangle}{\partial x_j}{u'}_j^p + \frac{1}{2}(\tau^{-1})_{lj}\frac{\partial\tau_{il}}{\partial x_k}{u'}_j^p{u'}_k^p, \\ d{u'}_i^p &= a_i^p dt + \sqrt{C_0\epsilon}\xi_i^p, \end{aligned} \tag{51}$$

where τ^{-1} is the tensor inverse to the stress tensor.

The setups of numerical experiments with RDMs and LSMs were close to particle advection conditions in LES (absorbtion at the altitude 100 m, ejection at $z_0 = 0.1$m and reflection at $z = 0$). The particles were generated continuously within two hours of modelling. The last hour was used for averaging. The models LSM0 and LSM1 use the value $C_0 = 6$. Three-dimensional model LSMT was applied with $C_0 = 6$ and $C_0 = 8$.

5.3 Modelling results

Figure ~~10 shows one-dimensional~~ 11 shows crosswind-integrated footprints f_s^y and the corresponding cumulative footprints F, computed by LES (bold solid lines, Δ_g=2.0 m) and by stochastic models described above. Footprints are shown for the sensor heights $z_M = 10$, 30 and 60 m.

The models RDM0, RDM1 and LSM1 provide very similar results. Faster mixing is observed in stochastic models below the altitude z_M = 10 m in comparison to LES. These differences are not crucial and are compensated in a cumulative footprints at the distances $x - x_M \sim 1000$ m. The differences can be explained either by insufficient subgrid mixing in LES or by inexact procedure of the data preparation for stochastic modelling. Very weak sensitivity of the models with respect to correlations of particle velocity components is observed as well. Thus, the results close to LES were obtained in stochastic models having the "diffusion limit" with the same or close vertical diffusion coefficient. The significant advantages of LSMs compared to RDMs were not observed in this particular flow.

The substantial disagreements to LES were obtained using three-dimensional Thomson model (Eq. 51) with $C_0 = 6$ and the model LSM0. The last one is designed for the isotropic turbulence and does not satisfy WMC under the conditions considered here. This model leads to overestimated mixing, and such bias does not vanish at large altitudes.

LSMT (Eq. 51) was proposed in (Thomson, 1987) as one of the possible ways to satisfy WMC in three dimensions. In our simulations the error of LSMT is substantial and grows with sensor height. This was shown by Sawford and Guest (1988), who derived the diffusion limit of Thomson's multidimensional model for Gaussian inhomogeneous turbulence and showed that the implied effective eddy diffusivity for vertical dispersion is:

$$K_s = \frac{2(\sigma_w^4 + \langle u'w' \rangle^2)}{C_0 \epsilon}. \tag{52}$$

Taking into account this expression and Eq. (13) which is valid for the one-dimensional LSM, one can estimate the appropriate value of C_0 for LSMT under the conditions considered here: $C_0 \approx 6(1.33^4 + 1)/1.33^4 \approx 8$ (we assume that $\sigma_w / |\langle u'w' \rangle|^{1/2} \approx \sigma_w / |\tau|^{1/2} \approx 1.33$). The results of LSMT with $C_0 = 8$ are in a close agreements with the results of other stochastic models and with the results of LES (open triangles in Fig. ~~10~~ 11a,c,e).

Turbulent Prandtl Pr and Schmidt Sc numbers computed using Eulerian approach are shown in Fig. ~~11~~ 12a. These numbers coincide and are approximately equal to 0.8 up to the altitude slightly less then 100 m, where the boundary condition for a scalar is applied. Schmidt numbers Sc were calculated also using the concentrations and the fluxes of Lagrangian particles. The models RDM0 and LSM1 provide the values of Sc close to the results of Eulerian model. Calculations by LSMT ($C_0 = 6$) result in $Sc \approx 0.5 - 0.6$, that is also the sign of the overestimated vertical mixing.

Two-dimensional footprints $f_s(x - x_M, y - y_M, z_M)$, computed by the models RDM0, RDM1 and LSM1 (~~pictures~~ figures are not shown here) were very close to LES results presented in Fig. ~~6~~ 8. In particular, this fact argues that the mechanism of formation of the region with negative values of f_s has a simple nature, which can be easily reproduced in the framework of the diffusion approximation.

The ~~cross-wind~~ crosswind mixing can be characterized by RMS of transversal coordinates of the particles depending on the mean distance from the source: $Y'^p(X^p) = \left\langle (y^p - Y^p)^2 \right\rangle^{1/2}$, where $X^p = \langle x^p \rangle$ and $Y^p = \langle y^p \rangle$ are the mathematical expectations of the particle position. Functions $Y'^p(X^p)$ are shown in Fig. ~~11~~ 12b. The models RDM0, RDM1, LSM1 and LSMT (with $C_0 = 6$) result in close horizontal dispersion. All the stochastic models predict slightly less intensive mixing in comparison to LES, that can be a consequence of the inaccurate data preparation algorithm, as well. If one neglects the anisotropy of eddy diffusivity than this dispersion would be substantially underestimated (see short-dashed line in Fig. ~~11~~ 12b, computed by RDM with the coefficients $K_s^{uu} = K_s^{vv} = K_s^{ww}$). One can see, that the choice $C_0 = 8$ in LSMT (open triangles) does not improve its overall performance because the improved vertical mixing is accompanied by the reduced dispersion of particles in the horizontal direction.

Wind direction rotation leads to widening of concentration trace from the point source (see thin dashed line in Fig. ~~11~~ 12b, computed with one-dimensional LSM). At larger distances from the source in the Ekman layer the crosswind dispersion of pollution should be defined by the joint effect of the wind rotation and vertical mixing, but not by the horizontal turbulent mixing.

6 Validation of ~~analytical~~ footprint parameterisations based on scaling approach

Footprint parameterisations that are assumed to be valid for a broad range of ~~boundary layer~~ ABL conditions and measurement heights ~~over the entire planetary boundary layer~~ were proposed in (Kljun et al., 2004) and recently in (Kljun et al., 2015). These parameterisations are based on a scaling approach. The parameters for these ~~analytical models~~ parameterisations were evaluated using backward Lagrangian stochastic particle dispersion model LPDM-B (Kljun et al., 2002). In turn, LPDM-B is based on the forward single particle Lagrangian stochastic model (see (Rotach et al., 1996) and (de Haan and Rotach, 1998)) satisfying WMC. The value of ~~Kolmogorov constant~~ parameter C_0 which was selected for LPDM-B stochastic model was set to 3 (see (Kljun et al., 2002)). In parameterisation of LPDM-B, the turbulent statistics and the wind velocity were assumed to be universal and depend on the surface heat and momentum fluxes, the roughness parameter and the boundary layer height. The exact formulas for all the universal non-dimensional functions under the stable stratification are not presented in (Kljun et al., 2015) and references therein, therefore direct comparison of the turbulence profiles with LES is not possible. Nevertheless, the final approximations (Kljun et al., 2004) and (Kljun et al., 2015) contain the input parameters, which can be determined from LES: the boundary layer height $z_i \approx 180$ m, Obukhov length $L/\kappa \approx 120$ m, friction velocity $U_* \approx 0.27$ m/s and roughness parameter $z_0 = 0.1$ m. These values were substituted into parameterisations (Kljun et al., 2004) and (Kljun et al., 2015). ~~Fig. 12~~ Fig. 13 shows the comparison of the ~~crosswind averaged~~ crosswind-integrated footprint functions f_s^y and cumulative footprints F, obtained by different models. The Thomson's model was used with $C_0 = 6, 4$, and 3 for the comparison.

Parametric models provide results which differ substantially from all the abovementioned approaches. Both of the models (Kljun et al., 2004) and (Kljun et al., 2015) predict faster mixing. One can see, that LSMT, which is itself too dispersive in comparison with 1-D LSMs and RDMs, does not reach the values predicted by parameterisations from (Kljun et al., 2004) and (Kljun et al., 2015), even if one chooses the smaller values of C_0. It means, that parameterisations of turbulence profiles must have significant impact and are one of the reasons for deviation between models from (Kljun et al., 2004) and (Kljun et al., 2015) and LES. ~~Besides, in~~ Finally, it can be seen from the Fig. ~~12 it is seen~~ 13, that the top boundary condition (absorbtion of particles at the height 100 m) does not affect ~~presented footprints .~~ the footprints obtained in LSMT.

7 Conclusions

Scalar dispersion and flux footprint functions within the stable atmospheric boundary layer were studied by means of LES and stochastic particle dispersion modelling.

It follows from LES results that the main impact on the particle dispersion can be attributed to the advection of particles by resolved and partially resolved "subfilter-scale" eddies. It ensures the possibility to improve the results of particles advection in discrete LES by the use of recovering of small-scale partially resolved velocity fluctuations. If one uses the LES model with the explicit filtering, then this recovering is straightforward and consists of application of the known inverse filter operator. Apparently, a similar method can be implemented for other LES when the spatial filter is not specified in an explicit form. This would require, however, the prior analysis of the modeled spectra to identify an effective spatial resolution and the actual shape of the implicit filter. For substantial improvement of particle transport statistics, it is enough to use subgrid Lagrangian stochastic model within the first computational layer only, where LES model becomes equivalent to simplified RANS-model.

When the particles are advected by a divergence-free turbulent velocity field, then the variance of the ~~particles~~ particle concentration can be accumulated at small spatial scales. In the considered case, it does not affect directly the ~~particles~~ particle advection by the large eddies and gives no significant influence on the results of footprint calculations. In those cases, when the instantaneous characteristics of the scalar field of particle concentration are important, the additional correction to particles velocities may be required. It can be done both through the introduction of stochastics, resulting in the diffusion of concentration, and through the "computationally inexpensive" ~~-~~divergent correction of the Eulerian velocity field.

Under the stable stratification, to calculate the flux footprint, it is preferable to use stochastic models, which describe the ~~particles~~ particle dispersion close to the process of scalar concentration diffusion with the effective coefficient $K_s^{ww}(z) = -\langle w's'\rangle / (\langle ds\rangle / dz)$ in a vertical direction. RDM and one-dimensional "well-mixed" LSM tested in this study are the examples of such stochastic models. The optimal value for the ~~"universal constant"~~ parameter C_0 for LSMs is found to be close to ~~6.~~ 6 under the conditions considered here. This value coincides with the estimation of ~~the value of~~ Kolmogorov Lagrangian constant in isotropic homogeneous turbulence. It provides additional justification for use of LSMs in stable ABL, due extending their of its applicability over a wider range of scales including the inertial subrange. Stochastic models that use smaller values ~~$C_0 \approx 4$~~ $C_0 \approx 3-4$ (this choice is widespread now) may produce extra mixing and the shorter footprints, ~~correspondingly.~~ respectively. Note that the estimation $C_0 = 6$ is based on the LES results combined with the SHEBA data (Grachev et al., 2013), where the nondimensional vertical velocity RMS was evaluated as $\tilde{\sigma}_w \approx 1.33$ (the exact estimation of this value in LES is restricted by the resolution requirements). In the cases when LSMs utilize smaller values of $\tilde{\sigma}_w$ the parameter C_0 should be reduced accordingly (for example, $C_0 \approx 4.7$ will be the best suited parameter for LSMs with the widely used value $\tilde{\sigma}_w \approx 1.25$ prescribed).

One-dimensional stochastic models can be supplemented by the horizontal ~~particles~~ particle dispersion in a simple way. Introduction of the correlation between particle displacement components in RDM does not improve or change results substantially. However, the coefficients of horizontal diffusion K_s^{uu} and K_s^{vv} for RDMs can be evaluated through the vertical diffusion coefficient K_s^{ww} multiplied by the square of velocity ~~components~~ component variances ratio.

Model LSM1, constructed as a combination of independent stochastic models in each direction (well-mixed in the vertical direction only) gives reasonable results although this model does not satisfy WMC in general. In contrast, the three-dimensional Thomson model with WMC and $C_0 = 6$ provides overestimated vertical mixing, which is manifested in a too small Schmidt number values and in ~~a~~ reduced lengths of the footprints. Thomson model with $C_0 = 8$ produces true mixing in vertical direction, but underestimates the mixing in crosswind direction.

Accordingly, one can recommend another well-mixed stochastic model proposed in (Kurbanmuradov and Sabelfeld, 2000). It was developed under the assumption that the vertical drift term does not depend on the horizontal velocity components, and the vertical component of this model coincides with LSM1. Prior to use, this model should be modified in an appropriate way to take into account the variation of momentum fluxes with height.

According to presented LES, the source area and footprints in stable ABL can be substantially more extended than those predicted by the modern ~~analytical footprint parameterizations~~ footprint parameterisations and LSMs. The following reasons were identified in this study: 1) too small values of the ~~Kolmogorov constant~~ parameter C_0 are used; 2) the possible overestimated vertical mixing provided by some stochastic models based on well-mixed condition; 3) universal functions for turbulent statistics that are likely to cause additional deviation in the case of stable turbulent Ekman boundary layer studied here.

8 Code availability/Data availability

The code of LES model is available by request for the scientific researches in cooperation with first author (and.glas@gmail.com). The data from LES are attached to the supplement. These data were prepared as it was discussed in Sect. 5.1 and can be used for the stochastic models evaluation. Besides, supplement contains the data for ~~cross-wind averaged~~ crosswind-integrated footprints and two-dimensional footprints obtained in LES (see ~~,~~ Fig.6 and Fig.9).

Appendix A: Assessing the influence of the artificial top boundary condition on the LES results

To confirm the small impact of the top boundary condition on the results presented above, an additional run was performed (LES with $\Delta_g = 6.25$ m and subgrid LSM, see Sect. 3.2.1(2)). The setup of this numerical experiment was identical to those described in Sect. 4.1, but all particles were retained inside the LES model domain after their ejection (reflection condition was prescribed at the top of the domain). The footprint functions f_s^y obtained in this run are shown by blue curves in Fig.A1a,b,c. The footprints from the particles, which attained the level $z = 100$ m at least one time (the particles were marked by the special identifier in numerical code), were also evaluated (see, dashed red lines in Fig.A1a,b,c). For comparison the footprints with the applied absorbtion of the particles at the level $z = 100$ m are shown by the green lines and the crosses in Fig.A1a,b,c. One can see, that the impact from the particles which were returned from the levels above 100 m is neglectfully small for the sensor heights $z_M = 10$ m and $z_M = 30$ m. For the level $z_M = 60$ m, the influence of the artificial boundary condition is visible beginning from the distances $x_M - x > 6$ km.

The functions $f_s^y(x_M - x, z_M, t_1, t_2)$ are presented in Fig. A1d. Here, $[t_1, t_2]$ is the interval of the time averaging (see, Sect.2.1), shown in the legend in seconds (here, t_1, t_2 is the time starting from the beginning of the particle ejection). One can see, that the footprints are developed sequentially, the fast and the intensive processes form the footprint function peak first, and it remains to be unchanged later. Figure A1d is included with the aim to demonstrate, that the shape and the value of the footprint function within a large enough range of the distances $x_M - x$ can be independent of the total vertical scalar flux value. The normalized vertical fluxes $\langle F_s(z_M)/F_s(0)\rangle_{[t_1,t_2]}$ are shown also and they grow approximately twice, depending on the time averaging interval.

Finally, we want to mention that this is very specific, and it may be different for different types of ABL. We select the described setup of the numerical experiment intentionally for the sake of convenience of the comparisons of statistics obtained by the Eulerian and the Lagrangian methods. This provides additional ability for the testing of Lagrangian particle transport routines implemented in the LES model code.

Acknowledgements. This research is implemented in framework of Russian-Finnish collaboration, funded within CarLac (Academy of Finland, 1281196) and GHG-Lake projects. Russian co-authors are partially supported by Russian Foundation for Basic Research (RFBR 14-05-91752, 15-05-03911 and 16-05-01094). Finnish co-authors acknowledges also the EU project InGOS, and National Centre of Excellence (272041), ICOS-FINLAND (281255), Academy professor projects (1284701 and 1282842) by Academy of Finland.

References

Anderson, P. S.: Measurement of Prandtl number as a function of Richardson number avoiding self-correlation. Boundary-Layer Meteorol., 131, 3, 345–362, 2009

Banta R. M. , Pichugina Y. L. and Brewer W. A.: Turbulent Velocity-Variance Profiles in the Stable Boundary Layer Generated by a Nocturnal Low-Level Jet. J. Atmos. Sci. 63, 1, 700–2719, 2006.

Barad M.: Project Prairie Grass, a field program in diffusion, vol 2. Technical Report Geophysical Research Papers No. 59, TR-58-235(II). Air Force Cambridge Research Center, Bedford, 1958. 209 pp

Bardina J, Ferziger J.H., Reynolds W.C.: Improved subgrid scale models for large-eddy simulation. Am. Inst. Aeronaut. Astronaut., paper 80-1357, 1980.

Basu S. and Porté-Agel F. Large-Eddy Simulation of Stably Stratified Atmospheric Boundary Layer Turbulence: A Scale-Dependent Dynamic Modeling Approach. J. Atmos. Sci. 2006, 63, 1, P. 2074–2091.

Beare, R.J., MacVean, M.K., Holtslag, A.A.M., Cuxart, J., Esau, I., Golaz, J.C., Jimenez, M.A., Khairoutdinov, M., Kosovic, B., Lewellen, D., Lund, T.S., Lundquist, J.K., McCabe, A., Moene, A.F., Noh, Y., Raasch, S., Sullivan, P. : An Intercomparison of Large-Eddy Simulations of the Stable Boundary Layer. Boundary-Layer Meteorol., 118, 2, 247–272, 2006.

Boughton B., Delaurentis J., Dunn W.: A stochastic model of particle dispersion in the atmosphere. Boundary-Layer Meteorol. 40, 1, pp 147–163, 1987.

Bhaganagar K. and Debnath M.: The effects of mean atmospheric forcings of the stable atmospheric boundary layer on wind turbine wake., J. Renewable Sustainable Energy 7, 013124, 2015

Businger, J. A., J. C. Wyngaard, Y. Izumi, and E. F. Bradley: Flux–profile relationships in the atmospheric surface layer. J. Atmos. Sci., 28, 2, 181–189, 1971.

Xuhui Cai , Jiayi Chen, Raymond L. Desjardins: Flux Footprints in the Convective Boundary Layer: Large-Eddy Simulation and Lagrangian Stochastic Modelling. Boundary-Layer Meteorol., 137, 1, 31–41, 2010.

Cuxart J., Holtslag A. A. M., Beare R. J., Bazile E., Beljaars A., Cheng A., Conangla L., Ek M., Freedman F. et al.: Single-Column Model Intercomparison for a Stably Stratified Atmospheric Boundary Layer. Boundary-Layer Meteorol., 118, 2, 273–303, 2006.

de Haan, P. and Rotach, M. W.: A Novel Approach to Atmospheric Dispersion Modelling: the Puff-Particle Model (PPM), Q. J. Roy. Meteorol. Soc., 124, 2771–2792, 1998.

Du S., Sawford B. L., Wilson J. D., and Wilson D. J.: A Determination of the Kolmogorov Constant (CO) for the Lagrangian Velocity Structure Function, Using a Second-Order Lagrangian Stochastic Model for Decaying Homogeneous Isotropic Turbulence, Phys. Fluids., 1, 3083–3090, 1995.

Durbin P.A.: Stochastic differential equations and turbulent dispersion. NASA Reference Publication 1103, NASA, 70p., 1983.

Durbin, P. A.: Comments on Papers by Wilson et al. (1981) and Legg and Raupach (1982), Boundary Layer Meteorol., 29, 409 – 411, 1984.

Finn, D., Lamb, B., Leclerc, M.Y., Horst, T.W.: Experimental evaluation of analytical and Lagrangian surface-layer flux footprint models. Boundary-Layer Meteorol., 80, 283–308, 1996.

Germano M., Piomelli U., Moin P. and Cabot W. H.: A dynamic subgrid-scale eddy viscosity model. Phys. Fluids. A, 3, 1760-1765, 1991.

Ghosal S., Lund T.S., Moin P., Akselvoll K.: A dynamic localization model for large eddy simulation of turbulent flows. J. Fluid Mech., 286, 229–255, 1995.

Glazunov A.V. : Large-eddy simulation of turbulence with the use of a mixed dynamic localized closure: Part 2. Numerical experiments: Simulating turbulence in a channel with rough boundaries. Izvestiya Atmospheric and Oceanic Physics, 45, 1, 25–36, 2009.

Glazunov A.V., Dymnikov V.P: Spatial spectra and characteristic horizontal scales of the temperature and velocity anomalies in convective atmospheric boundary layer. Izvestiya, Atmospheric and Oceanic Physics, 2013, 49, 1, 33–54, 2013.

Glazunov A.V.: Numerical simulation of stably stratified turbulent flows over flat and urban surfaces Isv. Atm. and Ocean. Phys. 50, 3, 236–245.

Glazunov A.V.: Numerical simulation of stably-stratified turbulent flows over urban-like surface. Spectra and scales, parameterization of temperature and velocity profiles, Atmospheric and Oceanic Physics, 50, 4, 356–368, 2014,

Glazunov A.V. and Stepanenko V.M.: Large eddy simulation of stratified turbulent flows over heterogeneous landscapes. Izvestiya, Atmospheric and Oceanic Physics, 51, 4, 351–361, 2015.

Grachev A.A., Andreas E.L, Fairall C.W., Guest P.S., Persson P.O.G.: On the turbulent Prandtl number in the stable atmospheric boundary layer. Boundary-Layer Meteorol. 125, 2, 329–341, 2007

Grachev A.A., Andreas E.L, Fairall C.W., Guest P.S., Persson P.O.G.: The Critical Richardson Number and Limits of Applicability of Local Similarity Theory in the Stable Boundary Layer. Boundary-Layer Meteorol., 147, 1, 51–82, 2013.

Grachev, A. A., Andreas, E. L., Fairall, C. W., Guest, P. S. and Persson, P. O. G.: Similarity theory based on the Dougherty–Ozmidov length scale. Q.J.R. Meteorol. Soc., 141, 1845–1856, 2015.

Haugen D.: Project Prairie Grass, a field program in diffusion, vol 3. Technical Report Geophysical Research Papers No. 59, TR-58-235(III). Air Force Cambridge Research Center, Bedford, 1959.

Hellsten Antti, Sofia-M. Luukkonen, Gerald Steinfeld, Farah Kanani-Suhring, Tiina Markkanen, Leena Jarvi, Juha Lento, Timo Vesala, Siegfried Raasch.: Footprint Evaluation for Flux and Concentration Measurements for an Urban-Like Canopy with Coupled Lagrangian Stochastic and Large-Eddy Simulation Models. Boundary-Layer Meteorol., 157, 2, pp 191–217, 2015.

Högström, U.: Review of Some Basic Characteristics of the Atmospheric Surface Layer, Bound.?Lay. Meteorol., 78, 215–246, 1996

Horst, T. W. and Weil, J. C.: Footprint Estimation for Scalar Flux Measurements in the Atmospheric Surface Layer. Boundary-Layer Meteorol., 59, 3, 279-296, 1992. Journal of the Meteorological Society of Japan

Kitamura Y.: Self–Consistency Validation of Subgrid Scale Parameterization Schemes in a Large–Eddy Simulation. J. of the Met. Society of Japan, 88, 5, 813–825, 2010

Kljun, N., Rotach, M. W., and Schmid, H. P.: A 3D Backward Lagrangian Footprint Model for a Wide Range of Boundary Layer Stratifications, Bound.-Lay. Meteorol., 103, 205–226, 2002.

Kljun, N., Rotach, M. W., and Calanca, P.: A Simple Parameterisation for Flux Footprint Predictions, Bound.-Lay. Meteorol., 112, 3, 503–523, 2004.

Kljun, N., Calanca, P., Rotach, M. W. and Schmid H. P.: A simple two-dimensional parameterisation for Flux Footprint Prediction (FFP), Geosci. Model Dev., 8, 3695-3713, 2015.

Kormann R. , Meixner F.: An analytical footprint model for non-neutral stratification. Boundary-Layer Meteorol., 99, 2, 207-224, 2001.

Kosoviĉ B. and Curry J. A. A Large Eddy Simulation Study of a Quasi-Steady, Stably Stratified Atmospheric Boundary Layer. J. Atmos. Sci., 57., 8., 1052–1068, 2000.

Kurbanmuradov O. , K. Sabelfeld: Lagrangian Stochastic Models For Turbulent Dispersion In The Atmospheric Boundary Layer. Boundary-Layer Meteorol., 97, 2, 191–218, 2000.

Leclerc, M. Y., Shen, S., Lamb, B.: Observations and large-eddy simulation modeling of footprints in the lower convective boundary layer. J. Geophys. Res. 102, 9323–9334, 1997.

Leclerc, M. Y., Meskhidze, N., Finn, D.: Comparison between measured tracer fluxes and footprint model predictions over a homogeneous canopy of intermediate roughness. Agric. For. Meteorol. 117, 145-158, 2003

Lien Ren-Chieh, D'Asaro Eric A.: The Kolmogorov constant for the Lagrangian velocity spectrum and structure function. Physics of Fluids., 14, 12, 4456–4459, 2002.

Liu S., Meneveau C., Katz J.: On the properties of similarity subgrid-scale models as deduced from measurements in a turbulent jet. J. Fluid Mech. 275, 83–119, 1994.

Maronga, B., Gryschka, M., Heinze, R., Hoffmann, F., Kanani-Suhring, F., Keck, M., Ketelsen, K., Letzel, M. O., Suhring, M., and Raasch, S.: The Parallelized Large-Eddy Simulation Model (PALM) version 4.0 for atmospheric and oceanic flows: model formulation, recent developments, and future perspectives, Geosci. Model Dev., 8, 2515-2551, 2015.

Meneveau C. and Katz J.: Scale-invariance and turbulence models for large-eddy simulation. Annu. Rev. Fluid Mech., 32, 1–32, 2000.

Michalek W. R., J. G. M. Kuerten, J. C. H. Zeegers, R. Liew, J. Pozorski, B. J. Geurts: A hybrid stochastic-deconvolution model for large-eddy simulation of particle-laden flow. Physics of Fluids, 25, 123302, 2013

Monin, A. S. and Yaglom, A. M.: Statistical Fluid Mechanics: Mechanics of Turbulence. Vol. 2, MIT Press, Cambridge MA, 1975.

Morinishi, Y., Lund, T. S., Vasilyev, O. V. and Moin, P.: Fully conservative higher order finite difference schemes for incompressible flow. J. Comp. Phys., 143, 1, 90–124, 1998.

Nieuwstadt F.T.M.: The turbulent structure of the stable, nocturnal boundary layer. J. Atmos. Sci., 41, 14, 2202–2216, 1984.

Nicolini G., G. Fratini, V. Avilov, J. A. Kurbatova, I. Vasenev and R. Valentini: Performance of eddy-covariance measurements in fetch-limited applications. Theoretical and Applied Climatology, 1–12, 2015.

Obukhov, A. M.: Structure of the Temperature Field in a Turbulent Flow, Izv. Akad. Nauk S.S.S.R., Ser. Geogr. and Geophys., 13, 58–69, 1949.

Piotrowski Z. P., Smolarkiewicz P. K., Malinowski S. P. and Wyszogrodzki A. A.: On numerical realizability of thermal convection. Journal of Computational Physics, 228, 17, 6268 – 6290, 2009.

Poggi D., Katul G. G. and Cassiani M. On the anomalous behavior of the Lagrangian structure function similarity constant inside dense canopies. Atmospheric Environment, 42, 4212–4231.

Rizza U., Degrazia G. A., Mangia C., Pereira E. and Filho E. Estimation of the Kolmogorov constant for the Lagrangian velocity spectrum and structure function under different PBL stability regimes generated by LES. Physica A 389, 4009–4017

Rotach M.W., Gryning S.E. and Tassone C.: A two-dimensional Lagrangian stochastic dispersion model for daytime conditions. Q. J. R. Meteorol. Soc., 122, 367–389, 1996.

Rotach, M. W., Gryning, S.-E., and Tassone, C.: A Two-Dimensional Lagrangian Stochastic Dispersion Model for Daytime Conditions. Quart. J. Roy. Meteorol. Soc., 122, 367–389, 1996.

Sawford, B. L., and F. M. Guest: Uniqueness and universality of Lagrangian stochastic models of turbulent dispersion, paper presented at 8th Symposium on Turbulence and Diffusion, San Diego, CA, Apr. 25-29, 1988, Preprints (A89-18205 05-47). Boston, MA, American Meteorological Society, 96 – 99, 1988.

Sawford B.L.: Recent developments in the Lagrangian stochastic theory of turbulent dispersion. Boundary-Layer Meteorol., 62, 1, 197–215, 1993.

Shotorban B., Mashayek F. A stochastic model for particle motion in large-eddy simulation. Journal of Turbulence, 7, 18, 2006

Steinfeld G., Raasch S. and Markkanen T.: Footprints in Homogeneously and Heterogeneously Driven Boundary Layers Derived from a Lagrangian Stochastic Particle Model Embedded into Large-Eddy Simulation. Boundary-Layer Meteorol., 114, 3, 503–523, 2008.

Stolz S., N. A. Adams, and L. Kleiser: An approximate deconvolution model for a large-eddy simulation with application to incompressible wall-bounded flows. Phys. Fluids, 13, 997–1015, 2001.

Thomson D.: Criteria for the selection of stochastic models of particle trajectories in turbulent flows. J Fluid Mech., 180, 529–556, 1987.

Thomson D., Wilson J.: History of the Lagrangian stochastic model for turbulent dispersion. In: Lagrangian models of the atmosphere. Geophysical Monograph 200. American Geophysical Union,
Washington, DC, 347 pp, 2013

Van Cittert, P.: Zum Einfluβ der Spaltbreite auf die Intensit$\ddot{a}$tsverteilung in Spektrallinien II. Z. Phys. 69, 298–308, 1931.

Weil J. C., Sullivan P. P. and Moeng C-H.: The Use of Large-Eddy Simulations in Lagrangian Particle Dispersion Models. J. Atmos. Sci., 61, 23, 2877-2887, 2004.

Wilson J., Thurtell G, Kidd G. Numerical simulation of particle trajectories in inhomogeneous turbulence. III. Comparison of predictions with experimental data for the atmospheric surface layer. Boundary-Layer Meteorol., 21, 4, 443–463, 1981.

Wilson J. D., Yee E.: A critical examination of the random displacement model of turbulent dispersion. Boundary-Layer Meteorol., 125, 3, 399–416, 2007.

Wilson J. D. and Sawford B. L.: Review of Lagrangian stochastic models for trajectories in the turbulent atmosphere. Boundary-Layer Meteorol., 78, 1, 101-210, 1996.

Wilson J. D.: Computing the Flux Footprint. Boundary-Layer Meteorol., 156, 1, 1-14, 2015.

Zhou, B. and Chow. F.K.: Large-eddy simulation of the stable boundary layer with explicit filtering and reconstruction turbulence modeling. Journal of the Atmospheric Sciences 68, 9, 2142–2155, 2011.

Zhou, B. and Chow. F.K.: Turbulence Modeling for the Stable Atmospheric Boundary Layer and Implications for Wind Energy. Flow Turbulence Combust 88, 255–277, 2012

Zilitinkevich S. S., Elperin T., Kleeorin N., Rogachevskii I., Esau I.: A Hierarchy of Energy- and Flux-Budget (EFB) Turbulence Closure Models for Stably-Stratified Geophysical Flows., 146, 3, 341–373, 2013.

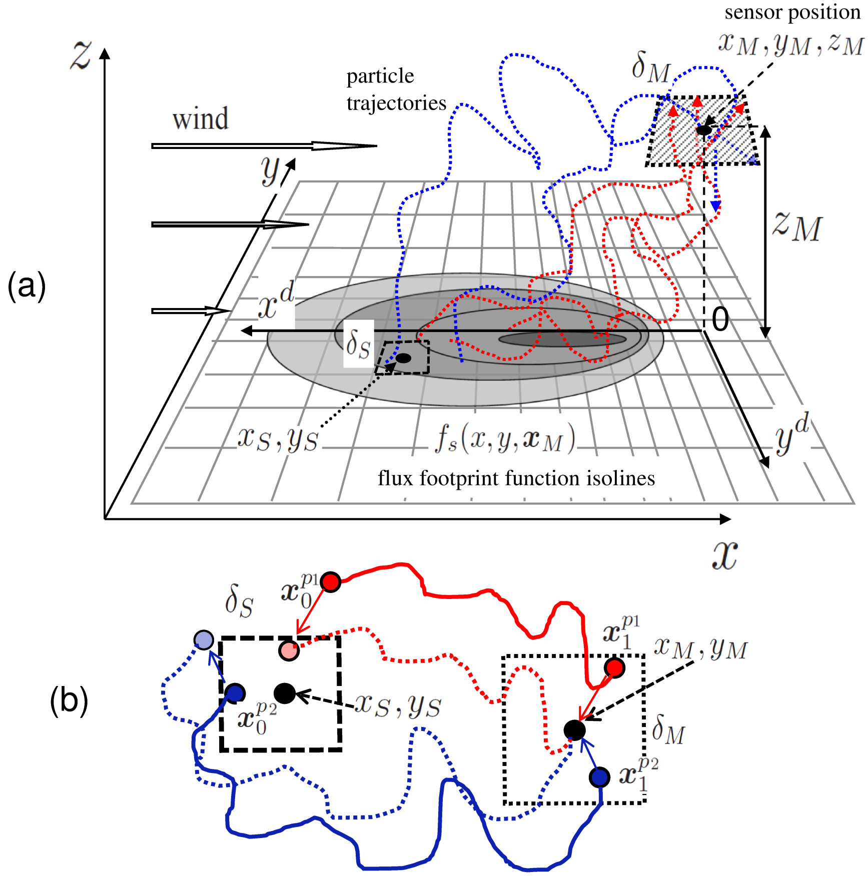

Figure 1. Schematic representation of footprint evaluation algorithm. (a) Setup of numerical experiment. (b) Example of two trajectories (red and blue bold curves). Shifted trajectories are shown by the dashed lines. Particle brings the impact into the value $f_s(x_S, y_S, \boldsymbol{x}_M)$ if it intersects the test area δ_M in vicinity of the sensor position $\boldsymbol{x}_M$ and the origin of modified trajectory belongs to the test area δ_S.

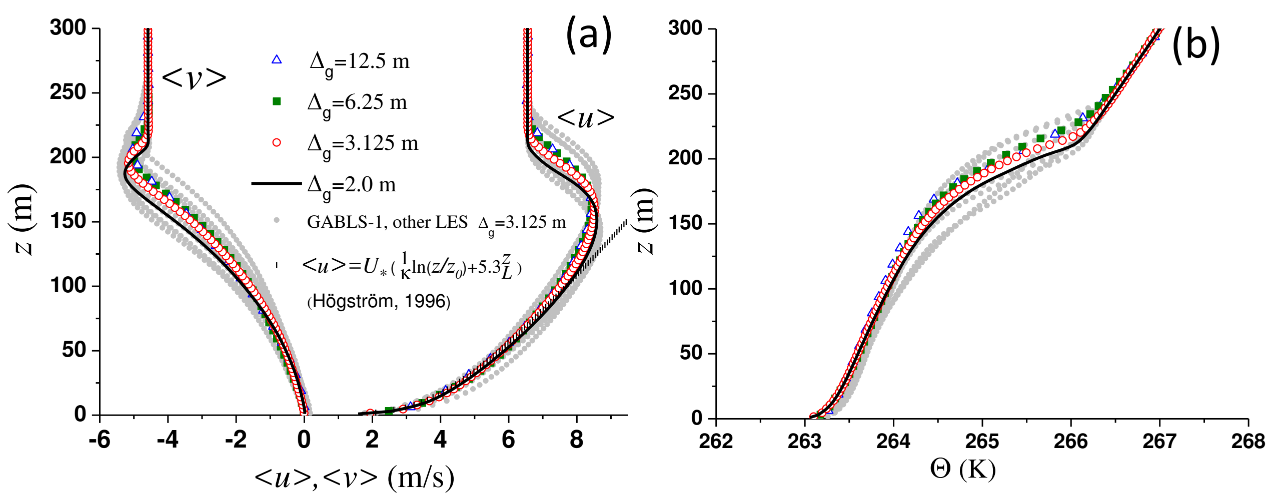

Figure 2. Mean wind velocity $\langle \boldsymbol{u} \rangle$ (a) and temperature $\langle \Theta \rangle$ (b) in runs with different grid steps (spatial step is pointed in legend). Gray dots are the data from other LES models obtained in (Beare et al., 2006) (wind velocity is rotated 35^o clockwise). 'Standard' wind profile for stable conditions in accordance with Högström (1996) is shown by the vertical dashes.

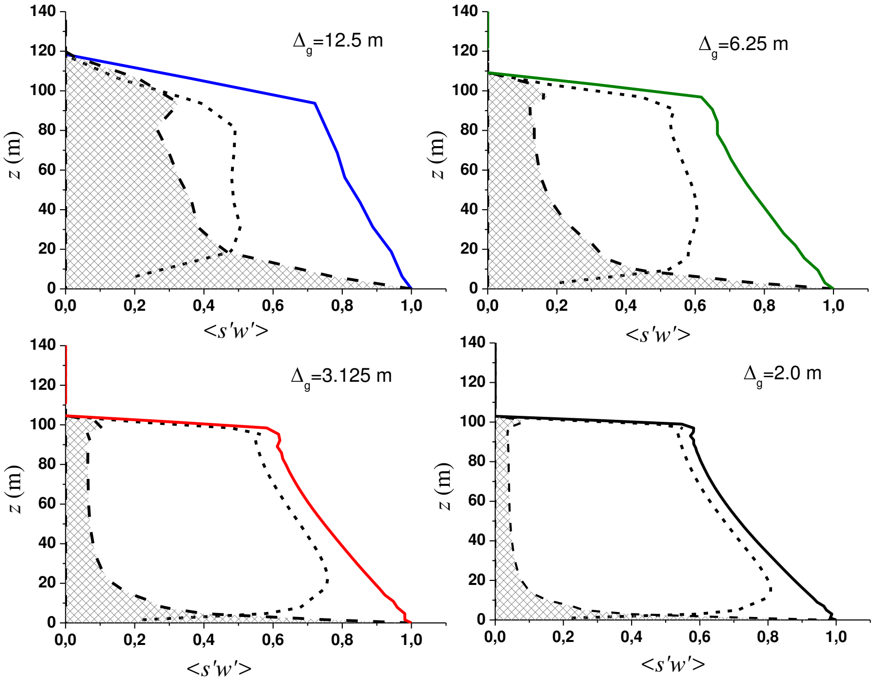

Figure 3. Total $F_s^{tot} = \langle \overline{s}\,\overline{w} \rangle + \langle \vartheta_3^s \rangle$ (solid lines), resolved $F_s^{res} = \langle \overline{s}\,\overline{w} \rangle$ (short-dashed lines) and "subgrid" $F_s^{sbg} = \langle \vartheta_3^s \rangle$ (long-dashed lines with shading) scalar fluxes in the runs with different grid steps Δ_g.

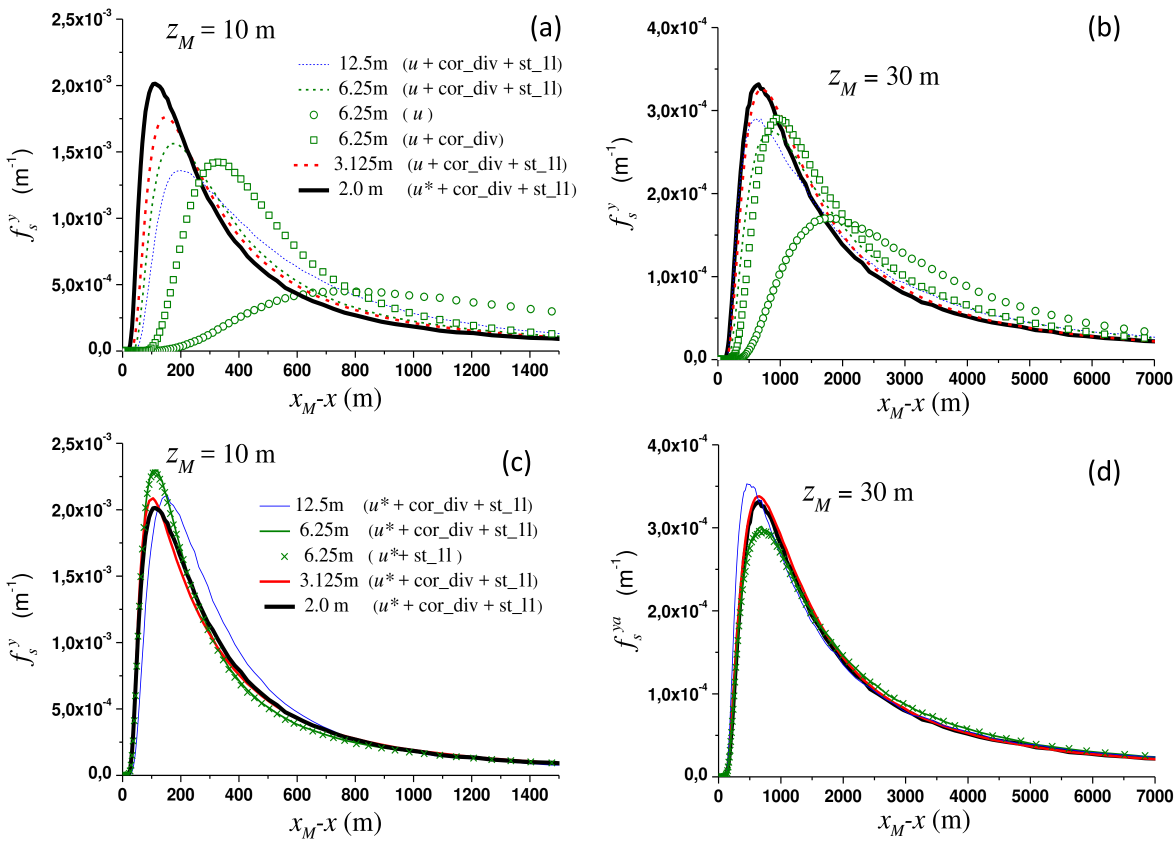

Figure 4. ~~Crosswind averaged~~ Crosswind-integrated scalar flux footprints f_s^y in stable ABL, computed by ~~the~~ different methods and with different grid steps; (a,c) sensor height z_M=10 m, (b,d) z_M=30 m. Grid steps and methods are indicated in the legend: u - particles are transported by a filtered LES velocity $\overline{\boldsymbol{u}}$; u^* - particles are transported by recovered velocity $\boldsymbol{u}^* = F^{-1}\overline{\boldsymbol{u}}$; cor_div - the additional correction of velocity (Eqs. 34, 35); st_1l - stochastic subgrid model (Eq. 28) is applied for the particles within the first computational grid layer.

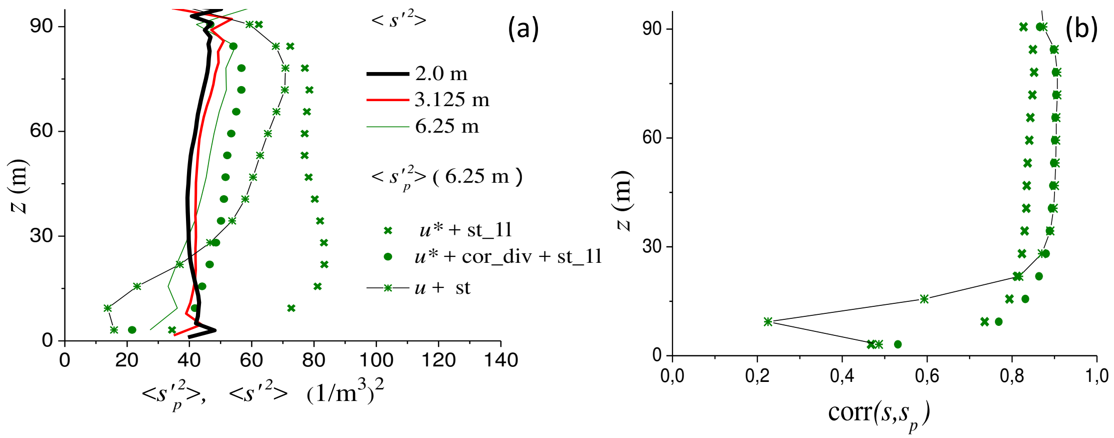

Figure 5. (a) Variance $\sigma_s^2 = \langle \overline{s}'^2 \rangle$ of concentration of Eulerian scalar (solid lines) and variance ~~$\sigma_{sp}^2 = \langle s_p'^2 \rangle$~~ $\sigma_{sp}^2 = \langle s_P'^2 \rangle$ of concentration ~~s_p~~ s_P, determined by Lagrangian particles (symbols); grid steps and the methods of calculations are shown in legend, symbolic notations are the same as in Fig. ~~3~~ 4; stars - stochastic model (Eqs. 28-32) is used throughout domain. (b) Correlation corr~~$(\overline{s}, s_p) = \langle \overline{s}' s_p' \rangle_{xyt} / (\sigma_{sp}\sigma_s)$~~ $(\overline{s}, s_P) = \langle \overline{s}' s_P' \rangle_{xyt} / (\sigma_{sp}\sigma_s)$ between "Eulerian" and "Lagrangian" concentrations. For remaining notations see the caption of Fig. ~~3.~~ 4.

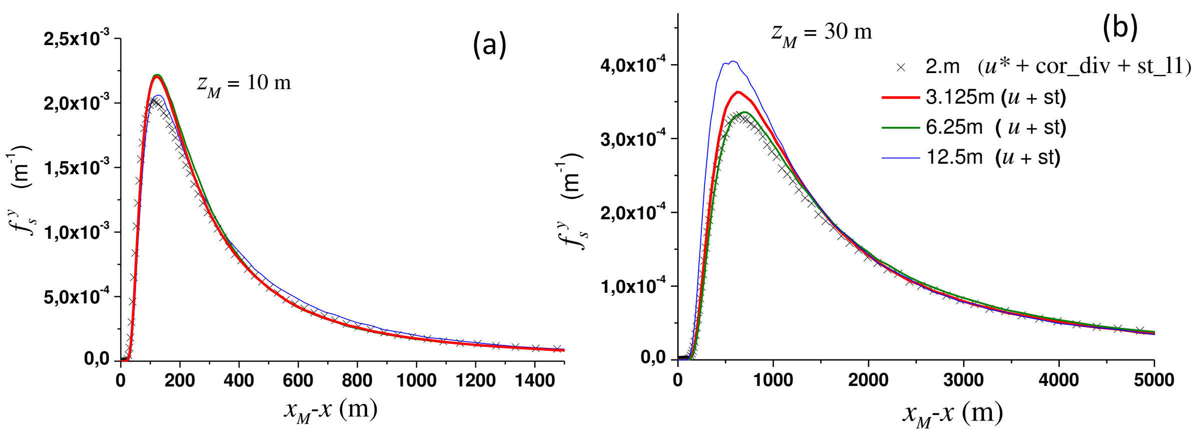

Figure 6. ~~Crosswind averaged~~ Crosswind-integrated scalar flux footprints f_s^y, computed using stochastic subgrid model (Eq. 28-32); (a) sensor height z_M=10 m, (b) z_M=30 m. Grid steps are given in the legend. Crosses denote footprints computed with subgrid LSM applied for the particles within the first grid layer only.

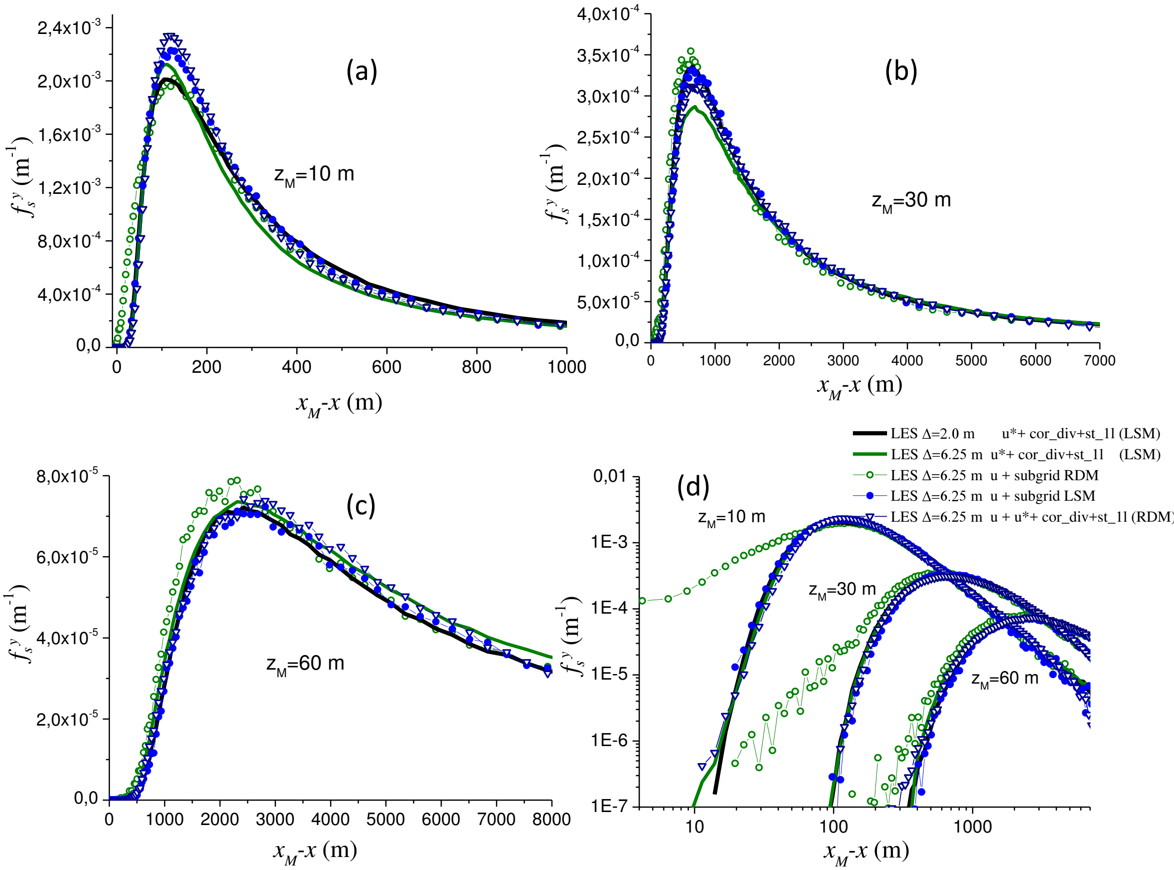

Figure 7. Crosswind-integrated scalar flux footprints f_s^y, obtained in LES with Δ_g = 6.25 m using different stochastic Lagrangian subgrid models RDM (Eq. 33) and LSM (Eqs. 28-32); The results obtained with these subgrid models applied within the first computational grid layer in combination with velocity recovering $\boldsymbol{u}^* = F^{-1}\overline{\boldsymbol{u}}$ and correction of velocity (Eqs. 34, 35) are also shown. Black lines are the footprints in LES with Δ_g = 2.0 m.

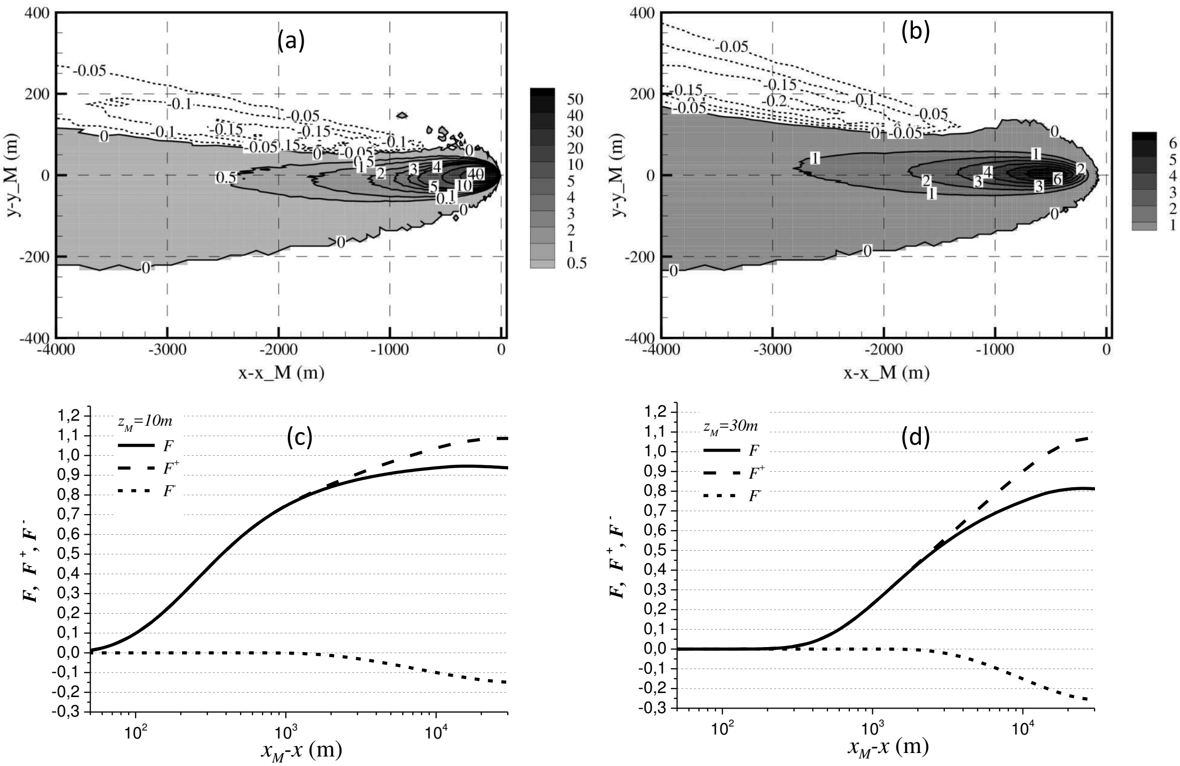

Figure 8. Two-dimensional footprints $f_s(x - x_M, y - y_M, z_M)$ ($\times 10^{-6}\mathrm{m}^{-2}$) for sensor height z_M=10 m (a) and z_M=30 m (b) and the corresponding ~~cross-wind integrated~~ crosswind-integrated cumulative footprints $F(x_M - x)$ (c) and (d); long dashed line - F^+ (impact of the area with positive values of f_s); short dashed line - F^- (impact of area with negative values).

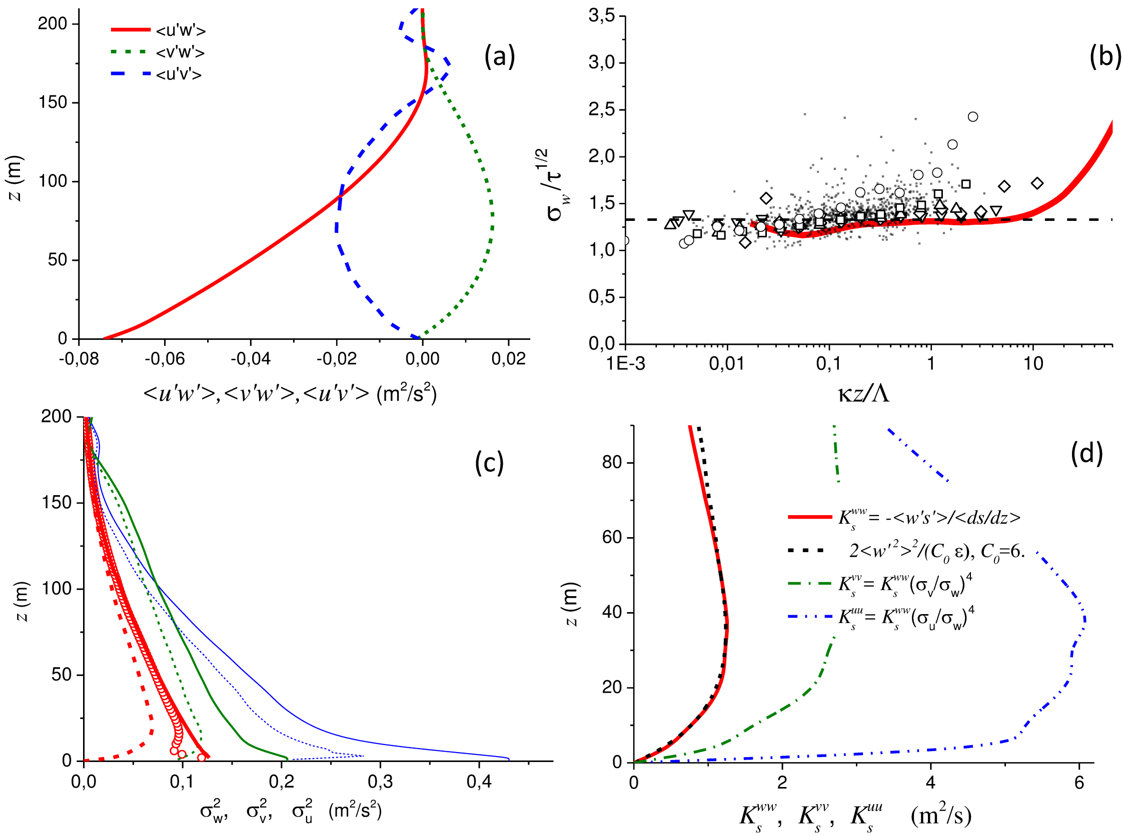

Figure 9. (a) Total momentum fluxes obtained in LES with Δ_g=2.0 m. (b) Normalized RMS of vertical velocity $\tilde{\sigma}_w = \sigma_w/|\tau|^{1/2}$ depending on a dimensionless parameter z/Λ (solid red line - estimation using LES data $\sigma_w = (\langle w^{*2}\rangle + 2/3E_{subgr})^{1/2}$; symbols - measurements (Grachev et al., 2013) at different ~~altitudes~~heights). (c) Variances of velocity components (dashed line - resolved fluctuation; solid lines - the final estimation for LSM; bold red lines - vertical component, ~~the~~ green curves of medium thickness - ~~cross-wind~~ crosswind component, blue thin lines - longitudinal component, circles - evaluation of σ_w^2 by ~~the formula~~ Eq. (41)). (d) Vertical effective eddy diffusivity K_s^{ww} (red solid line - coefficient calculated by the gradient and flux of scalar; dashed line - estimation of coefficient using ~~formula~~ Eq. (13) with $C_0 = 6$); estimations of diffusion coefficients in ~~cross-wind~~ crosswind direction K_s^{vv} (green dash-dot line) and coefficient in longitudinal direction K_s^{uu} (blue dash-dot-dot line).

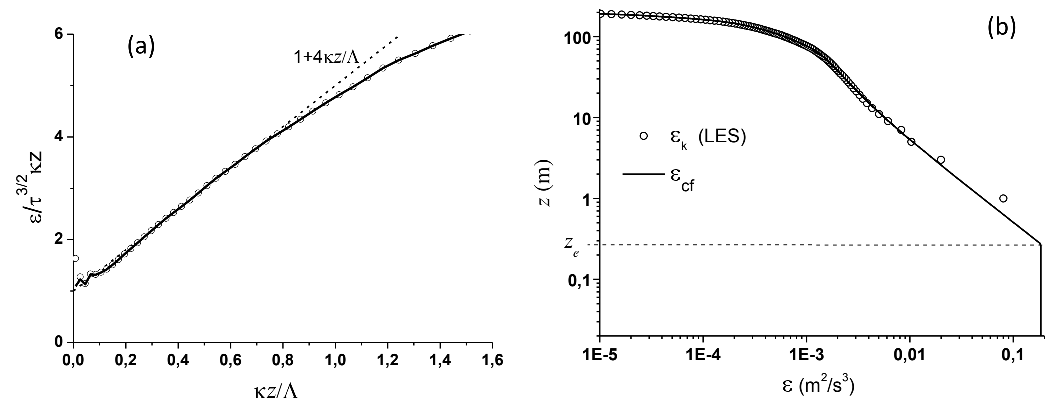

Figure 10. (a) Discrete (LES) nondimensional dissipation $\cancel{\epsilon_{\Delta k} z_k/|\tau|^{3/2}}$ $\epsilon_{\Delta k}\kappa z_k/|\tau|^{3/2}$ (circles), corrected values (solid line), universal function (Eq. 44) (dashed straight line). (b) Simulated discrete dissipation $\epsilon_{\Delta k}$ (circles) and corrected dissipation $\epsilon_{cf}(z)$ for LSM (solid line). Dashed horizontal line denotes the height z_e, which was chosen in order to equalize the integral values of the corrected dissipation and the discrete dissipation.

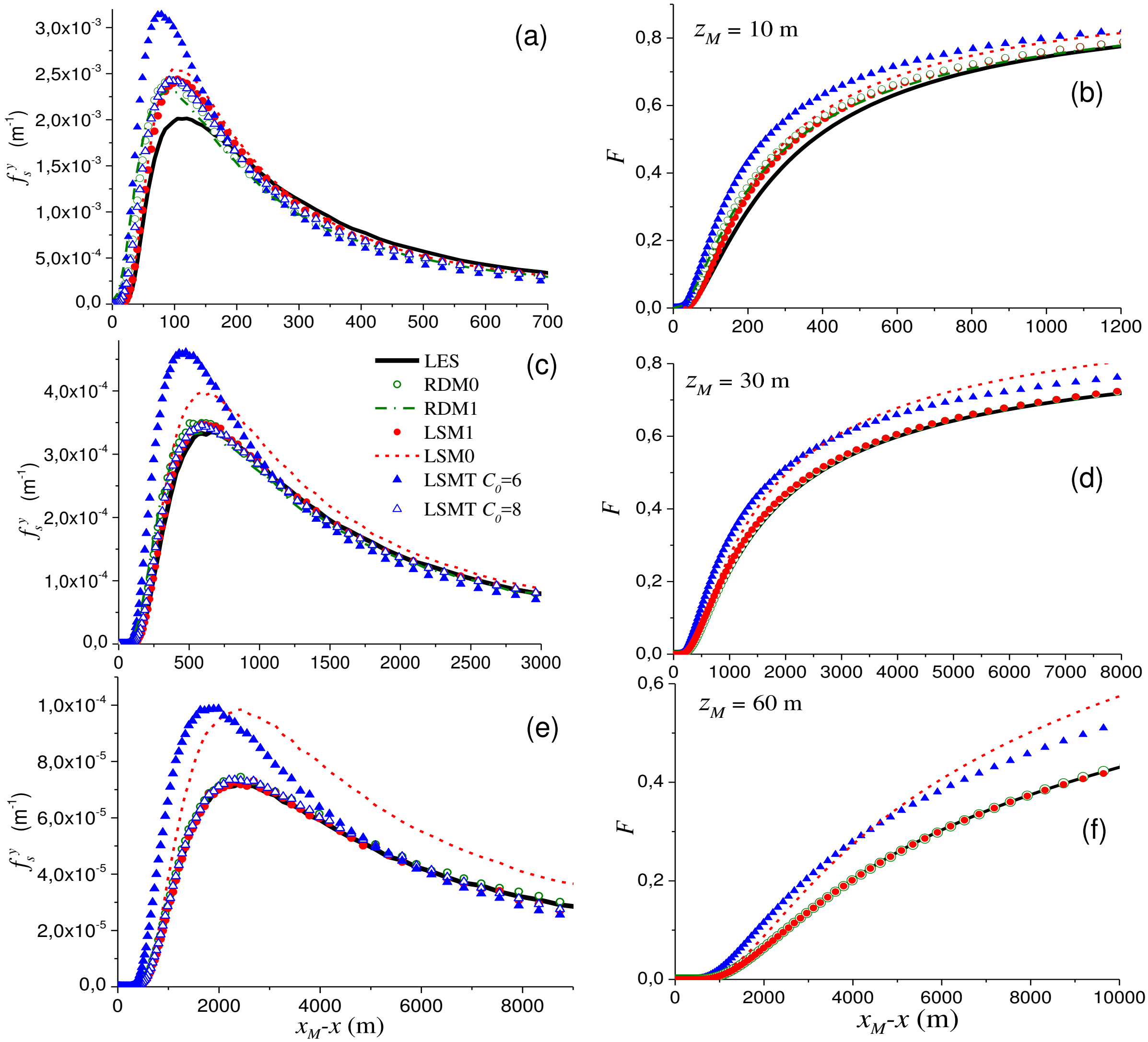

Figure 11. ~~One-dimensional~~ Crosswind-integrated footprints f_s^y (a,c,e) and cumulative footprints F (b,d,f) for sensor height z_M = 10 m (a,b), z_M = 30 m (c,d) and z_M = 60 m (e,f). Solid lines - LES with grid steps Δ_g=2.0 m. ~~Black~~ Blue triangles - LSMT (Thomson, 1987) with $C_0 = 6$, open triangles - LSMT with $C_0 = 8$. Short-dashed line - LSM0 (Lagranian stochastic model without well-mixed condition). ~~Black~~ Red circles - LSM1 (LSM with WMC for vertical mixing). Open green circles - RDM0 (uncorrelated random displacements model). Dash-dot green line - RDM1 (random displacements model with correlation between displacement components).

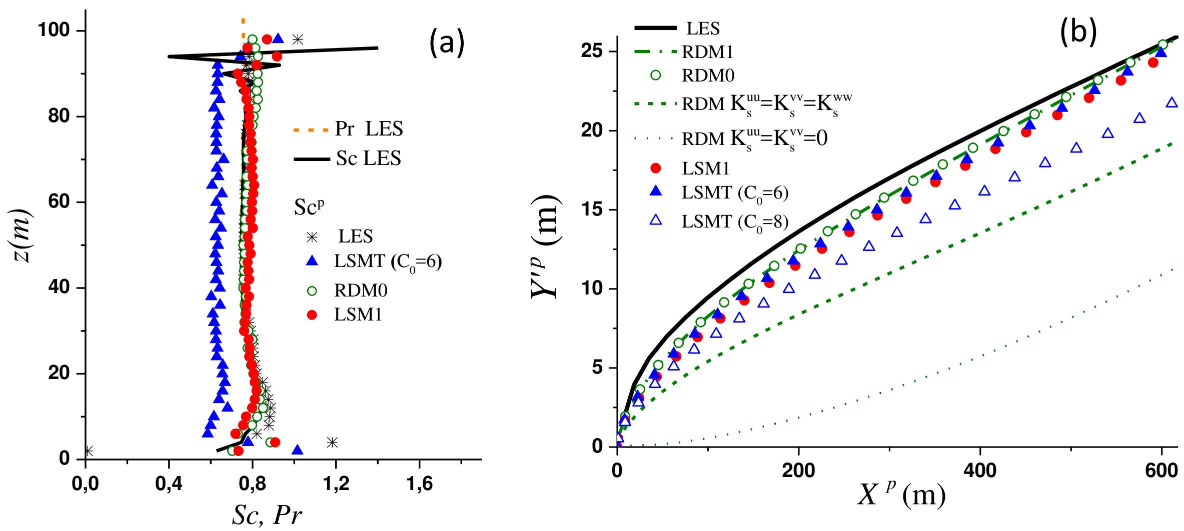

Figure 12. (a) Prandtl number Pr (dashed line) and Schmidt number Sc (solid line), computed using Eulerian scalars. Symbols - Schmidt numbers Sc, computed using the Lagrangian particles in LES, LSMs and RDMs. (b) RMS of the crosswind position of particle $Y'^p = \left\langle (y^p - Y^p)^2 \right\rangle^{1/2}$ depending on the mean longitudinal position $X^p = \langle x^p \rangle$. Dashed lines - RDM with $K_s^{uu} = K_s^{yy} = K_s^{ww}$ and one-dimensional RDM $K_s^{uu} = K_s^{vv} = 0$.

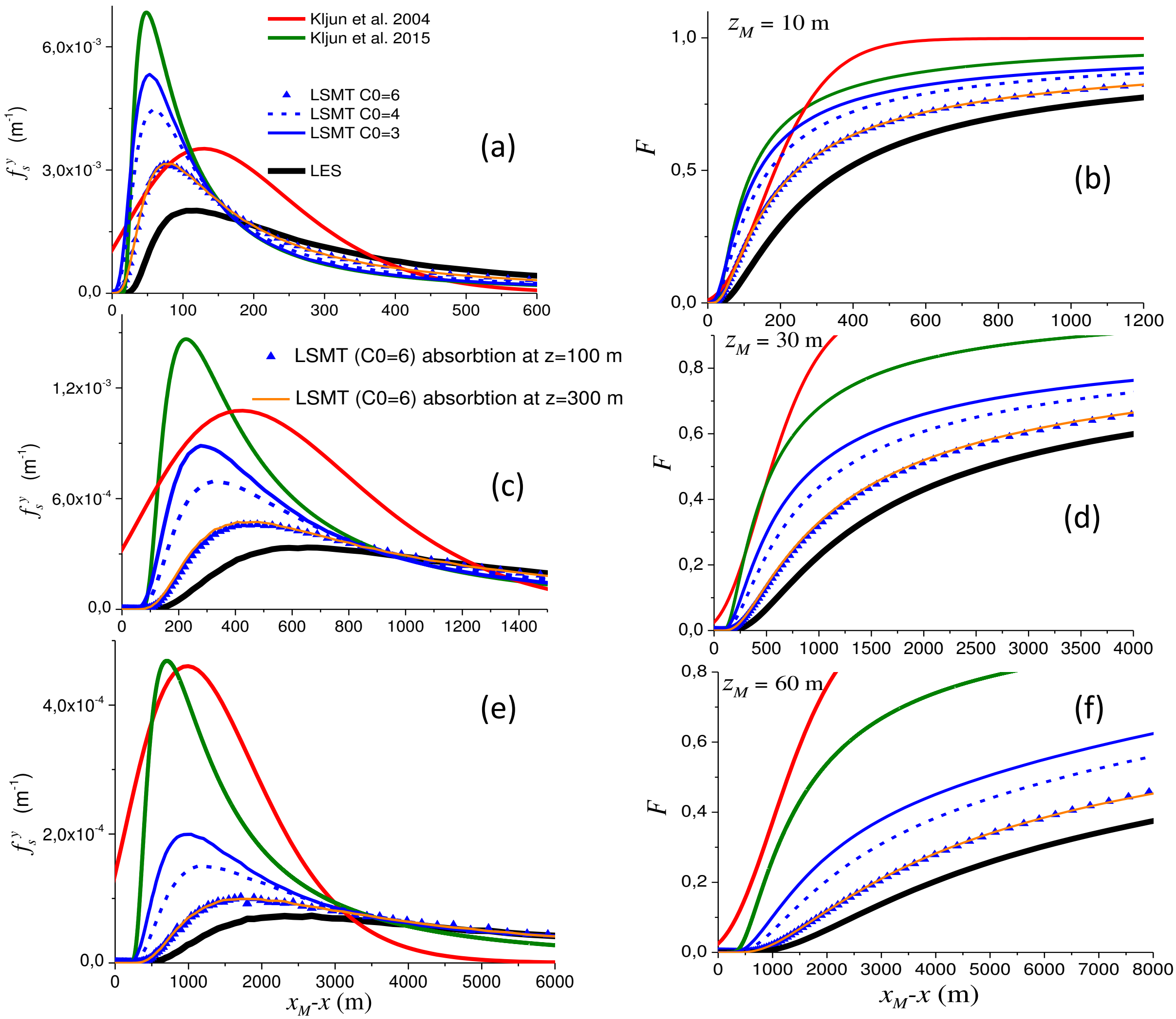

~~One-dimensional footprints f_s^y (a,c,e) and cumulative footprints F (b,d,f) for sensor height z_M = 10 m (a,b), z_M = 30 m (c,d) and z_M = 60 m (e,f). Solid lines - LES with grid steps Δ_g=2.0 m. Triangles - LSMT (Thomson (1987) model), $C_0 = 6$, absorbtion at z=100 m. Orange curves LSMT, $C_0 = 6$, absorbtion at z=300 m. Dashed blue lines - LSMT, $C_0 = 4$. Solid blue lines - LSMT, $C_0 = 3$. Red lines - parameterisation (Kljun et al., 2004). Green lines - parameterisation (Kljun et al., 2015).~~

Figure 13. Crosswind-integrated footprints f_s^y (a,c,e) and cumulative footprints F (b,d,f) for sensor height z_M = 10 m (a,b), z_M = 30 m (c,d) and z_M = 60 m (e,f). Solid lines - LES with grid steps Δ_g=2.0 m. Triangles - LSMT (Thomson (1987) model), $C_0 = 6$, absorbtion at z=100 m. Orange curves LSMT, $C_0 = 6$, absorbtion at z=300 m. Dashed blue lines - LSMT, $C_0 = 4$. Solid blue lines - LSMT, $C_0 = 3$. Red lines - parameterisation (Kljun et al., 2004). Green lines - parameterisation (Kljun et al., 2015).

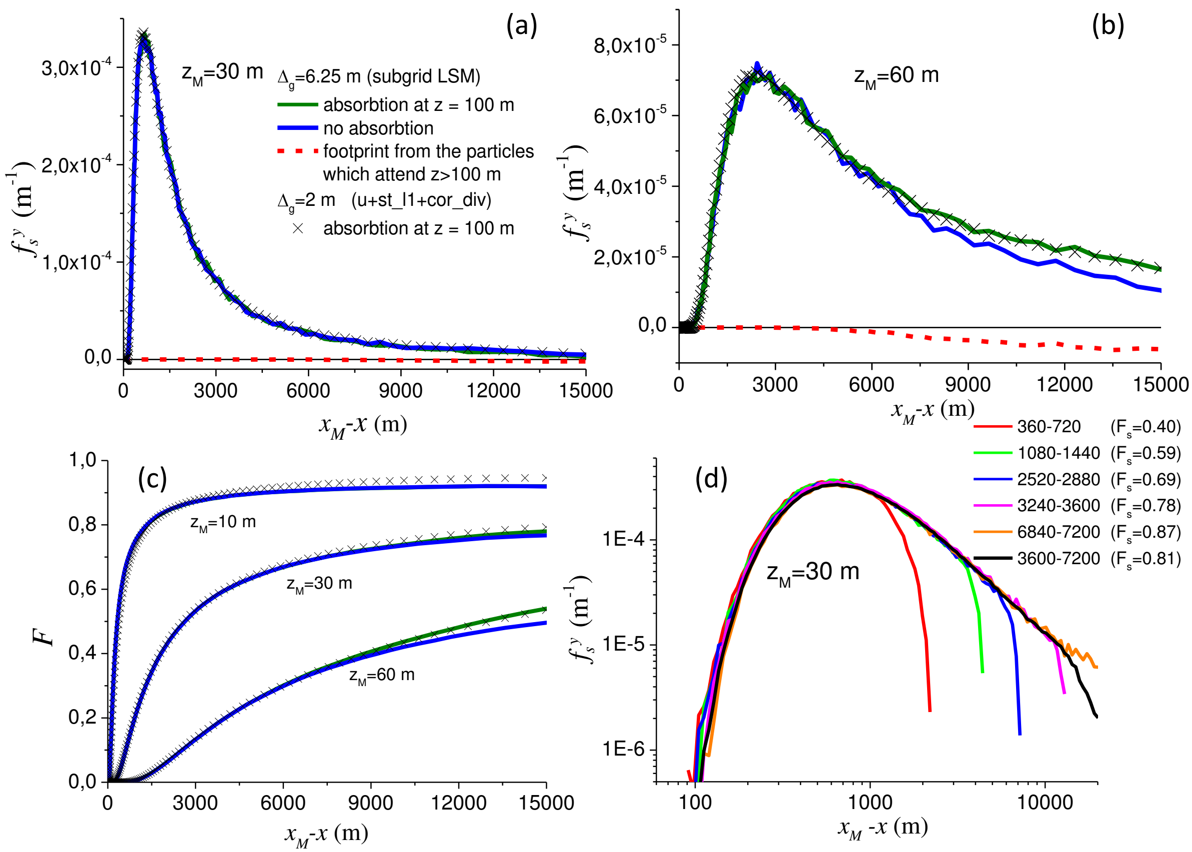

Figure A1. The footprint functions f_s^y (a,b) and the cumulative footprints F (c) obtained without the prescribed absorbtion (blue lines) in comparison with the results of simulation where the absorbtion is imposed at the level $z = 100$ m (green lines). Red dashed lines are the footprints from the particles which attained the level $z = 100$ m. (d) - Footprints obtained with the different intervals of averaging $[t_1, t_2]$ (shown in seconds in the legend), the normalized vertical concentration fluxes $\langle F_s(z_M)/F_s(0)\rangle_{[t_1,t_2]}$ are shown in brackets.